MICROCOPY RESOLUTION TEST CHART

NATIONAL BUREAU OF STANDARDS-1963-A

DESIGN AND ANALYSIS OF A SUBCRITICAL
AIRFOIL FOR HIGH ALTITUDE,
LONG ENDURANCE MISSIONS

THESIS

AFIT/GAE/AA/82D-1

Iftikhar Ahmad
Flt Lt   PAF

DEPARTMENT OF THE AIR FORCE

AIR UNIVERSITY (ATC)

AIR FORCE INSTITUTE OF TECHNOLOGY

Wright-Patterson Air Force Base, Ohio

83 02 022121

DESIGN AND ANALYSIS OF A SUBCRITICAL
AIRFOIL FOR HIGH ALTITUDE,
LONG ENDURANCE MISSIONS

THESIS

AFIT/GAE/AA/82D-]   Iftikhar Ahmad
                                     Flt Lt   PAF

DTIC

DESIGN AND ANALYSIS OF A SUBCRITICAL

AIRFOIL FOR HIGH ALTITUDE LONG

ENDURANCE MISSIONS

THESIS

Presented to the Faculty of the School of Engineering

of the Air Force Institute of Technology

Air University

in Partial Fulfillment of the

Requirements for the Degree of

Master of Science

by

Iftikhar Ahmad, B.E.

Flt Lt   PAF

Graduate Aeronautical Engineering

December 1982

Approved for public release; distribution unlimited.

Preface

This thesis topic was proposed by the Air Force Wright Aeronautical Laboratories. It is based on the concept of inverse airfoil design. It interested me because inverse methods were a part of my studies at AFIT and the thesis promised to cover two-dimensional boundary layers in some detail. The topic is also of current interest to the U.S.A.F.

I take this opportunity to thank "Allah" who gave me the strength to complete this project. I wish to express sincere gratitude to my thesis advisor, Major Mike Smith, whose understanding of Aerodynamics is impressive. His suggestions during the study and while compiling the draft were invaluable. I also wish to thank Major Eric Jumper and Doctor Milton Franke for their useful guidance. Thanks are also due to Mr Russel Osborn, Dr Jo Shang and Mr Charles Gallaway who provided maximum support and guidance while I was working at AFWAL. I appreciate the patience and diligence of Mrs Anna Lloyd who typed my thesis. Last, but not the least, I acknowledge the patience with which my wife took the late hours and the weekends not only during the thesis, but druing my whole stay at AFIT.

<div align="right">Iftikhar Ahmad</div>

Table of Contents

List of Figures

List of Figures (contd)

List of Symbols

Symbol	Explanation
AR	aspect ratio
a_m, b_m	power-series coefficients
$C_{D,i}$	induced-drag coefficient
$C_{D,p}$	parasite-drag coefficient
C_D	boundary-layer dissipation coefficient
C_f	boundary-layer skin-friction coefficient
C_L	lift coefficient
C_p	pressure coefficient
c	airfoil chord, m
c^*	reference airfoil chord, m
c_d	section profile-drag coefficient
c_f	flap chord, m
c_l	section lift coefficient
$c_{l,ns}$	section lift coefficient without correction due to separation
c_m	section pitching-moment coefficient about quarter-chord point
D^*	dissipation function for laminar boundary layer
F	complex potential function
g	acceleration due to gravity, m/s^2
g_1	slope of panel at beginning of panel
g_2	slope of panel at end of panel
H_{12}	boundary-layer shape factor, δ_1/δ_2
H_{12}^*	modified boundary-layer shape factor for calculation of section profile-drag coefficient
H_{32}	boundary-layer shape factor, δ_3/δ_2

I_a	total number of airfoil segments
i	$= \sqrt{-1}$
K	constant in upper-surface pressure-recovery function
$\overline{K}$	constant in lower-surface pressure-recovery function
K_H	exponent of upper-surface closure contribution
$\overline{K}_H$	exponent of lower-surface closure
K_R	desired value of K_S
K_S	sum of exponents of upper- and lower-surface closure contributions, $K_H + \overline{K}_H$
K_{tol}	tolerance on achievement of K_R
l	length, m
n	variable number
n_c	number of points on ζ unit circle
n_p	number of subpanels in one panel
n_q	number of points on airfoil, $n_c + 1$
P	real part of $\ln \dfrac{dz}{d\zeta} - \ln (1 - \dfrac{1}{\zeta})$ on circle $e^{i\phi}$, point
Q	conjugate harmonic function of $P(\phi)$
R	Reynolds number based on free-stream conditions and airfoil chord
R_{δ_2}	Reynolds number based on local conditions and boundary-layer momentum thickness
r	roughness factor
s	source distribution; arc length along airfoil surface, m
s_{sep}	arc length along which boundary layer is separated, m
s_T	arc length for transition from forward portion of airfoil to flap, m

s_{turb}	arc length along which boundary layer is turbulent including s_{sep}, m
t	airfoil thickness, m
t^*	reference airfoil thickness, m
U	potential-flow velocity, m/s
U'	$= \dfrac{dU}{dx}$, s^{-1}
U_∞	free-stream velocity, m/s
u	x-component of boundary-layer velocity, m/s
V	aircraft speed, m/s
v	absolute value of complex velocity; local velocity on airfoil, m/s
v^*	local velocity on airfoil for velocity specification in design method, m/s
v_0	normal velocity at surface in boundary-layer method, m/s
w	pressure-recovery function
$\bar{w}$	complex velocity, $ve^{-i\theta}$
$\vec{w}$	vector of velocity induced by panel at point (ξ, η)
w_t	tangential component of velocity induced by panel at end of panel
w_η	η-component of $\vec{w}$
w_ξ	ξ-component of $\vec{w}$
x	airfoil abscissa, m; axis in streamwise direction, tangential to surface in boundary-layer method
x_s	chord location of beginning of closure-contribution region, m
x_T	chord location of transition, m
x_w	chord location of beginning of main pressure-recovery region, m
y	airfoil ordinate, m; axis normal to surface in boundary-layer method

z	complex variable, $x + iy$
α	angle of attack relative to zero-lift line, deg
α^*	angle of attack relative to zero-lift line for velocity specification in design method, deg
α_c	angle of attack relative to chord line, deg
α_i^*	α^* for ith segment of ξ circle or airfoil, deg
$\alpha_{i,le}^*$	α^* for last segment of upper surface, deg
α_0	angle of zero lift, deg
β	inner normal angle, rad
Γ	circulation
γ	vorticity
γ_i	vorticity at beginning of panel
γ_j	vorticity at end of panel
γ_p	parabolic-vorticity factor
Δ	incremental change in quantity
Δc_ℓ	section lift-coefficient correction due to separation
$\Delta\alpha$	angle-of-attack correction due to separation, deg
$\Delta\phi$	angle between points on ξ unit circle, $\dfrac{2\pi}{n_c}$
δ	slope of airfoil surface near trailing edge, rad
δ_f	flap deflection, positive downward, deg
δ_1	boundary-layer displacement thickness
δ_2	boundary-layer momentum thickness
δ_2'	$= \dfrac{d\delta_2}{dx}$
δ_3	boundary-layer energy thickness
δ_3'	$= \dfrac{d\delta_3}{dx}$

ε^*	skin-friction function for laminar boundary layer
ζ	complex variable
η	panel ordinate
θ	argument of complex velocity; twist angle, deg
λ	$= \dfrac{\phi_w}{\Delta\phi}$
$\overline{\lambda}$	$= \dfrac{\overline{\phi}_w}{\Delta\phi}$
λ^*	$= \dfrac{\phi_s}{\Delta\phi}$
$\overline{\lambda}^*$	$= \dfrac{\overline{\phi}_s}{\Delta\phi}$
μ	exponent of upper-surface main pressure recovery
$\overline{\mu}$	exponent of lower-surface main pressure recovery
ν	kinematic viscosity, m^2/s
ν_i	$= \dfrac{\phi_i}{\Delta\phi}$
$\nu_{i,\ell e}$	$= \dfrac{\phi_{i,le}}{\Delta\phi}$
ξ	panel abscissa
ρ	air density, kg/m^3
σ	panel length
τ	shear stress, $kg/m \cdot s^2$
τ_0	skin friction, $kg/m \cdot s^2$
τ_1	angle between ξ-axis and line from beginning of panel to point (ξ, η), rad
τ_2	angle between ξ-axis and line from end of panel to point (ξ, η), rad
ϕ	argument of ξ
ϕ_{Ia}	arc limit of lower-surface trailing edge
ϕ_i	arc limit on ζ unit circle
$\phi_{i,\ell e}$	arc limit of leading edge

ϕ_s	arc limit of beginning of upper-surface closure-contribution region
$\bar{\phi}_s$	arc limit of beginning of lower-surface closure-contribution region
ϕ_w	arc limit of beginning of upper-surface main pressure-recovery region
$\bar{\phi}_w$	arc limit of beginning of lower-surface main pressure-recovery region
ψ	integration variable
ω	total amount of upper-surface main pressure recovery
$\bar{\omega}$	total amount of lower-surface main pressure recovery
ω'	initial slope of upper-surface main pressure recovery
$\bar{\omega}'$	initial slope of lower-surface main pressure recovery
∞	infinity

Subscripts:

i,j	index; $1,2,3,\ldots,\infty$
le	leading edge
lim	limit
ls	lower surface
max	maximum
min	minimum
sep	separation
te	trailing edge
us	upper surface

Abstract

An airfoil was designed using the 'inverse design' method. The airfoil was tailored to meet the requirements of high altitude, long endurance missions. The cruise Mach number was 0.65 so compressibility effects were included. In the procedure used, a basic airfoil was generated to meet the thickness and moment requirements. It was then refined to ensure desired behaviour of the boundary layer at the operating angles of attack. Computer codes designed by Richard Eppler were used for this study. The airfoil was anlayzed by using a viscous effects analysis program designed by Shang et al and a comparison was made with results obtained through Eppler's code.

I. INTRODUCTION

The United States Air Force is interested in the potential for high altitude, long endurance, remotely piloted vehicles to perform a variety of reconnaissance, survilliance and relay missions. The mission requires that the vehicle operate above 55,000 feet for at least 24 hours. The mission is to be performed at least 250 nautical miles away from home base. The aircraft should be able to take off and land using conventional runways (Ref 11).

High altitude, long endurance missions are ideal potential applications of subcritical airfoils. The wing accounts for a large percentage of total aircraft drag on such aircraft. This leads to the study of airfoils with a high lift to drag ratio. Such airfoils can result in substantial fuel savings when used on aircraft performing long endurance missions.

A substantial amount of research has been carried out in order to develop airfoils with high lift and low drag characteristics. But it has remained limited to low speed because of the applications, i.e., sailplanes, gliders, etc. It has been found that aircraft using jet engines can operate ecnomically at high subsonic speeds. Thus efforts are now being made to design subcritical airfoils for high subsonic flight.

Problem

The basic requirement for this study was as follows: To design an airfoil with the following characteristics:

1. A critical Mach number of 0.65.

1

2. A nominal thickness ratio of 15%.

3. As high a design lift coefficient as possible.

4. A low drag coefficient through extensive laminar flow at a Reynolds number range of 1.5 to 6.5 million on the airfoil.

5. As wide a drag bucket as possible.

Scope

The scope of this study is well defined by the design specifications. This study was limited to a theoretical investigation only and it did not include fabrication and wind tunnel testing of the airfoil. The Mach number was limited to 0.65 and the Reynolds number range varied from 1.5 million to 6.5 million. The requirements of high lift, low drag, low thickness ratio and a wide drag bucket indicate that a high lift to drag ratio was sought in this design.

General Approach

The study consisted of three basic parts which are discussed here.

The first step was to use some scheme in order to design a basic airfoil shape that satisfied the design requirements. This required the use of some computer program which could use design requirements as input to give the airfoil shape as output. An inverse program designed by Eppler (Ref 5) was used in this study to accomplish this part.

The second step involved the analysis of the airfoil under viscous flow conditions. It included the study of boundary layer behaviour in order to determine the extent of laminar and turbulent flow. Location of transition point and study of flow separation were also a

part of this step. A viscous flow computer code designed by Eppler was used to investigate the viscous behaviour of the airfoil.

To accomplish the two steps mentioned above, the airfoil was required to meet all the design requirements. This implied an iterative solution of the problem. Various parameters were changed gradually in order to reach a stage where all requirements were fulfilled.

The final step was to verify the results obtained from the first two steps. The viscous flow results obtained by using Eppler's computer code were compared with another viscous flow analysis scheme. A computer program designed by Shang, Hankey and Dowyer (Ref 2) was used in this step. A comparison of the results obtained from the two programs is presented in the report.

Development

In this report, the analysis of design parameters is given in Chapter II. Chapter III covers the design procedure and results followed by comparison of results in Chapter IV. Conclusions and recommendations are given in Chapter V. The historical survey of airfoil development and the theory used in this study are included in the appendices.

3

II. ANALYSIS OF DESIGN PARAMETERS

In the design process it is required first of all to decide upon the goals that have to be achieved. The goals for this study were mentioned in the introduction. They will be discussed in some detail here.

Mach Number Range. According to the specifications for this design, the airfoil should have a critical Mach number of 0.65. The significance of this limit can be understood by realizing that the critical Mach number will restrict the values of $\frac{V}{V_\infty}$ and C_p on the airfoil surface. Also to be understood is the fact that M = 0.65 falls in the category of high subsonic flow and thus the compressibility effects can not be neglected. Prandtl-Glauert relations are used to take care of these effects in calculation of $\frac{V}{V_\infty}$ and C_p. The calculations are presented in Appendix B, where it can be seen that for a critical Mach number of 0.65 the value of $\frac{V}{V_\infty}$ is limited to 1.4172 and the value of C_p is limited to -1.0085. These are important considerations for shaping the desired velocity profile. It should be noted that a lower critical Mach number would result in higher values of $\frac{V}{V_\infty}$ and lower values of C_p.

Reynolds Number Range. The design specifications lay down a Reynolds number range of 1.5 to 6.5 million for this airfoil. This is a very interesting condition because the two extremes of this range lie in two different design areas. The 1.5 million Reynolds number is generally considered to be a "low" number whereas 6.5 million is considered "high". At low Reynolds numbers, the laminar boundary layer is quite stable. But an adverse pressure gradient

exists on the aft part of the airfoil. This implies the existence
of a turbulent boundary layer in the aft region. Due to the stability
of the laminar boundary layer, it is difficult to promote and con-
trol transition at low Reynolds numbers.

In case of high Reynolds numbers, the flow is predominantly
turbulent over the airfoil because the laminar boundary layer is very
unstable; thus at high Reynolds numbers one has to consider the ad-
vantages of early transition and existence of fully developed
turbulent boundary layers while avoiding separation of flow.

In all cases the designer is concerned about the phenomenon
of boundary layer separation. Separation causes a great increase
in the pressure drag and a laminar separation also causes poor initial
conditions for the turbulent boundary layer. Thus the designer must
ensure that either there is no separation of flow or that the separa-
tion is restrictred to the area close to the trailing-edge at all the
flight Reynolds numbers.

Wide Drag Bucket. This design stresses that the width of the
"low drag bucket" should be as high as possible at all Reynolds numbers.
The physical significance of the drag bucket was explained in Appendix
A. During the design phase a wide drag bucket implies that the range
of angles of attack at which the flow remains laminar on the upper
and the lower surface be as large as possible. This requirement ties
in with another phenomenon, i.e., the thickness to chord ratio of the
airfoil. It is explained in Appendix A that the thicker airfoils have
a wider drag bucket. Thus the width of the drag bucket is restricted
by the t/c ratio. The designer has to try and get the maximum width
consistent with the t/c ratio.

Thickness to Chord Ratio. A t/c = 15% was specified for this airfoil design. This thickness ratio limits the width of the "low drag bucket" as explained in the previous section. A study of NACA laminar flow airfoils indicates that a drag bucket width of 2° is associated with a t/c of 15%. The designer has to try and increase the width beyond 2° in order to show an improved design.

High lift. It is desired that the design lift coefficient of the airfoil be as high as possible consistent with the other design restraints. Actually the application of this airfoil—as described in the introduction—is such that a high lift airfoil is not desired. The requirement is for an airfoil which should have the highest possible L/D ratio at cruise conditions. This also implies that cruise is the design condition. Thus the designer has to try and increase the c_ℓ and decrease the c_d as much as possible in order to meet this requirement.

Low Moment. Although the limits for the moment of the airfoil have not been spelled out in the introduction but it is imperative to have a low moment in order to avoid the requirements of a large tail structure. A large tail would result in unnecessary drag increase.

A low moment results from increasing the laminar length on the lower surface and decreasing the laminar length on the upper surface. But it has already been stated that the requirements of low drag imply a long laminar length on the upper surface. Thus the designer is again faced with conflicting requirements and he has to discover the optimum solution.

The moment requirement thus goes into the decision regarding the shape of the velocity profile, as do all the other design specifications.

Stall Characteristics. It is important to design the airfoil in such a manner that the possibility of stall within the operating angle of attack range is eliminated. Stall can occur due to flow separation over the whole airfoil as a result of a leading edge laminar separation bubble or due to the movement of the separation point to the leading edge. The latter condition is avoided through stabilizing the laminar part of the flow and by controlling the turbulent part in order to restrict separation to the region near the trailing-edge. For the leading edge laminar bubble, the remedy is to modify the velocity profile such that no suction peaks occur close to the leading edge within the desired angle of attack range.

It can be seen that the formulation of a basic velocity profile becomes quite involved due to all the design limiations. The designer has to develop a profile that will result in all the conditions being satisfied up to the desired level.

Basic Velocity Profile

The formulation of a velocity profile is the most important step in the design of the airfoil. This profile determines the shape of the airfoil and it also determines the behaviour of the boundary layer. The velocity profile can be divided into different segments. This disttribution is explained in Figure 1.

Nose Region. The nose region includes the area starting at the forward stagnation point and ending at about 8% of chord on the upper

7
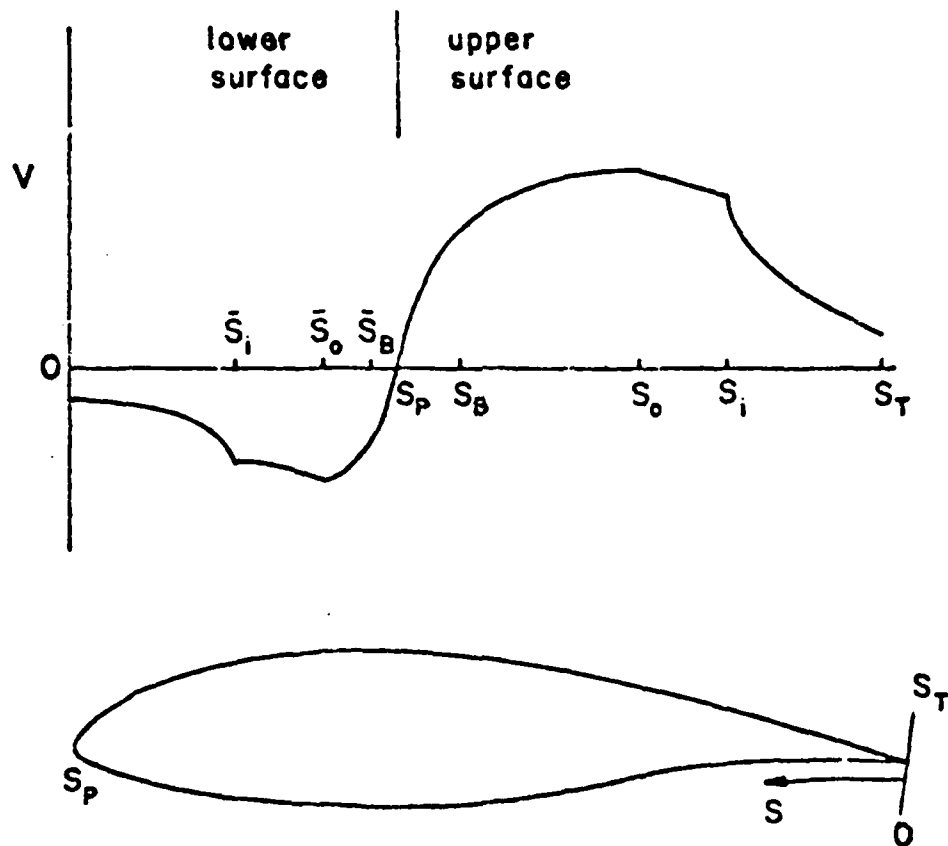
$S_P - S_B$ = Nose region

$S_B - S_O$ = Acceleration region

$S_O - S_T$ = Pressure recovery region

Figure   1   General Form of the Airfoil Velocity Distribution(Ref. 15)

surface. In this region the velocity rises very quickly from zero to the peak value at each angle of attack. The velocity distribution here should be such that no leading edge stall can take place within the operating range of angles of attack.

Acceleration Region. This region extends from the end of the nose region up to the beginning of the pressure recovery area. In this region it is desirable to have favourable or extremely low adverse pressure gradients to maintain laminar flow resulting in reduction of skin friction drag.

Pressure Recovery Region. This region represents the area where a strong adverse pressure gradient exists. It extends from the end of acceleration region up to the trailing-edge. This region is of great importance because the control of flow in this region is necessary in order to have good lift and drag characteristics. It is desirable to have the flow transition to turbulent conditions when entering this region. Different people have come up with various schemes to achieve this. They include the introduction of instability range as recommended by Wortmann (Ref 21) and the turbulent development region advocated by Miley (Ref 13). The shape of the pressure recovery plays an important part in determining the behaviour of the boundary layer. It has been found that a concave pressure recovery profile results in lower c_d values and delays separation of the turbulent boundary layer.

Lower Surface. The lower surface velocity distribution can have all the components mentioned above or it can be only one component where the flow is accelerating. It is desirable to have only accelerating flow on the lower surface in order to maintain laminar flow

at the desired angle of attack. It is also observed that a pressure recovery region on the lower surface causes an undesirable moment increase on the airfoil. But in some situations it is practical to have a laminar segment and then a pressure recovery region on the lower surface. This is done to avoid flow separation on the lower surface at high Reynolds numbers.

III. DESIGN PROCEDURE AND RESULTS

The design procedure followed during the study will be described in this chapter. The most important factor in this procedure is to understand the significance of each input parameter and to interpret correctly the output of the program. It is therefore in order to start by describing the input and output for the computer program used in the study.

Description of Input and Output Parameters

Input Parameters. The input for the design part consists of a set of α^* and ϕ values and the pressure recovery parameters for the upper and lower surface. Using the circle as the plane for input, the circle is divided into many segments. The angle for each segment is related to the chord length on the airfoil by the relation

$$\frac{x}{c} = \frac{1}{2} (1 + \cos\phi)$$

So at $\phi = 0°$, $\frac{x}{c} = 1.0$ and at $\phi = 180$, $\frac{x}{c} =$ zero. For each segment on the circle a value of α^* is specified. This value signifies the angle of attack at which the velocity will have a constant value over that segment. The arc limits—and all other data depending upon arc limits, i.e., ϕ_w, ϕ_s, etc.—are not specified in degrees, rather they are specified relative to the point numbers. The airfoil points computed are images of equidistant points on the ζ circle (see Figure 2). Any number of points on the circle can be specified as long as it is divisible by four. So

11
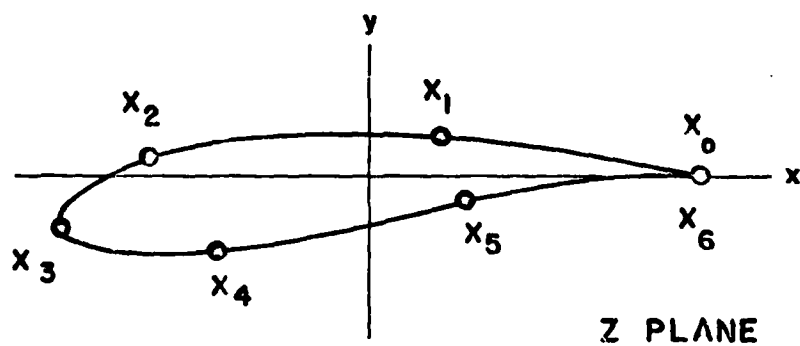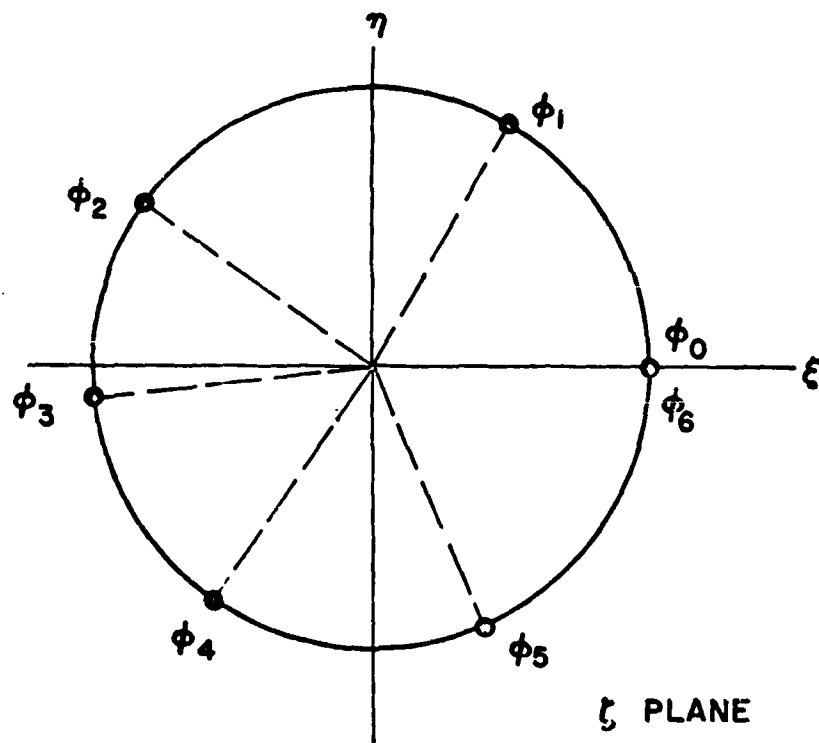
Figure 2   Segmenting the Interval $(0, 2\pi)$ for the Velocity Specifi-
cation $v^*(\phi)$ and the Angle of Attack Specification
$\alpha^*(\phi)$

$$\Delta\phi = 2\pi/n_c = 360°/n_c$$

where n_c is the number of points. $n_c = 60$ was used in this study be-
cause it gave an optimum number of points on the airfoil surface.
Now we define

$$\nu_i = \phi_i/\Delta\phi$$

which is used to input arc limits to the computer. For example
$\nu_i = 15$ means $\phi_i = 90°$ which on the airfoil would indicate the mid
chord of upper surface. A set of ν_i and α^* values are presented
in Table I along with the corresponding ϕ_i and x/c values (Ref 10).

Table I

Example Input Values

	ϕ_i	ν_i	α^*	x/c
i = 1	141.0°	23.5	8°	0.11
i = 2	165°	27.5	10°	0.017
i = 3	ϕ_1, ℓ_e	0	12°	0.0
i = 4	360°	60	2°	1.0

The value $\nu_{i,\ell e}$ is specified as zero but the exact location of
the front stagnation point is computed by the program. In the data
given above the circle, and therefore the airfoil, will have four
segments.

The second part of input consists of the pressure recovery
specification for both surfaces of the airfoil. Five values are
input for each surface. The first number indicates $\phi_s/\Delta\phi$, i.e.,

13

the number of circle segments which the program can vary to return a closed airfoil. The second number specifies the number of circle segments for the pressure recovery, i.e., $\phi_w/\Delta\phi$. The third number specifies the iteration mode for the pressure recovery. This number determines the interpretation of the fourth and the fifth number also. These iteration modes and the recovery parameters in each mode are given in Table II.

Table II

Pressure Recovery Modes

Mode	Parameter 1	Parameter 2
0	K	μ
1	ω'	ω
2	μ	ω

In addition to the ten numbers specified above, a design iteration mode, desired trailing-edge thickness, a tolerance in achieving the trailing-edge thickness, and the integration scheme have to be specified. The detailed description for these parameters can be found in Ref 7.

The above information is enough to solve the transcendental equation and find the airfoil shape. The next step is to specify the angles of attack at which the characteristics of the airfoil are desired. The program can at this stage be used to analyze the airfoil by the paneling method. The input for boundary layer analysis consists of a set of Reynolds numbers along with a transition mode. The transition modes are as follows:

14

$M_u = 0$ – Transition at laminar separation.

$M_u = 1$ or 2 – Fixed transition at given location on upper and lower surface.

$M_u = 3$ – Natural transition (see equation D-18)

$M_u > 3$ – Transition with roughness factor $r = M_u - 3$.

The boundary layer calculations are carried out for all values of angle of attack specified in the earlier input.

Program Output. The program output can be divided into two parts, i.e., numerical and graphical. The numerical output consists of the airfoil coordinates, $\frac{V}{V_\infty}$ or C_p values for specified angles of attack, a detailed printout of boundary layer development on the upper and lower surfaces for each set of Reynolds number and angle of attack, and a summary of C_l, C_m and C_d values at each angle of attack and Reynolds number.

The graphical output consists of plots of $\frac{V}{V_\infty}$ vs x/c, $R_{\delta 2}$ vs H_{32}, C_l vs C_d, C_l vs α, C_m vs α, $\frac{x}{c}$ turbulent vs x/c, and x/c separation vs x/c.

A reader interested in further details on program input and output is referred to Ref 7 which contains all the details with examples.

Design Process

The requirements for this design imply a design velocity distribution shown in Figure 3. It shows an accelerating flow on the whole lower surface. This is done to ensure laminar flow all along the lower surface. On the upper surface we have a nose region followed by a long region of acceleration. This implies laminar
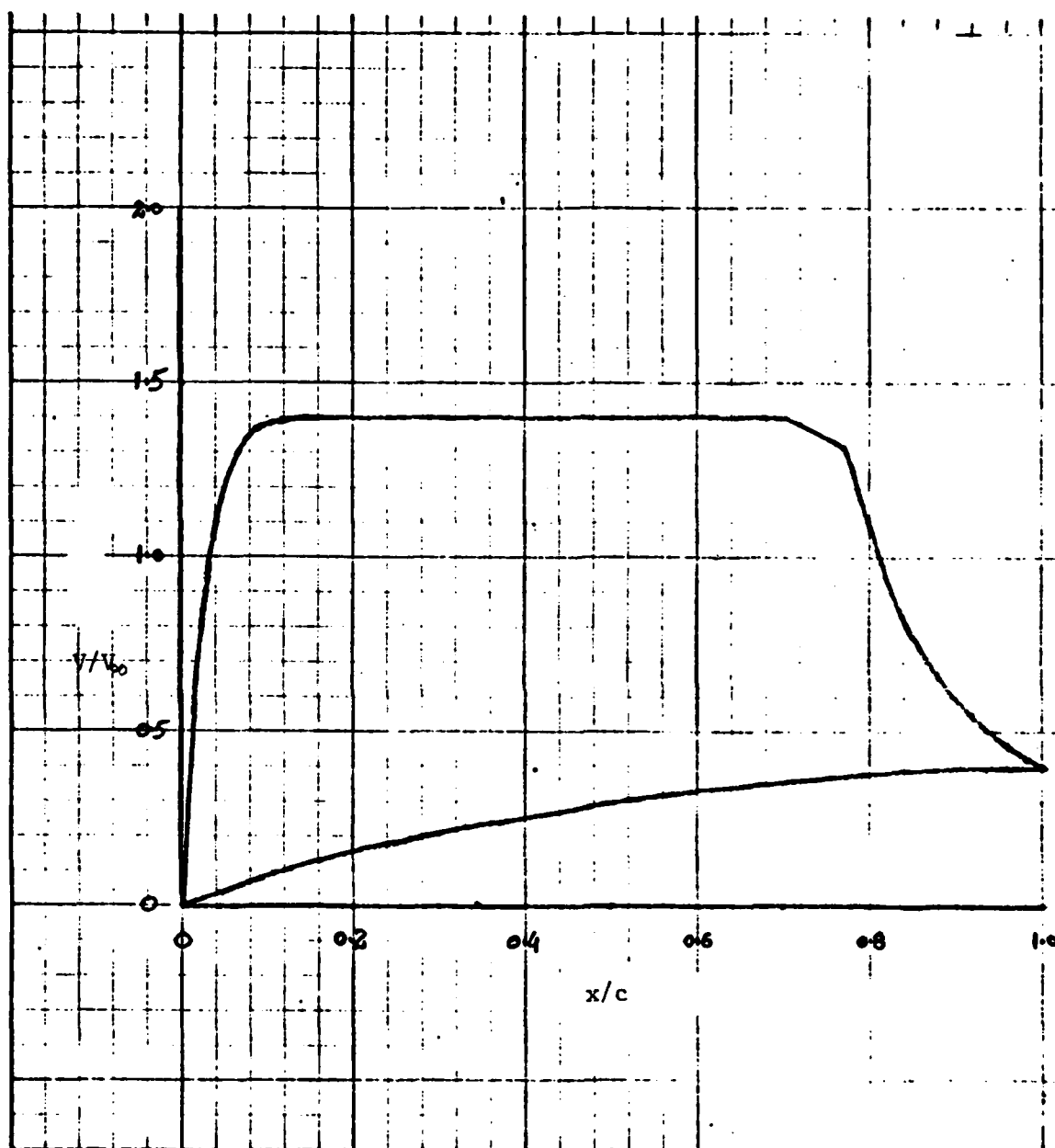
15

Figure 3.   Desired Velocity Distribution at αDesign

flow over about 80% of the upper surface at design conditions. Finally on the upper surface we have a pressure recovery region which has a concave shape in order to avoid separation of the turbulent boundary layer. The pressure recovery parameters are specified such that no laminar separation takes place prior to transition. The numbers initially chosen for this type of profile were:

$$\nu_1 = 8.5 \qquad \alpha_1^* = 5.0 \qquad \text{Recovery area (upper surface)}$$

$$\nu_2 = 27.5 \qquad \alpha_2^* = 5.0 \qquad \text{Acceleration range}$$

$$\nu_3 = 0 \qquad \alpha_3^* = 10.0 \qquad \text{Leading edge (nose region)}$$

$$\nu_4 = 60 \qquad \alpha_4^* = 1 \qquad \text{Lower surface}$$

With these, a closing contribution $\lambda^* = \overline{\lambda}^* = 4.0$ was used. On the upper surface recovery specification mode 2 was used and $\lambda = 8.5$ was used with $\mu = 10.0$ and $\omega = 6.5$. On the lower surface no recovery was specified so the $\overline{\lambda}$ value was put equal to zero. All other pressure recovery numbers were realistic on the lower surface also. Iteration mode six with $K_R = 4$ was used in order to achieve a realistic trailing-edge shape.

The above values resulted in an airfoil that was 17.38% thick and which had a positive $C_{m_0} = .0187$. In order to bring these values to the specified limits, iterations on α^* values had to be carried out. The final values in the design process are:

$$\nu_1 = 8.5 \qquad \alpha_1^* = 5.0$$

$$\nu_2 = 27.5 \qquad \alpha_2^* = 7.45$$

$$\nu_3 = 0 \qquad \alpha_3^* = 12.0$$

$$\nu_4 = 60 \qquad \alpha_4^* = 5.0$$

17

$$\mu = \overline{\mu} = 10.0 \qquad , \; \omega = \overline{\omega} = 6.5$$

$$\lambda = 8.5 \qquad \overline{\lambda} = 5.0$$

$$\lambda^* = \overline{\lambda}^* = 4.0$$

The result was an airfoil with $t/c = 15.01\%$ and $C_{m_0} = -.1282$. It can be noted that a small pressure recovery region had to be introduced on the lower surface.

The shape of the airfoil and the velocity distributions for some angles of attack are shown in Figure 4. The airfoil was given the number 2500.

In this phase, it was required to have another airfoil with the same t/c and C_{m_0} range, which could be a competitor when viscous flow analysis was carried out. For the second design it was decided to change the velocity distribution a little bit. A pressure recovery region was introduced on the lower surface and it extended from mid-chord to the trailing-edge. The upper surface profile was to be the same as in airfoil 2500. This was done in order to study the effects of a long pressure recovery region on the lower surface. Also it was intended to increase the camber of the airfoil so as to have higher C_l values.

In this case, again, a lot of iterations were carried out to reach the final result and the final values are:

Airfoil 2510 $\qquad t/c = 15.04\% \qquad\qquad C_{m_0} = -.1226$

$$\nu_1 = 8.5 \qquad \alpha_1^* = 5.0$$

$$\nu_2 = 27.5 \qquad \alpha_2^* = 5.0$$

$$\nu_3 = 0 \qquad \alpha_3^* = 10.8$$
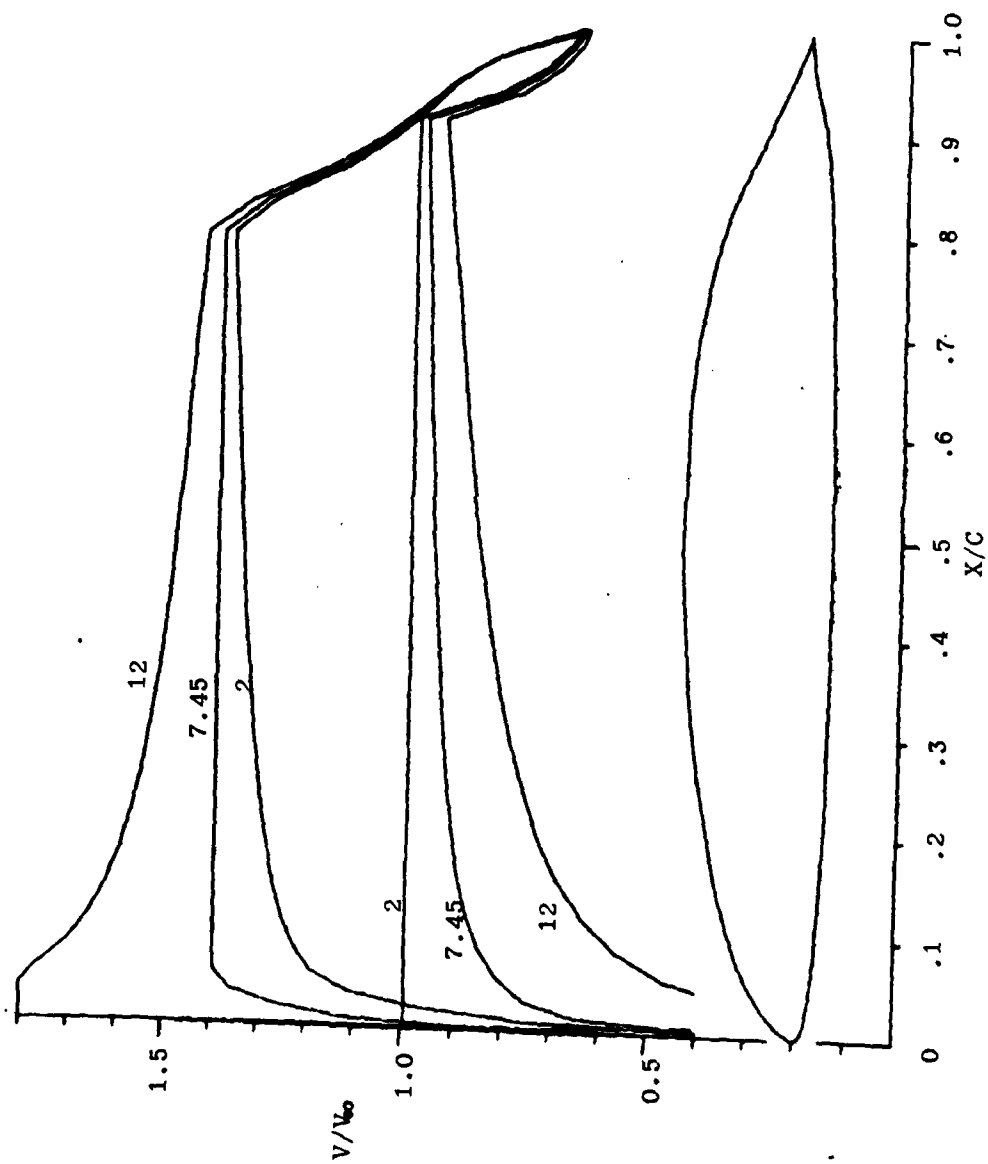
$$\nu_4 = 60 \qquad \alpha_4^* = 2.0$$

Figure 4. Velocity Profile;Airfoil 2500

upper surface: $\lambda = 8.5$, $\lambda^* = 4.0$, $\mu = 10.0$, $\omega = 6.5$ iteration mode = 6

lower surface: $\lambda = 14.5$, $\lambda^* = 4.0$, $\mu = 10.0$, $\omega = 6.5$ $K_R = 0$

The airfoil shape with the velocity profiles is shown in Figure 5.

Analysis of Airfoils. The analysis phase consisted of looing at the velocity and pressure coefficient values on the airfoils at different angles of attack to determine the range of angles of attack fit for cruise at M = 0.65. Next, the boundary layer behaviour was investigated, i.e., the extent of laminar and turbulent flow, separation length and the C_l, C_d and C_m values. All these values were checked for Reynolds number range of 1.5 to 6.5 million. The detailed results for each airfoil are given in Appendix E and Appendix F.

The section characteristics of airfoil 2500 are shown graphically in Figure 6 and Figure 7. Figure 8 and Figure 9 contain the characteristics of airfoil 2510. It can be seen from the figures mentioned above that airfoil 2500 has a narrower drag bucket width at all Reynolds numbers when compared to airfoil 2510. Airfoil 2500 has much longer separation lengths at various angles of attack when compared to airfoil 2510. The C_{m_0} value is also higher for airfoil 2500.

In view of the above it was decided to restrict further work to airfoil 2510 only. On this airfoil it was observed that at $R = 1.5 \times 10^6$ the airfoil had a "bubble analog" longer than .03 at several angles of attack. This condition signifies the presence of a laminar separation bubble at the transition location. In order

20
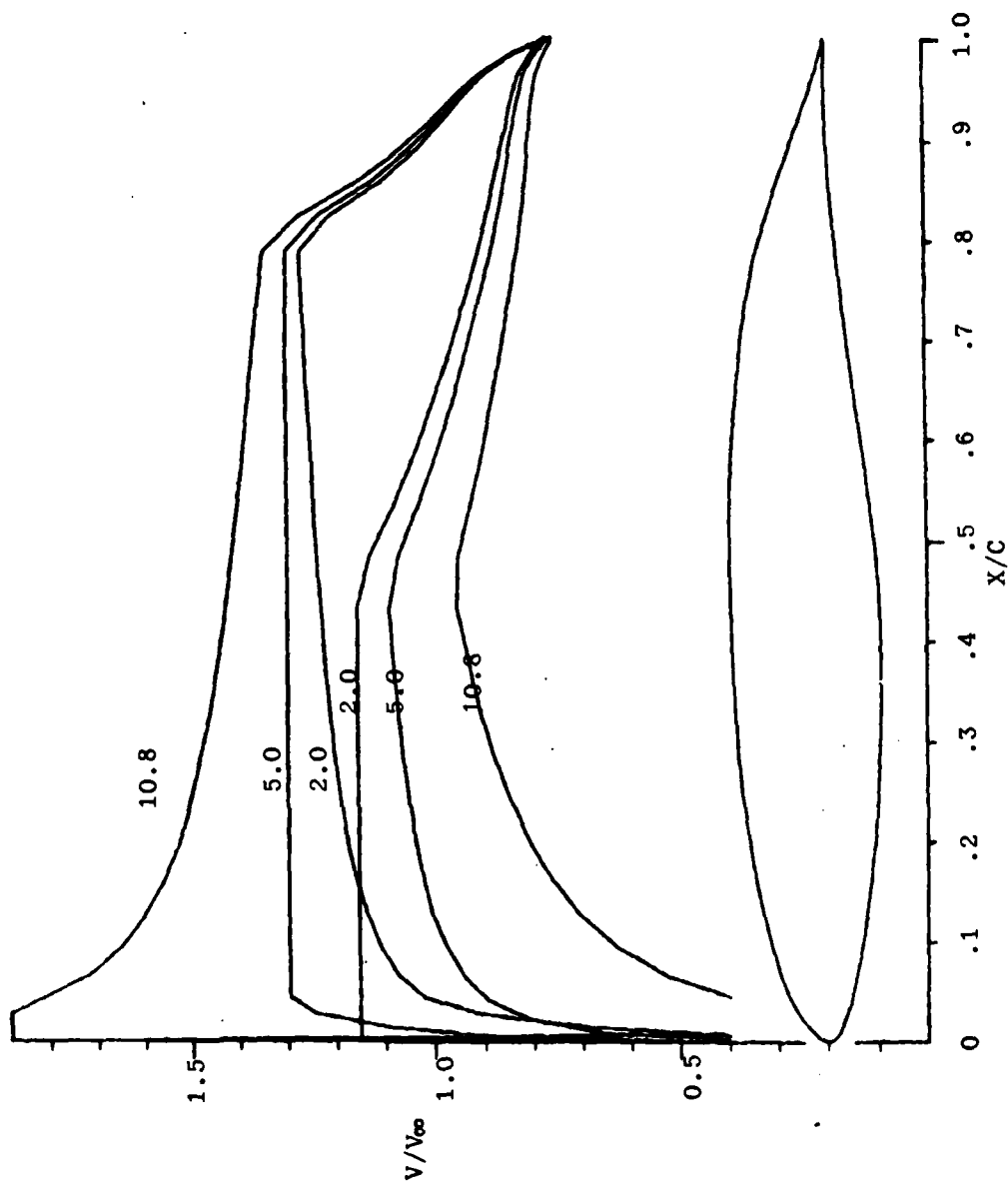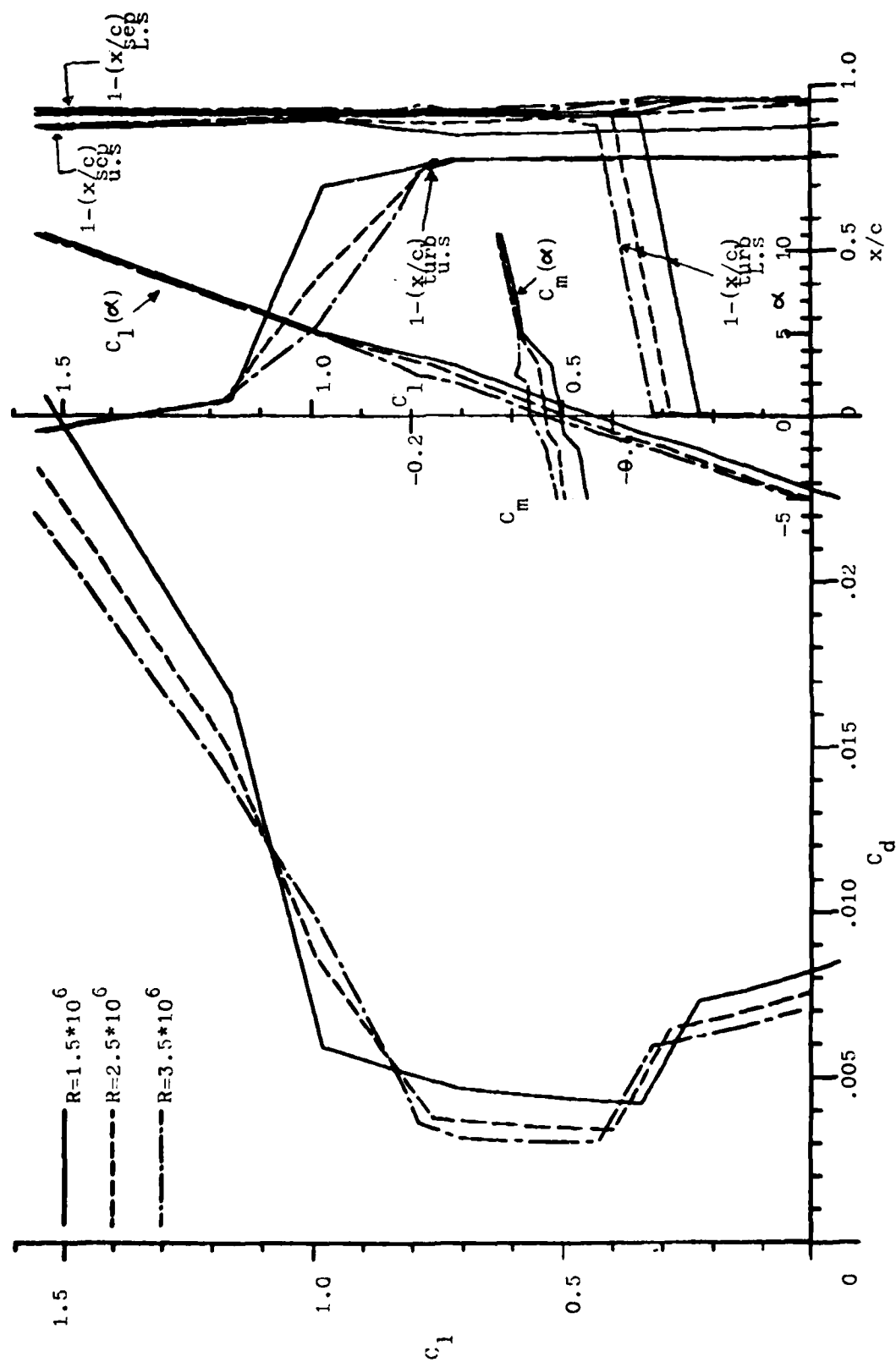
Figure 5. Airfoil 2510;velocity profile
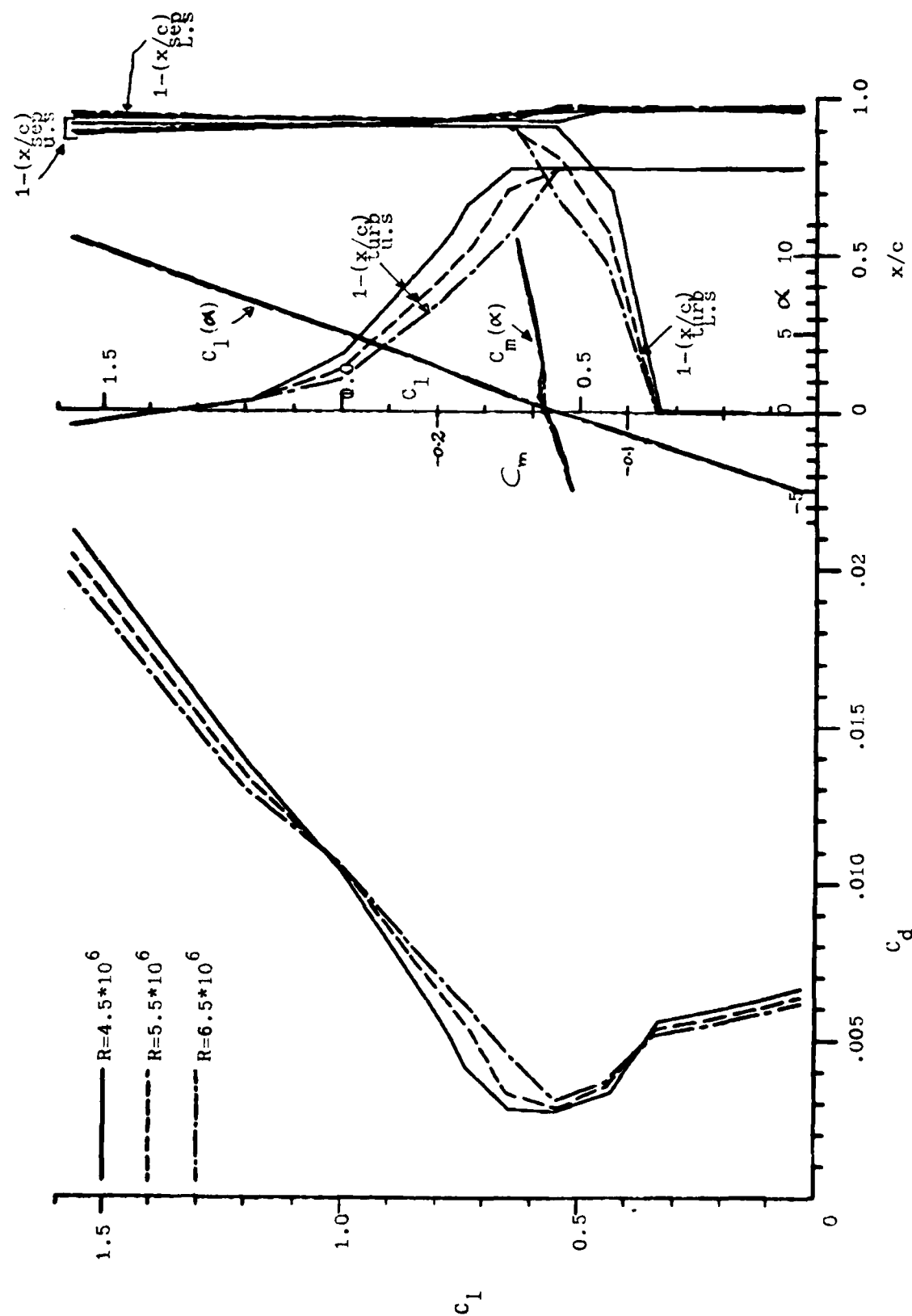
Figure 6. SECTION CHARACTRISTICS:AIRFOIL 2500

Figure 7.   SECTION CHARACTRISTICS:AIRFOIL 2500 (cont.d)
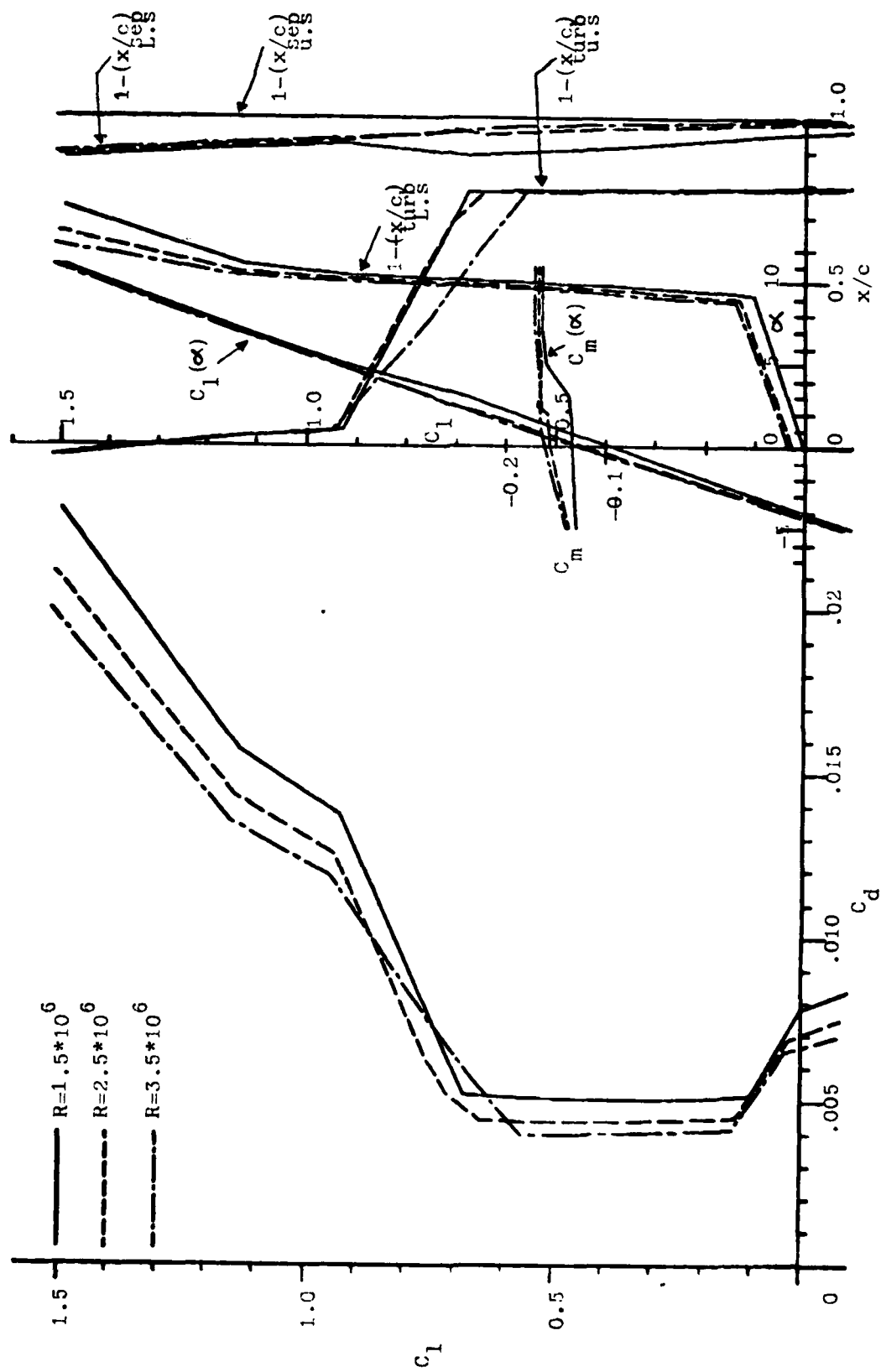
Figure 8. SECTION CHARACTRISTICS:AIRFOIL 2510
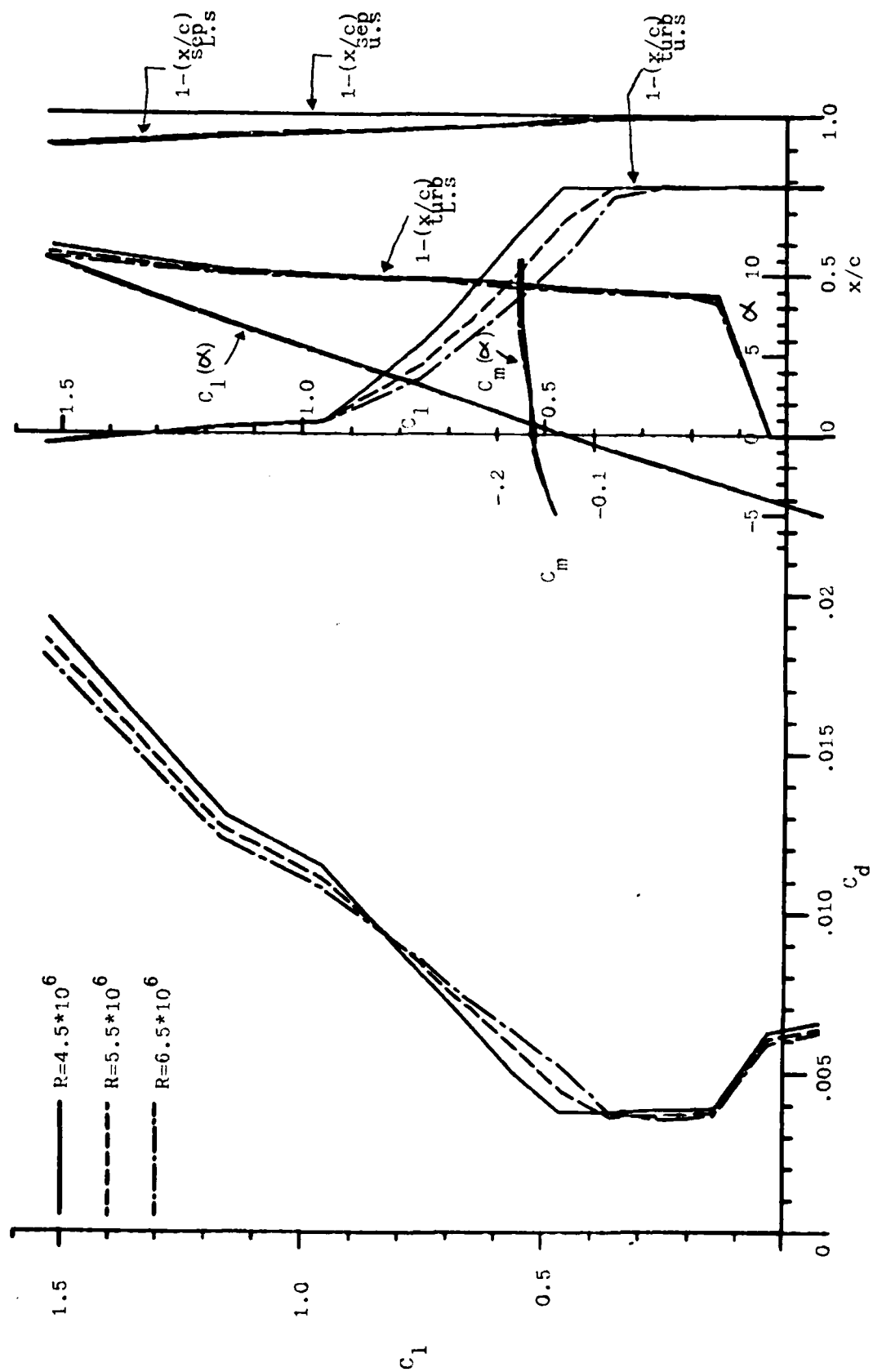
Figure 9. SECTION CHARACTRISTICS:AIRFOIL, 2510(contd)

to ensure "no laminar separation" the bubble analog has to be avoided.

This was achieved by reducing the pressure gradient at the transition location. The value of λ was increased to 9.5 and the resulting profile was analyzed. It was found that the problem of bubble analog was completely resolved. It was also found that the section characteristics of this new profile were satisfying all the design requirements. Thus it was decided to retain the new profile as the final airfoil. It was given the number 2700. The airfoil shape along with velocity profiles at selected angles of attack is shown in Figure 10. The section characteristics of airfoil 2700 are displayed in Figure 11 and Figure 12.

Results. A summary of results, obtained by analysis of airfoil 2700, is presented here. The detailed results are attached as Appendix G.

The airfoil has a thickness ratio of 15% which is the desired value. It has a C_{m_0} of -.1112 which is reasonably small and so it does not pose any problems with respect to the tail size.

The value of pressure coefficient remains greater than -1.008 at angles of attack ranging from -2.5° to +2.5°. Thus the airfoil can be used for cruising at $M = 0.65$ at any of the angles of attack within this range.

The drag bucket width is 5° at a Reynolds number of 1.5 million and reduces to 3° at a Reynolds number of 6.5 million. This is a substantial improvement upon the NACA 64 and 65 series laminar flow airfoils that have a bucket width of 2° associated with $t/x = 15\%$. It is also noted that the value of C_d at the drag bucket is 0.0052 for a Reynolds number of 1.5×10^6 and it reduces to a value of .0039
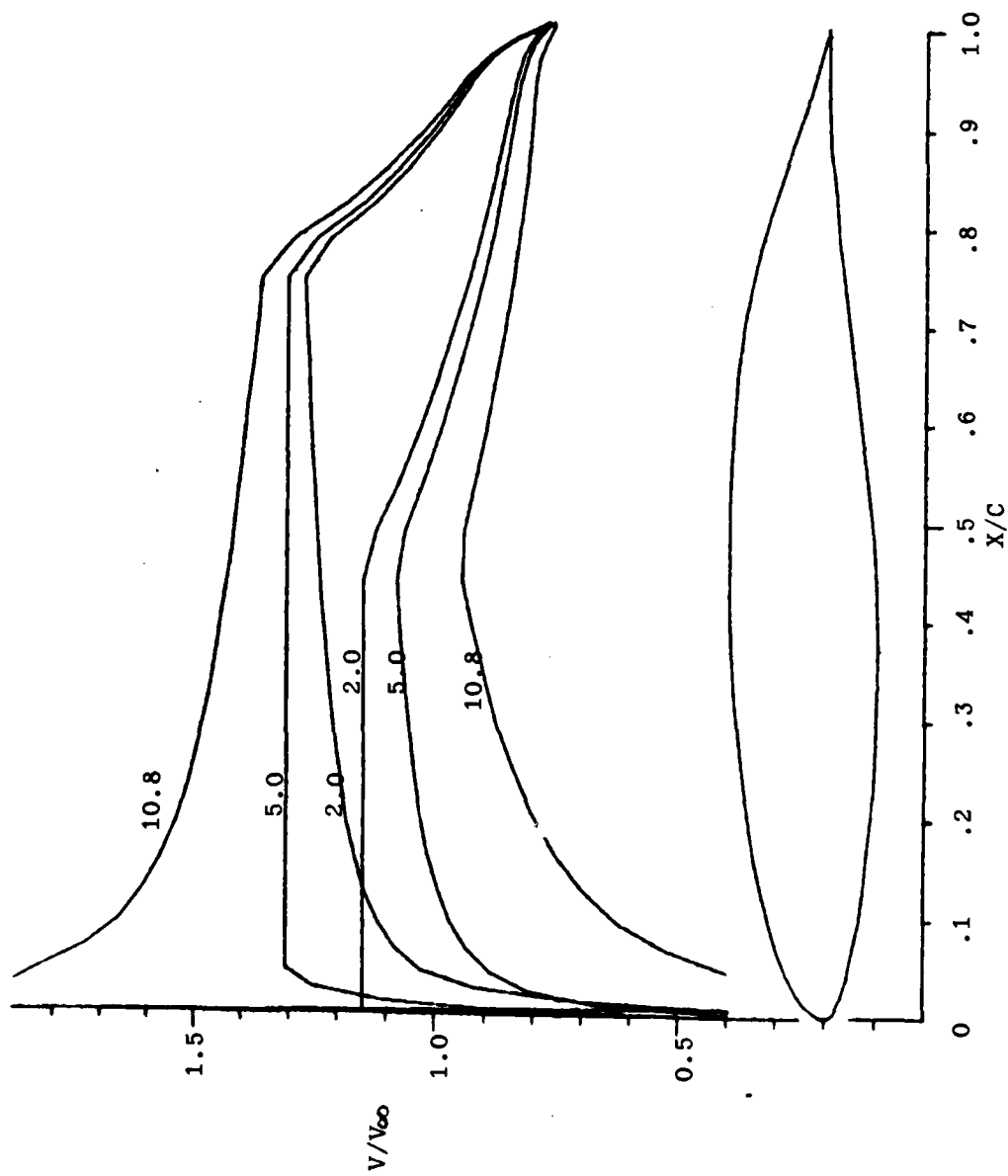
Figure10 . Velocity profile;Airfoil 2700
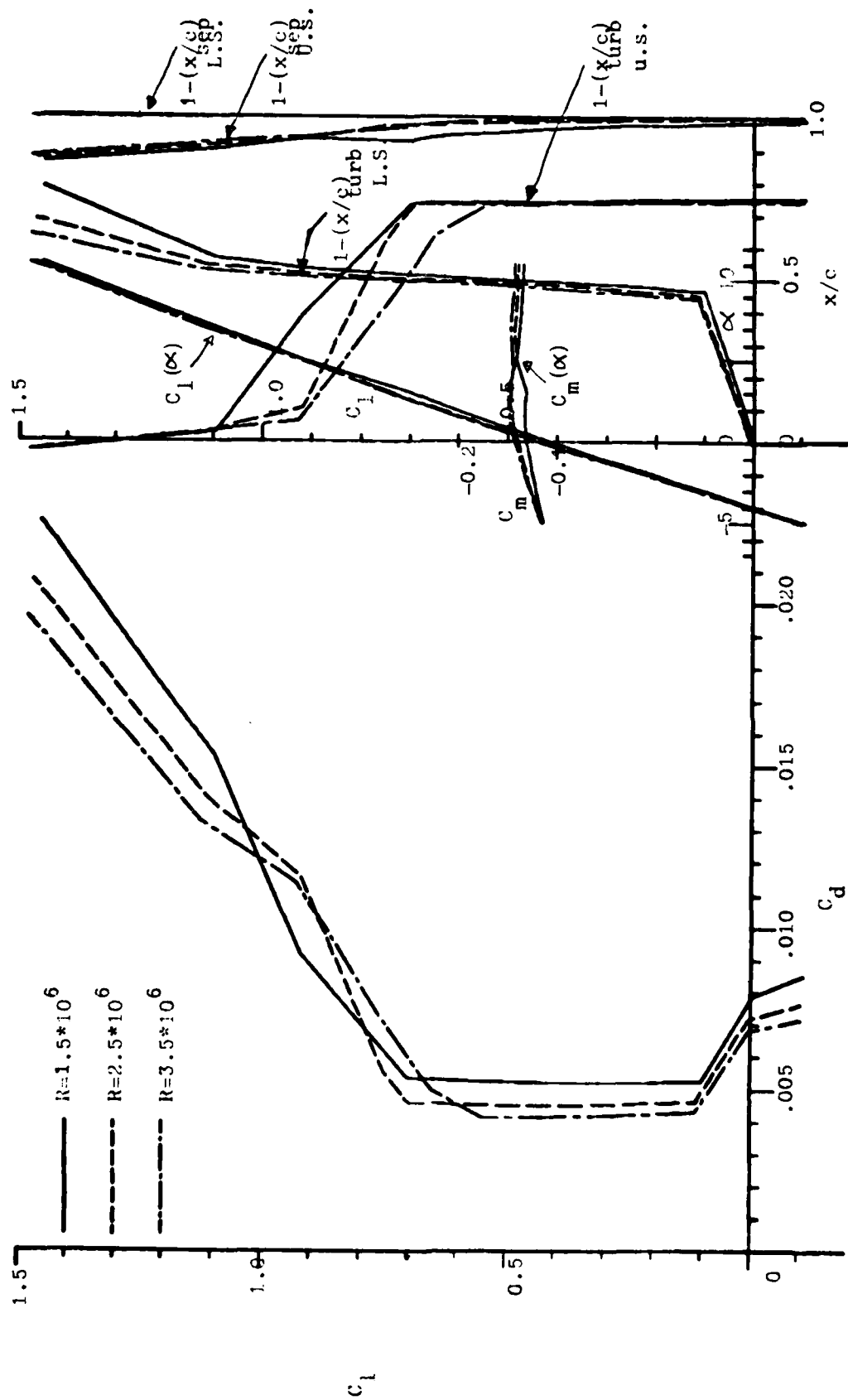
Figure 11 . SECTION CHARACTERISTICS:AIRFOIL 2700
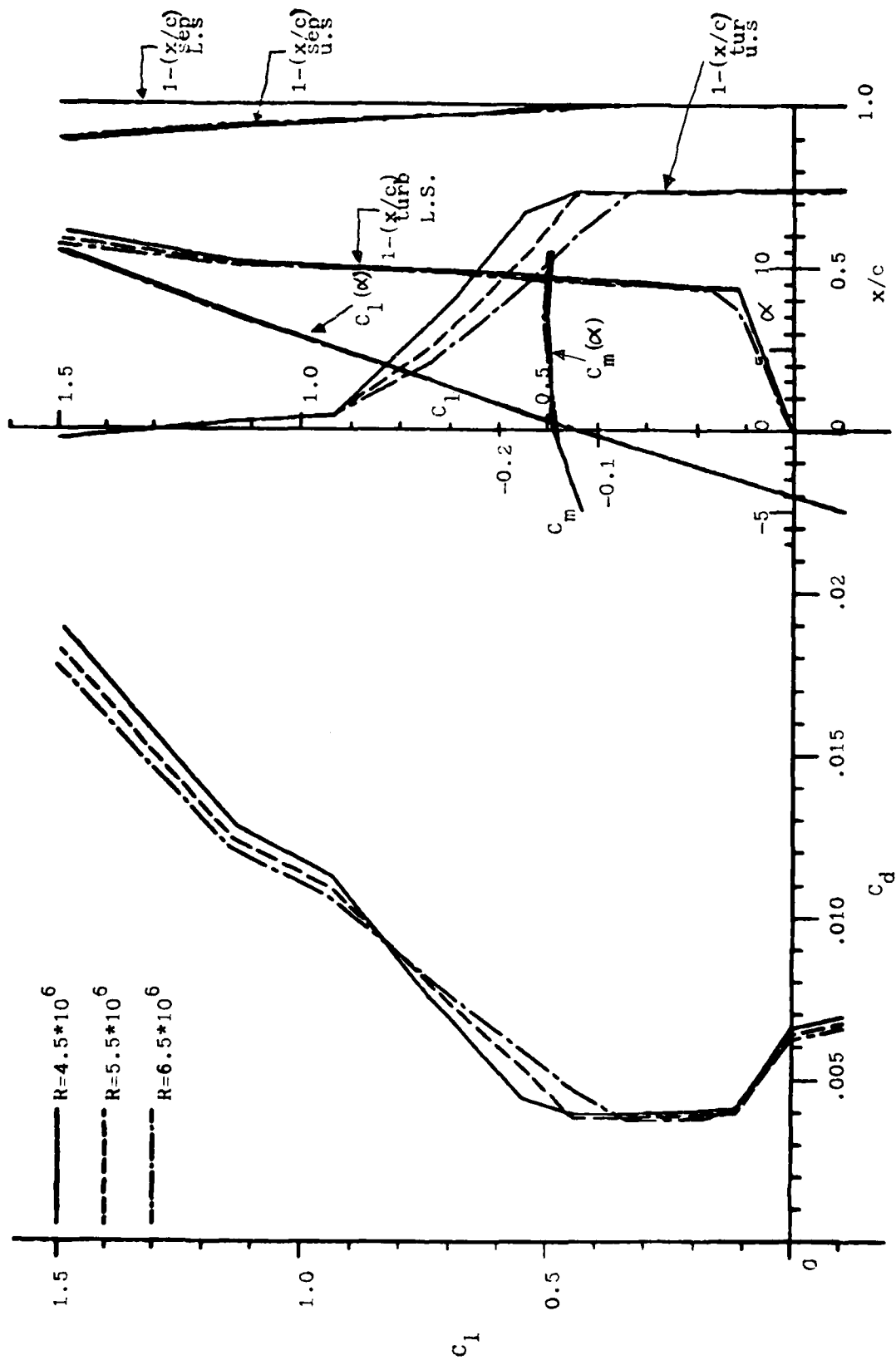
Figure 12. SECTION CHARACTRISTICS:AIRFOIL 2700(contd)

for $R_e = 6.5 \times 10^6$. These values—when compared to the NACA airfoils—are either equal or lower. Thus the objective of widening the drag bucket has effectively been met.

The airfoil has a laminar length of 0.75c on the upper surface and 0.5c on the lower surface. It has no laminar separation and turbulent separation is restricted to the last 5% of the chord on the upper surface within the operating range of this airfoil. On the lower surface no separation is indicated. These qualities result in very low drag values and good lift coefficient values.

Finally one has to consider the most significant factor, i.e., the L/D ratio. The behaviour of the L/D value at different angles of attack and Reynolds numbers is shown in Figures 13 - 18. The peak value in five cases is above 100. And the cruise condition L/D ($\alpha = 2°$) is above or very close to 100 in all cases. These are considered good L/D values for airfoils in this category.

Figure 10 shows the velocity profiles of airfoil 2700. Actually two sets of data are plotted in this diagram, one from the design mode and the other from the analysis mode where paneling techniques were used. The difference between the two curves can hardly be observed. This implies that the inverse method was very accurate in converting the velocity profile into an airfoil shape.
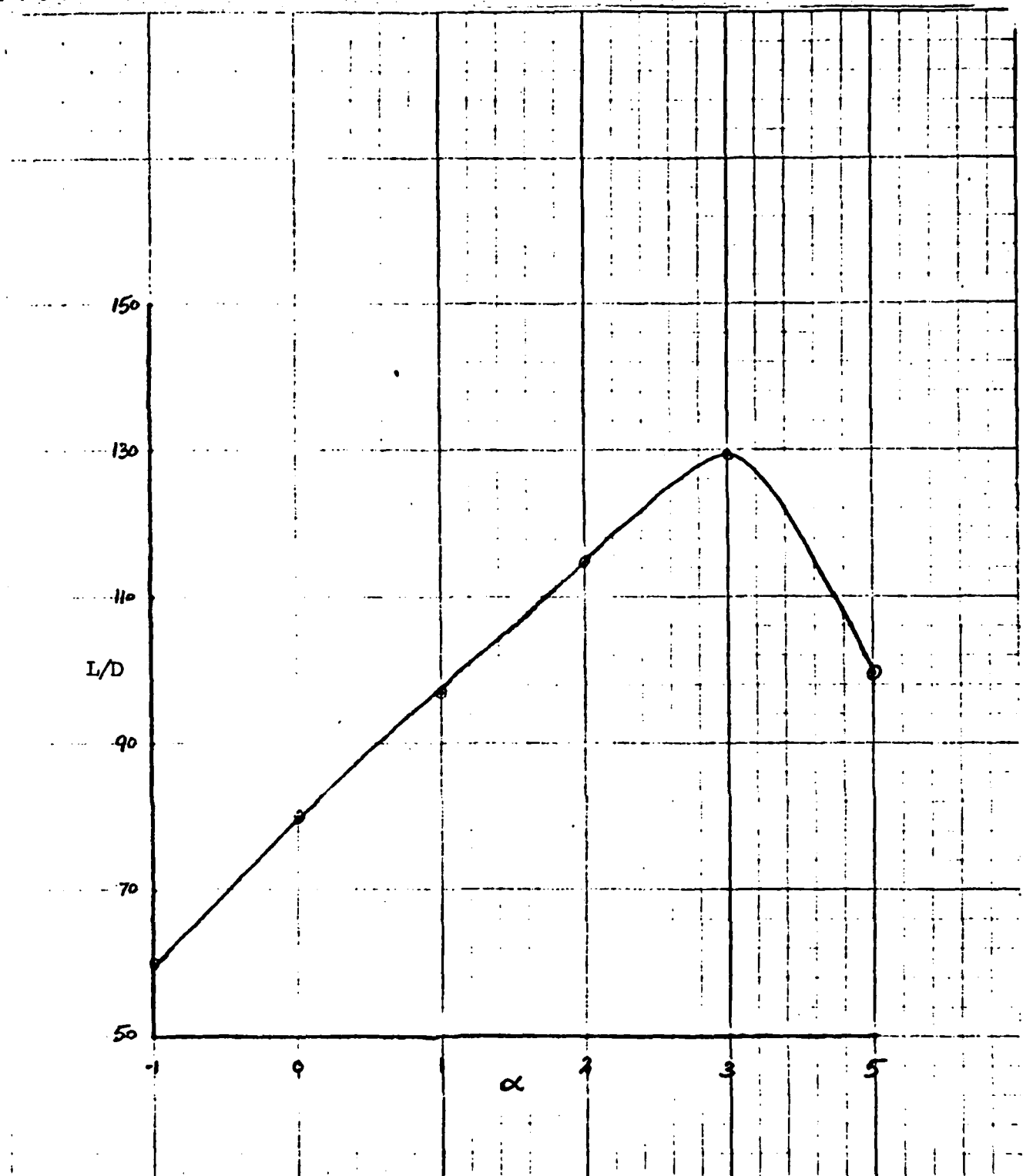
Figure 13. Airfoil 2700, L/D vs α: R=1.5x10^6
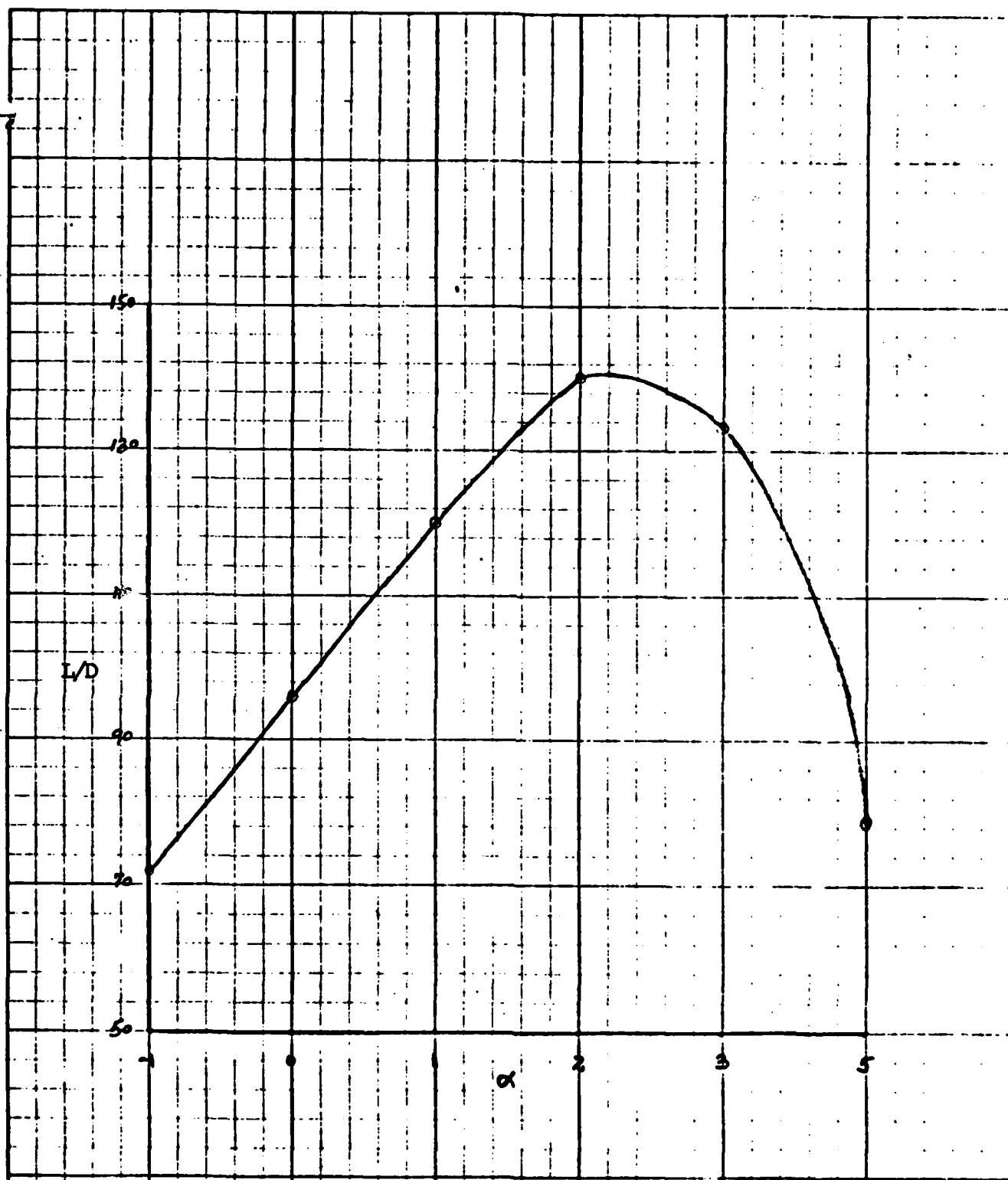
Figure]4.Airfoil 2700, **L/D** vs α: **R=2.5x10**[6]

L/D

16₀

13₀

11₀

9₀

7₀

5₀

-1 0 1 α 2 3 5
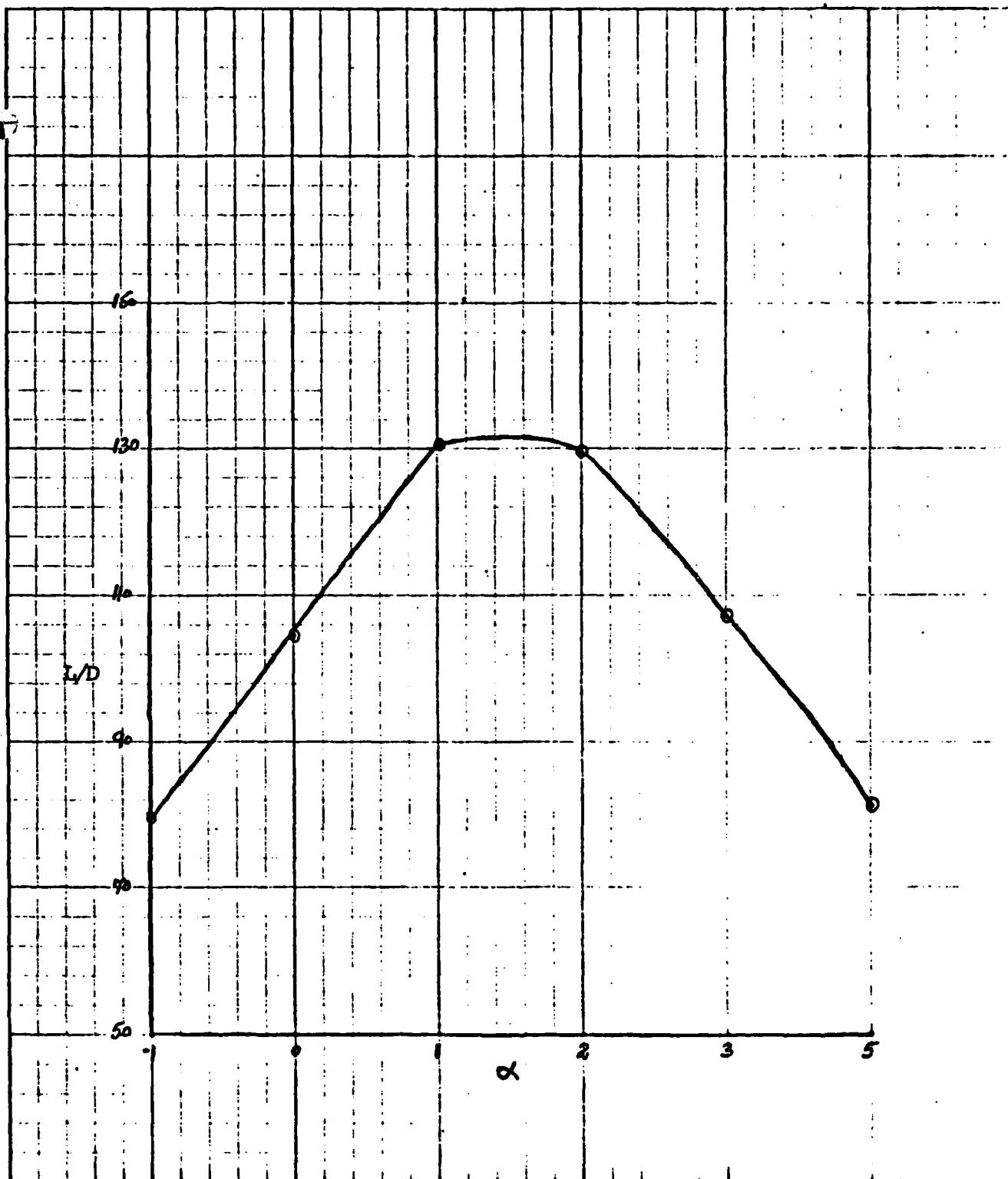
Figure 15. Airfoil 2700, L/D vs α: R=3.5x10⁶

15
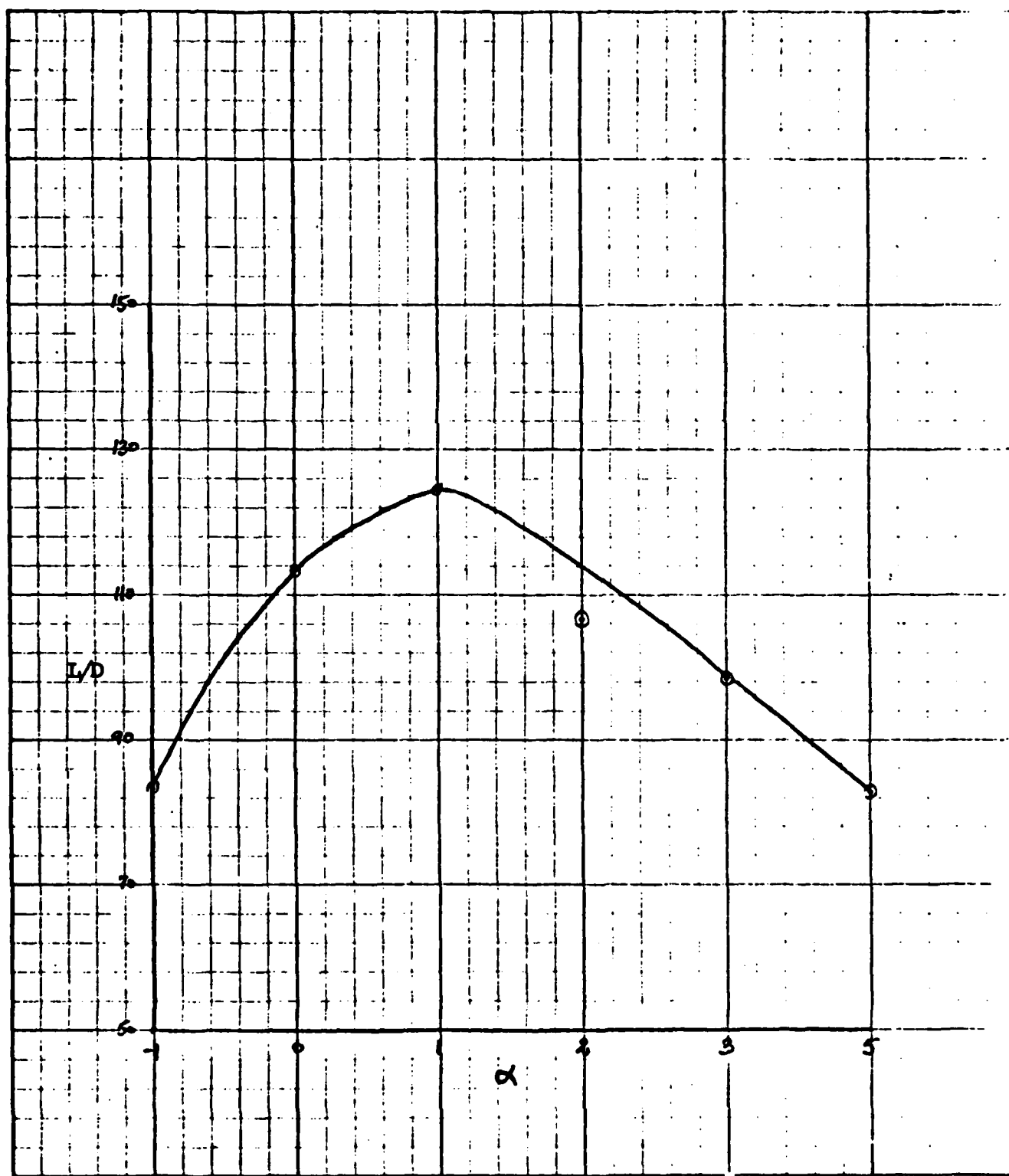
Figure 16. Airfoil 2700, **L/D** vs α: R=4.5x10^6
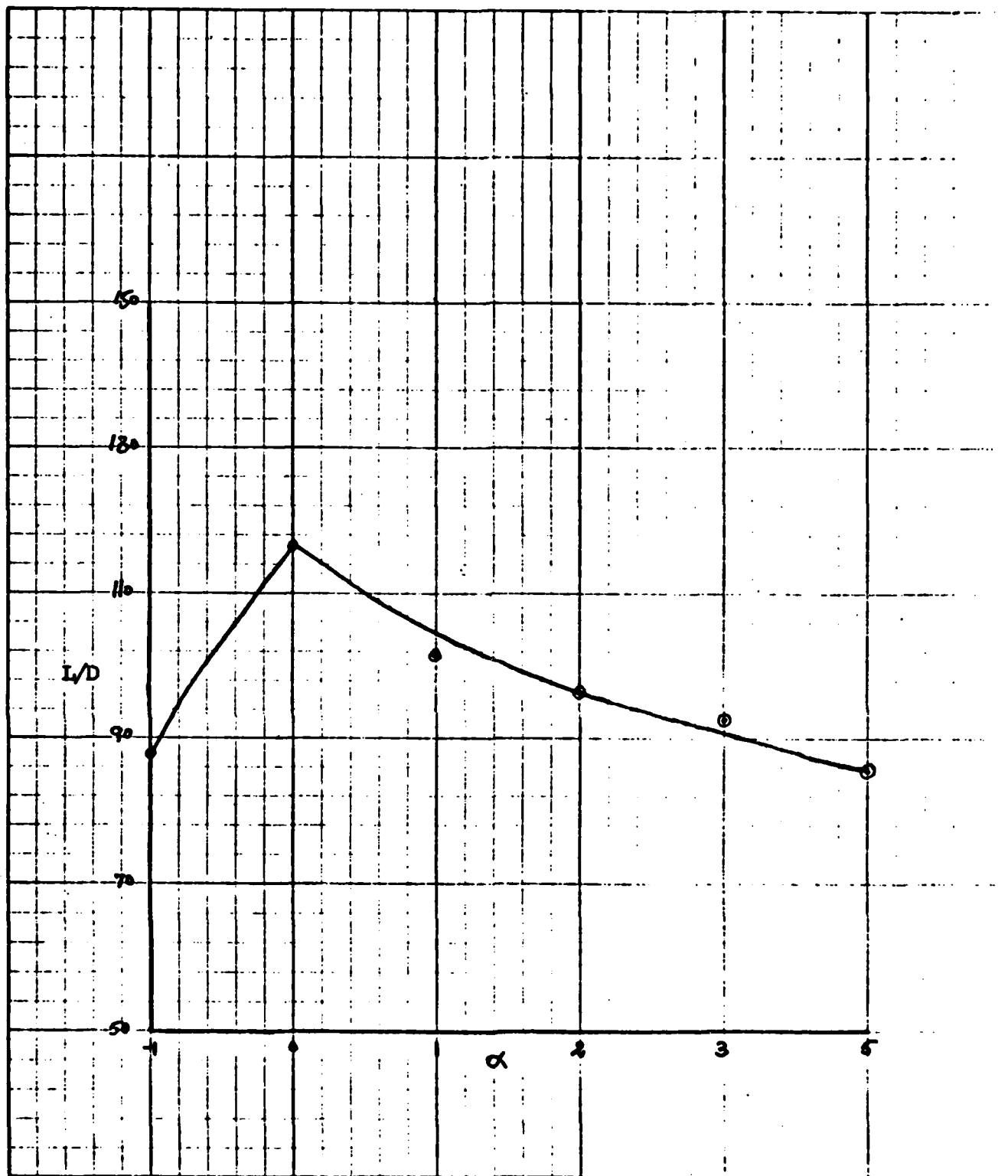
Figure 17. Airfoil 2700, L/D vs α: R=5.5x10^{6}
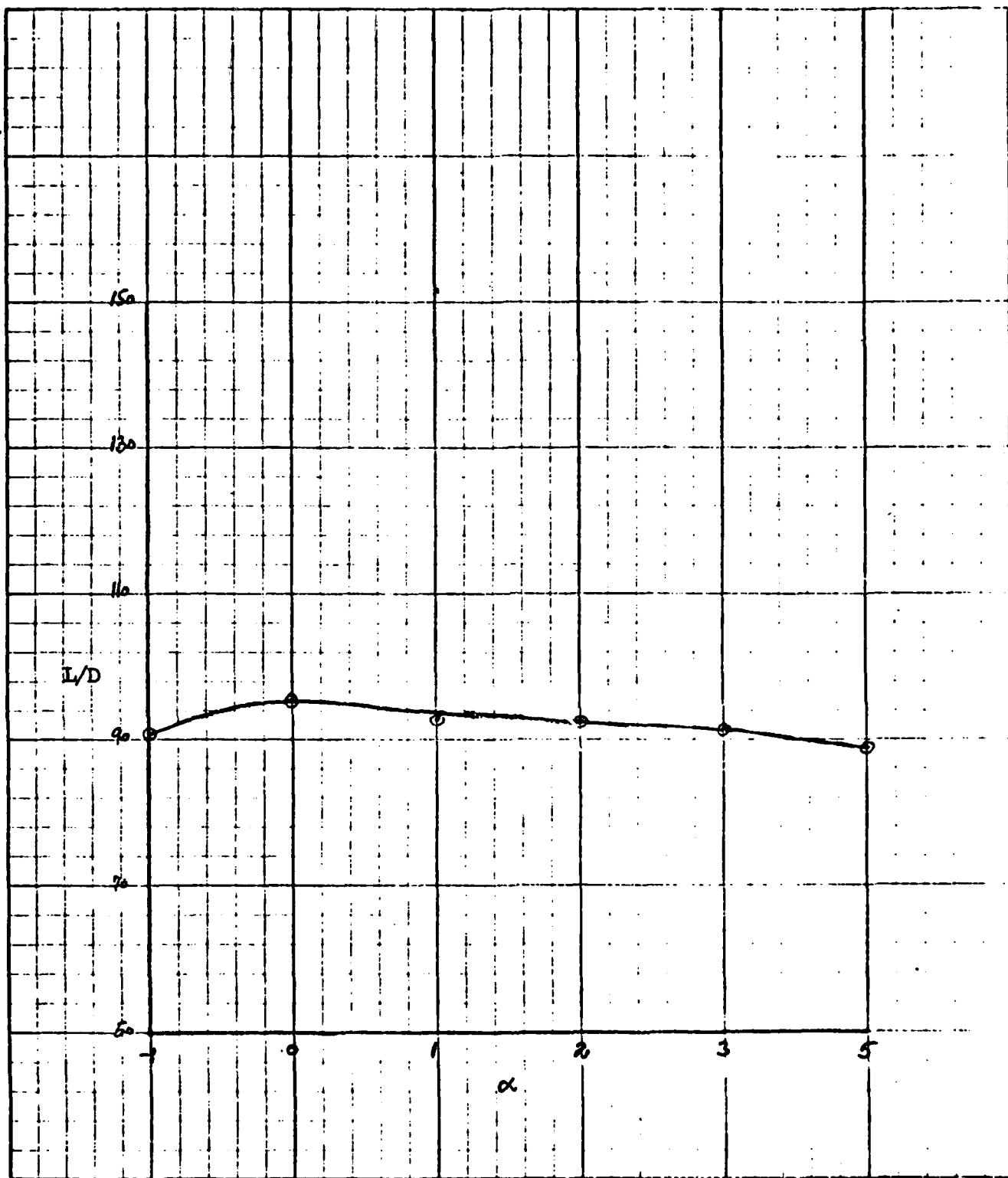
Figure 18. Airfoil 2700, L/D vs α: R=6.5x10^6

IV. COMPARISON OF RESULTS

After designing and analyzing the airfoil by using Eppler's computer code, it was decided to compare results by running the same airfoil through a different viscous flow analysis scheme. A computer program, written by Shang, Hankey and Dowyer (Ref 2,18) was available. The program was used for analysis of boundary layers, using the eddy viscosity model. A description of the principles used in this program is given in Appendix H.

The aim in using this eddy viscosity model was to verify that the extent of laminar and turbulent flow as indicated by Eppler's code agreed with results obtained from this model. This program was not used for the calculation of section characteristics like C_l, C_d, etc. The program input includes the airfoil coordinates, pressure coefficient at each airfoil coordinate, Reynolds number, altitude and temperature data, and some information about the desired output. The output includes the C_f, momentum thickness, displacement thickness, Reynolds numbers based on momentum and displacement thickness, etc. at each airfoil station. The velocity profile of the boundary layer can be obtained at any number of airfoil stations. Separation of flow is indicated by a rapidly decreasing friction coefficient. But at separation, the program stops further execution, so the analysis stops if separation is indicated anywhere on the airfoil. In this program the surface is approximated by a flat plate, so the upper and the lower surfaces have to be analyzed separately. It may be pointed out that values of C_d can be calculated by using the C_f values obtained from this program.

The analysis was carried out on airfoil 2700. The test conditions (input to the program) were a simulation of design operation, i.e., altitude of 60,000 feet and a free stream mach number of 0.65. The airfoil was numerically tested at various angle of attack and Reynolds number combinations.

The results indicated that flow separation was taking place at transition on both surfaces of the airfoil at all angles of attack and Reynolds numbers. On further analysis it was found that adverse pressure gradient—even of a low magnitude—caused the indication of separation. It was, however, confirmed that there was no tendency of leading edge stall within the operating range of angles of attack. It was also confirmed that the extent of laminar flow, on both surfaces of the airfoil, matched very closely with the results obtained from Eppler's program.

It was concluded that the eddy viscosity model was very sensitive to adverse pressure gradients. The results of this analysis reaffirmed the validity of Eppler's laminar flow analysis method. However, his criterion for prediction of flow separation and transition to turbulent flow could not be verified. The two numerical schemes are based on different principles. Eppler has incorporated a lot of empirical data in the solution of turbulent flow and transition problem (see Appendix D).

The conflict in results obtained from the two viscious flow codes emphasizes the importance of wind tunnel testing. The actual performance of the airfoil can only be judged in the wind tunnel or by carrying out flight tests. These tests can establish the validity of theoretical models.

A comparison of results obtained from the two computer codes is presented in Table 1. Only 2° angle of attack is considered in this example. Similar results were obtained for other angles of attack.

Table 1

Comparison of Results

$$\alpha_c = 2°$$

Reynolds Number	x/c Laminar (upper)		x/c Laminar (lower)	
	Eppler	Shang, et al	Eppler	Shang, et al
1.5×10^6	0.735	0.731	.505	0.495
2.5×10^6	0.730	0.728	.496	0.490
3.5×10^6	0.637	0.63	.490	.485
4.5×10^6	0.492	0.485	.486	0.480
5.5×10^6	0.396	0.38	0.482	0.475
6.5×10^6	0.328	0.32	0.474	0.470

V. CONCLUSIONS AND RECOMMENDATIONS

Conclusions

1. This study was started with the intent of designing an airfoil with the characteristics specified in the introduction. This goal was achieved and airfoil 2700 is the product of this study.

2. All design goals were met.

3. The validity of Eppler's design method was confirmed by the use of paneling techniques.

4. The validity of Eppler's laminar flow analysis method was confirmed by the results obtained from the eddy viscosity model designed by Shang et al.

5. The validity of Eppler's criterion for prediction of transition and for analysis of turbulent boundary layers could not be confirmed because conflicting results were obtained by using the computer code designed by Shang et al.

6. The flow anlaysis program designed by Shang et al was found to be very sensitive to adverse pressure gradients.

Recommendations

1. This study should be continued in order to refine the present airfoil. This can be achieved by using some of the recently developed theories to predict the behaviour of the boundary layer. By using these techniques the airfoil shape may be modified such that there is no separation at all and the extent of turbulent flow is optimum.

2. Another interesting topic would be to study the effect of boundary layer control on the characteristics of the airfoil.

The improvement in C_l and reduction in C_d may be substantial if techniques like suction and blowing are utilized.

3. It is also recommended that the theoretical results be verified by building the airfoil and then testing it in a wind tunnel. That would be a test of the accuracy of theoretical design methods.

Bibliography

1. Abbot, Ira H. and Von Doenhoff, Albert E. Theory of Wing Sections. New York: Dover Publications, Inc., 1959.

2. Beauregard, A. J., "An Analytical Study of the Effects of Mass Transfer on a Compressible, Turbulent Boundary Layer", Master's Thesis, Air Force Institute of Technology, 1976.

3. Eppler, R. Direct Calculation of Airfoils from Pressure Distribution. NASA TT F-15, 1974.

4. Eppler, R. Practical Calculation of Laminar and Turbulent Bled-off Boundary Layers. NASA TM-75328, 1978.

5. Eppler, R. and Somers, Dan M. Low Speed Airfoil Design and Analysis. NASA CP-2045, Part I, 73-99, 1979.

6. Eppler, R. "Turbulent Airfoils for General Aviation", Journal of Aircraft, Vol. 15(2): 93-98, February 1978.

7. Eppler, R. and Somers, Dan M. A Computer Program for the Design and Analysis of Low Speed Airfoils. NASA TM-80210, 1980.

8. Eppler, R. Laminar Airfoils for Reynolds Number Greater than $4x10^6$. NTIS N69-28178. 1969.

9. Eppler, R. Results of the Combined Application of Boundary Layer and Profile Theory. NASA TT F-15416, 1974.

10. Gallaway, Charles R. Interactive Computer Inverse Airfoil Design Procedure. AFFDL-TM-77-14-FXM, 1977.

11. Gallaway, Charles R. Application of Advanced Airfoils to High Altitude Long Endurance Remotely Piloted Vehicles. AFFDL-TM-77-10-FXM, 1976.

12. Kuethe, Arnold M. and C how, Chuen-Yen. Foundation of Aerodynamics. New York: John Wiley and Sons, 1976.

13. Miley, S. J. "An Analysis of the Design of Airfoil Sections for Low Reynolds Numbers", Doctoral Dissertation: Mississippi State University, 1972.

14. McMasters, J. H. and Hendersen, M. L. "Low-speed Single-element Airfoil Synthesis", Technical Soaring, Vol VI(2): 1-21.

15. Narramore, J. C., Olander, R. D., and Stearman, R. D., The Development of a Computer Aided Airfoil Design Procedure including Preliminary Wind Tunnel Experiments on a Low Reynolds Number, High Lift Section. AF-AFOSR 71-1998, 1976.

16. Schlichting, H. Boundary Layer Theory, New York: McGraw Hill Book Company, 1979.

17. Schlichting, H. and Truckenbrodt, E. Aerodynamics of the Airplane. New York: McGraw Hill Book Company, 1979.

18. Shang, J. S., Hankey, W. L., and Dowyer, D. L. Numerical Analysis of Eddy Viscosity Models in Supersonic Turbulent Boundary Layers. AFSC ARL 74-004, 1974.

19. Stratford, B. S. "The Prediction of Separation of Turbulent Boundary Layer", Journal of Fluid Mechanics, Vol 5: 1-16, 1959.

20. Wortmann, F. X., "A Critical Review of Physical Aspects of Airfoil Design at Low Mach Numbers", MIT Symposium 1972, Technology and Science of Motorless Flight, Cambridge, Mass.

21. Wortmann, F. X., "Airfoils with High Lift to Drag Ratio at a Reynolds Number of About One Million."

Appendix A

HISTORICAL DEVELOPMENT

Historical Review

Airfoil design started when man--in his desire to fly--copied the wings of different birds. Until early 20th Century, airfoil "design" was a largely empirical process drawing inspiration from birds. In 1915 the NACA was formed and it started an experimental research program. A huge mass of data was accumulated by this program. The procedure was to develop families of wing sections by a systematic experimental approach. During the experiments a basic section was chosen to start with and tests were conducted by varying the different section parameters. Ultimately the desired shape was obtained after many experiments. The results of all experiments were preserved and were published as airfoil section catalogs to aid designers. Such work was also carried out at Göttingen in Germany. During this period the theoretical base was limited to potential flow theory.

By the mid 1930s the influence of viscous scale effects had been acknowledged, and boundary layer theory had been developed. The boundary layer concepts were qualitatively incorporated in the design of airfoils which resulted in the famous NACA 6-series "laminar flow" airfoils. These airfoils were used extensively by designers for the next twenty years. Some designers made modifications to these designs in order to get desired results, but the basic material remained unchanged.

The big change came with the introduction of digital computers in the late 1950s. The equations of potential flow and viscous flow

45

theory were very well understood at that time but they could not be applied fully in design because of the labour involved in computation. It was difficult to solve the system of equations resulting from the application of basic equations even in the problem of simple airfoils in a real fluid. Thus, until that time, theory was only used as a guide to the experimental research work. In the wind tunnels it was easy to see "what" happened but there were hardly any clues to "why" it happened. Thus it was necessary to go beyond the 'design by testing' phase and to come up with practical, quantitative solutions to the equations of viscous flow.

Computers made it possible to solve the complex systems of equations in reasonable amounts of time. The computer based methods were successfully applied by Wortmann (Ref 20) and the results were cataloged as airfoils of the FX-series. Many others have since used the computer not only to design airfoils but to analyze and test them under real flow conditions. Computers led to the advent of what we call "computational aerodynamics" today. A survey of the progress of airfoil design is shown in Figure 19. (Ref 14).

Laminar Flow Airfoils

The experimental work showed that a laminar boundary layer could be maintained on an airfoil if the wing surface was smooth and a slightly favourable pressure gradient was maintained. This was the theory underlying the development of laminar flow airfoils. The criterion used for their design was to maintain laminar flow up to a certain chord length at a certain angle of attack. After

1000 - 1920

EMPIRICAL

Potential flow theory
(Joukowski airfoil)

1920 - 1940

GOTTIGEN
NACA - 4 DIGIT

NACA
5-DIGIT

1940 - 1950

NACA
6-SERIES

Moderate to high
camber and thick-
ness. General
aviation, saliplanes

THIN, LOW CAMBER

JET TRANSPORT

low speed

high speed (M<1)

1960 - Present day

WORTMANN

EPPLER

NASA GA( )

LIEBECK

HENDERSON, etc.

Super critical and
advanced technology
transonic airfoils

PEARCEY, GARABE-
DIAN, KORN,
WHITCOMB

Figure 19.   Single Element Airfoil Evolution (Ref. 4)

that point the pressure was allowed to increase linearly back to its trailing edge value. These airfoils attained 30 to 50 percent smaller minimum profile drag than older airfoils with the same thickness.

A study of laminar flow airfoils indicates that at the design angle of attack, favorable pressure gradient maintains laminar flow up to the position of peak suction which results in the production of minimum frictional drag. This is shown in the case of 3 NACA air-foils in Figure 20 (Ref 15). The logical conclusion of this discussion is that the position of peak suction should be moved as far back as possible so as to have the minimum possible drag. But this is not true, because moving the peak suction back results in a steeper pres-sure recovery near the trailing edge which results in increased pres-sure drag due to thicker turbulent boundary layer. It may even cause separation. Thus we conclude that, with respect to drag, there is an optimum aft limit for peak suction in case of every airfoil.

Another factor to be considered is off-design operation. Referr-ing to Figure 20, it can be observed that at an angle of attack of 1.3°, the flow characteristics have changed. The peak suction point moves forward suddenly. This can result in an adverse pressure gradient causing instability of the laminar flow which ultimately leads to turbulence and greatly increased frictional drag. If the behaviour of laminar flow airfoils is studied over a range of angles of attack, the well known "bucket" effect becomes immediately obvious. There is a range of angles of attack at which the drag has a minimum value; above and below that range, there is a sudden increase in drag. If the values of C_l and C_d for all angles
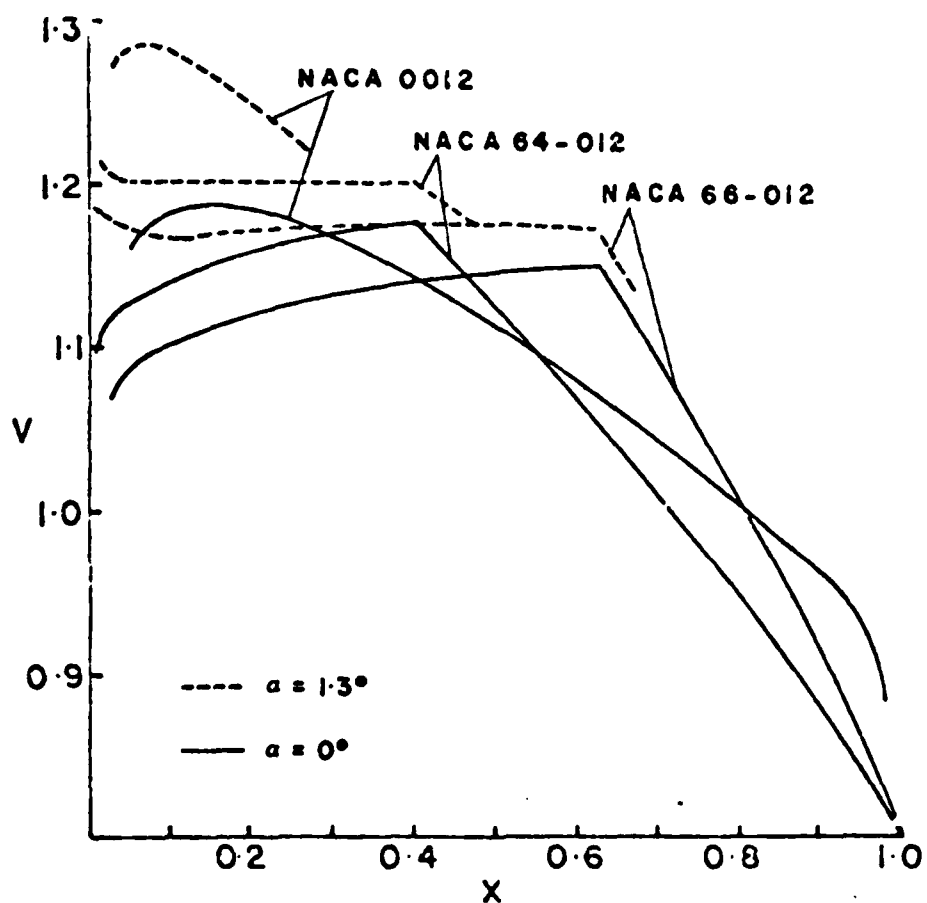
Figure 20. Velocity Distributions of three 12 percent thick NACA Airfoils at Two Angles of Attack (Ref. 15)

are plotted, the curves depict the "drag bucket". This is seen in Figure 21 (Ref 15) where such curves (also called drag polars) for four laminar flow airfoils are drawn. The drag bucket is the area where C_d has the minimum value. This phenomenon is absent in case of older airfoils because on those airfoils the transition position changes gradually over the angle of attack range.

The drag bucket concept is useful to define a range of angles of attack within which the airfoil can operate most efficiently. But even within this range the point of maximum efficiency can be found; i.e., the angle of attack at which the C_l/C_d ratio is a maximum. The width of the "drag bucket" is closely connected to minimum drag and thickness of the section in case of laminar flow airfoils. It can be seen in Figure 21 that the thicker sections have a wider drag bucket but the minimum drag value is lower for the narrow drag buckets. By going over such results for a large number of airfoils the relation between the drag bucket width and the thickness becomes very clear. The width of the drag bucket is normally indicated by the range of angle of attack over which the minimum drag is maintained. For example, in 65_2-415 airfoil, the subscript '2' indicates that the difference between the two angles of attack-- at which the drag starts to increase from its minimum value--is 2 degrees. A study of such numbers shows that in NACA airfoils a bucket width of 2° is associated with a thickness ratio of 15%. Thus an improvement can only be claimed if this interdependence is changed such that a wider low drag range is achieved with the same thickness and minimum drag value.
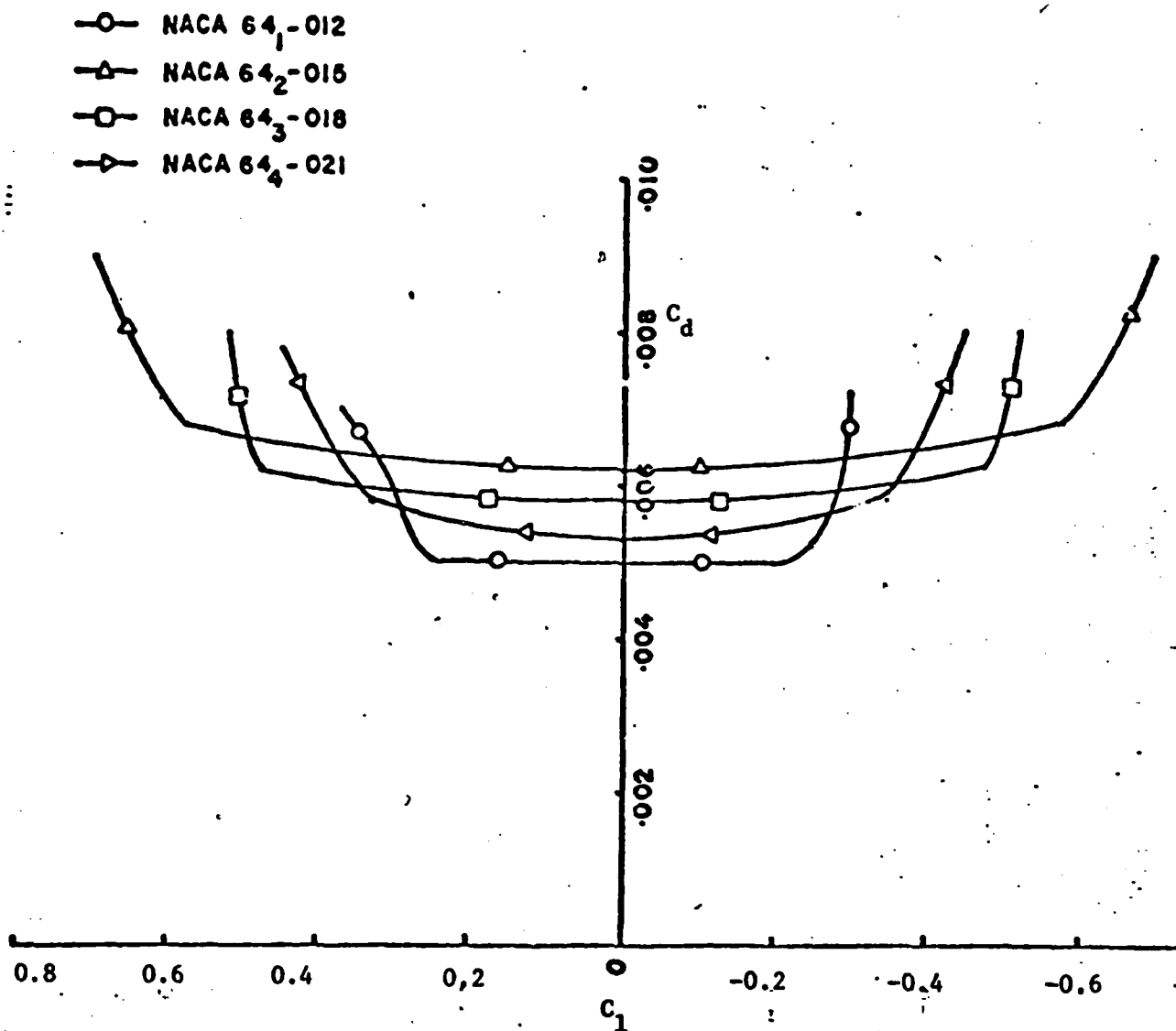
Figure 21.　Drag Polars of four NACA Laminar Airfoils (Ref. 15)

Further Developments

The study of laminar flow airfoils was very useful because it led to the fact that a low drag airfoil is designed from a specified velocity distribution. The velocity distribution is used to control the boundary layer. It showed the importance of the velocity distribution, i.e., the lift, moment, and the development of the boundary layer (drag) are direct results of the velocity distribution. Also the velocity distribution defines the profile of the airfoil.

Analytical techniques have been developed such that boundary layer theory can be applied to the flow about an airfoil in two ways. First the boundary layer development can be determined for a given potential flow velocity distribuiton. Second, the potential flow field, or at least some of its properties, can be determined for a given boundary layer development. The second is known as the inverse or design problem. In such problems the potential flow velocity distribution is specified and the airfoil shape is computed. But this shape has to be consistent with the desired boundary layer develcpment.

Since the time of the development of NACA laminar flow airfoils, boundary layer and potential flow theories have been steadily improved. The flow around an airfoil can now be defined more exactly. Also the boundary layer behaviour can be predicted much more accurately. The use of complex variables in potential flow theory has led to conformal mapping techniques, also the use of digital computers has resulted in fast solutions of complex boundary layer

equation systems. Methods are now available by which the boundary layer transition and the behaviour of the turbulent boundary layer can be controlled.

Control of Turbulent Boundary Layers

It is understood that all airfoils have an adverse pressure on the surface close to the trailing edge. This adverse pressure causes transition of laminar flow to turbulent flow. Thus it is imperative to have a way of controlling the development and behaviour of turbulent boundary layers so as to ensure low drag penalties. Studies have shown that suitable velocity distributions on the airfoil can result in turbulent boundary layers which do not separate near the trailing edge of the airfoil. But in order to shape the velocity distribution a procedure is needed through which separation of the boundary layer can be predicted. Such a method was devised by B. S. Stratford (Ref 19) and it provides a velocity distribution which recovers a given pressure difference in the shortest chord length without separation of flow. This velocity distribution is shown in Figure 22 (Ref 13) and it is compared to the conventional linear distribution used on NACA laminar flow airfoils. In Figure 22, θ indicates the momentum thickness and H stands for the boundary layer form parameter.

Transition Control

On NACA laminar flow airfoils the velocity distribution is such that the favourable pressure gradient changes suddenly to an adverse pressure gradient. This is also true of many airfoils with
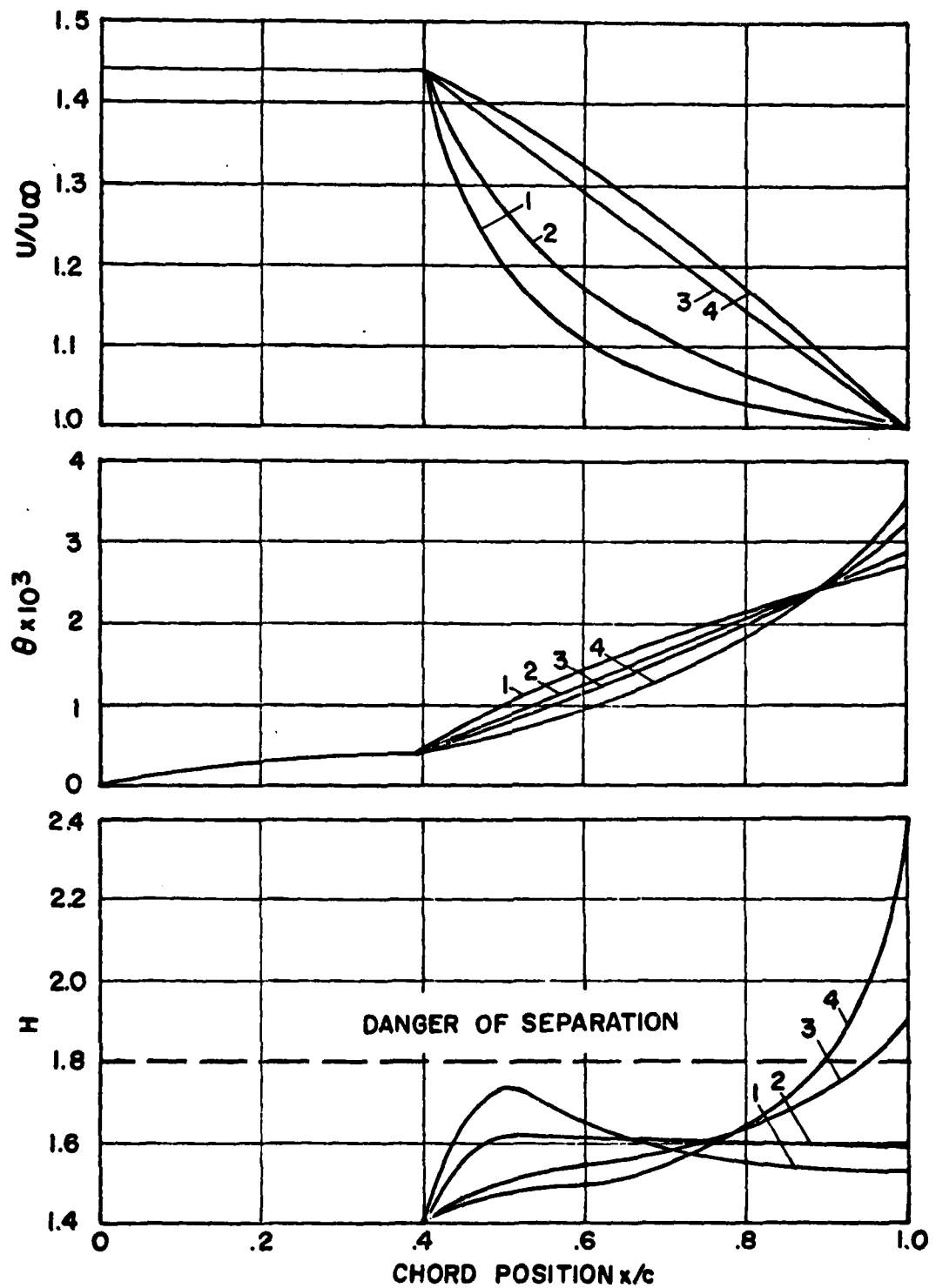
Figure 22 Influence of the Shape of the Pressure Recovery Velocity
Distribution on Momentum Thickness and Form Parameter
(Ref 13)

54

concave pressure recovery regions. This abrupt change of pressure gradient results in the creation of "laminar separation bubbles." The separation bubble is a region where the laminar flow separates but then it immediately becomes turbulent and reattaches to the air- foil surface. The separation bubbles cause an unnecessary increase in the drag by causing thickening of the boundary layer. The ef- fect of the separation bubble can be seen in Figure 23 (Ref 15).

F. X. Wortman (Ref 20) discovered that it is possible to con- trol transition by introducing an "instability range" between laminar and turbulent flows. A slight negative pressure gradient is maintained in this region. This results in absence of laminar sep- aration but introduces a high instability of the laminar flow. The result is transition from laminar to turbulent flow without separa- tion.

Wortman has shown that the instability range combined with con- cave pressure recovery can enhance the performance of an airfoil up to 18 to 20 per cent. Comparison of a NACA laminar flow airfoil and a Wortman airfoil with the same drag bucket width is shown in Fig 24 (Ref 15). It can be seen that the 19.1% thick Wortman airfoil has 18% less drag than the 18% thick NACA airfoil and its minimum lift is higher.

In the case of airfoils designed for very low Reynolds numbers, S. J. Miley (Ref 13) suggests placing a turbulent development region after the instability region so that the turbulent boundary layer is fully developed before facing the steep adverse pressure gradient in the concave recovery region. A velocity distribution to achieve this purpose is shown in Figure 25.
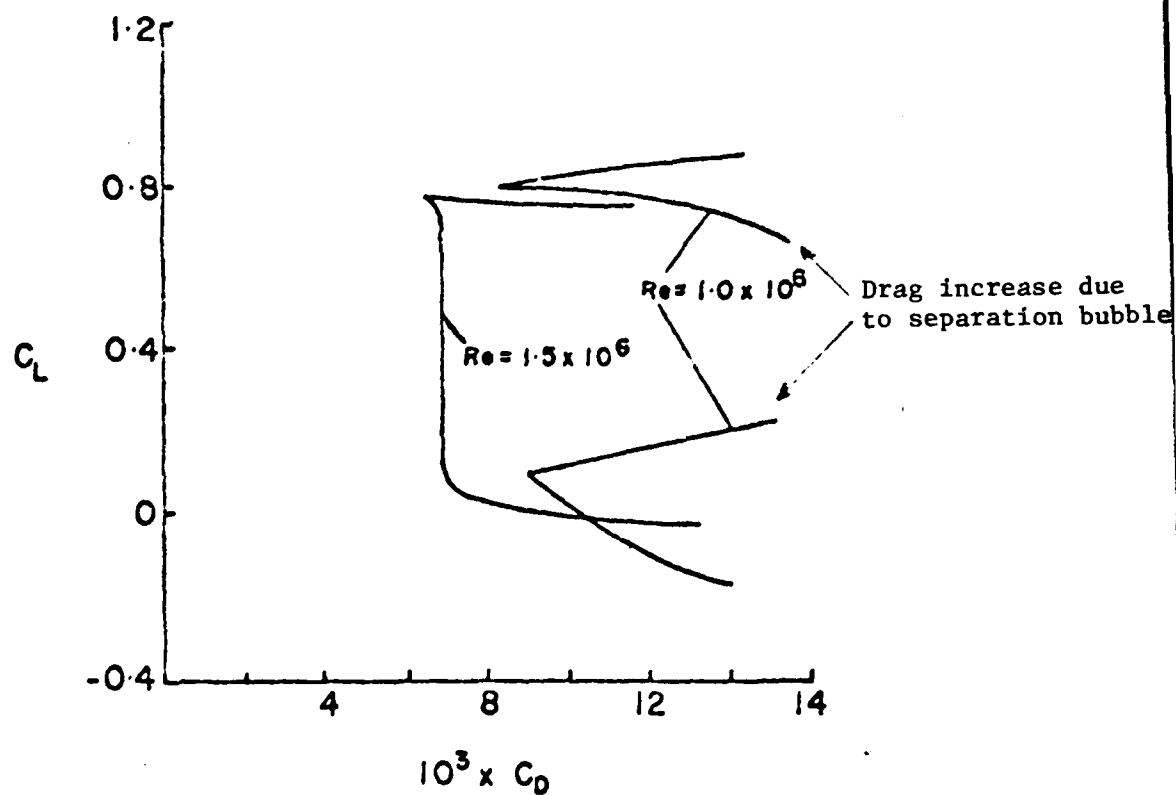
Figure 23   Lift-drag Curve of 20 percent Thick
            Airfoil for two Reynolds Numbers Illustrating
            Effect of Laminar Separation Bubble in
            Pressure Recovery Region (Ref 15)

56
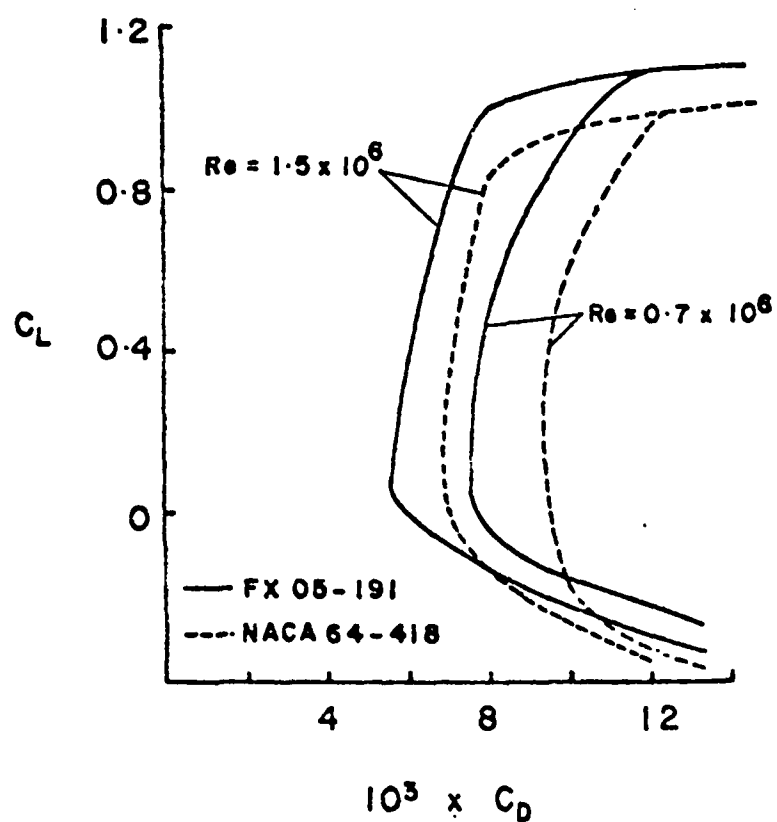
Figure 24   Comparison of the Lift-drag Curves
of the NACA 64-418 and the FX05-191
Airfoil Sections at two Reynolds Numbers
(Ref 15)
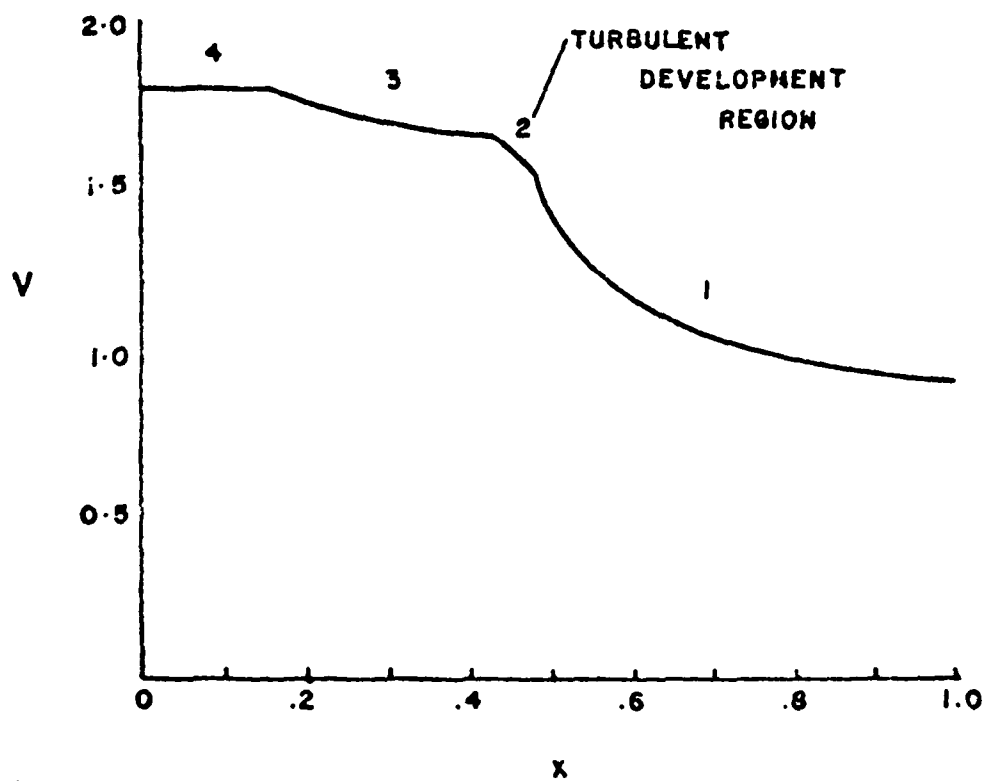
Figure 25   Upper Surface Velocity Distribution
Showing Miley's Turbulent Development
Region   (Ref 13)

Computation Procedures

The above discussion deals with the properties of velocity distributions over an airfoil. A very important objective is to get a suitable airfoil shape from the given velocity distribution. To go slightly further, a procedure is also needed to verify that the airfoil actually depicts the boundary layer behaviour which was predicted by the velocity distribution.

Such procedures have been developed and they apply conformal mapping techniques for the design of an airfoil from a given velocity distribution. The boundary layer analysis is based on the current knowledge available to the scientist working on the problem.

One such method was devised by Richard Eppler (Ref 5). The method was later converted into a computer program which could be used for design and analysis of airfoils. This method was used for the present design project and it will be discussed in detail in the next chapter.

Summary

A brief history of the development of airfoil sections has been presented followed by a survey of the concepts that led to present day computerized design of airfoils.

$$\text{Calculation of } C_p \text{ and } \frac{V}{V_\infty}$$

Given: $M_{critical} = 0.65$

Unknown: C_p critical

$\frac{V}{V_\infty}$ critical

Using the relationship

$$C_{p_{cr}} = \frac{2}{KM_{cr}^2} \left[\left\{ \frac{(K+1)/2}{1+[(K-1)/2]M_{cr}^2} \right\}^{\frac{K}{K-1}} -1 \right]$$

(Ref 12)
Page 263

where

$C_{p_{cr}}$ = critical pressure coefficient

M_{cr} = critical Mach number

x = 1.4 for air

we get

$$C_{p_{cr}} = \frac{2}{(1.4)(0.65)^2} \left[\left\{ \frac{1.2}{1+0.2(0.65)^2} \right\}^{\frac{1.4}{-.4}} -1 \right]$$

$$C_{p_{cr}} = -1.00852$$

Now $C_p = 1 - \left(\frac{V}{V_\infty} \right)^2$

or $-1.00852 = 1 - \left(\frac{V}{V_\infty} \right)^2$

so $\frac{V}{V_\infty} = 1.4172$

Thus the critical C_p and $\frac{V}{V_\infty}$ values are:

$$C_p = -1.00852$$
$$\frac{V}{V_\infty} = 1.4172$$

60

Appendix C
AIRFOIL DESIGN AND ANALYSIS METHOD

It is understood that the properties of an airfoil depend upon the potential flow velocity distribution around it. One such distribution is shown in Figure 26 (Ref 13). This figure shows the velocity distribution on the upper and lower surface for α_u and α_L, where α_u and α_L are the angles of attack at which a flat plate velocity gradient is observed on the upper and the lower surface respectively. In the insert of the same figure it is shown that α_u and α_L form the boundaries of the "drag bucket." To use the parameters of this figure in order to design an airfoil, a suitable inverse solution method is needed. That method should be able to come up with an airfoil shape that will produce the specified velocity distributions at specified angles of attack.

Richard Eppler used the concepts of conformal mapping and complex variables to come up with such a method. He converted the numerical scheme into a computer code. This code was utilized in the present study. The computer code includes a design program which yields the airfoil shape based on the desired velocity profile. The second part of the code uses aerodynamic paneling technique to anlayze the designed airfoil.

The conformal mapping procedure and Eppler's calculation scheme will be discussed in some detail in the following sections. Discussion of Eppler's method is based on Refs 3, 5 and 13.

Conformal Mapping

Plane, irrotational, and incompressible flow can be represented by an analytical function of the complex argument $Z = x + iy$:

61
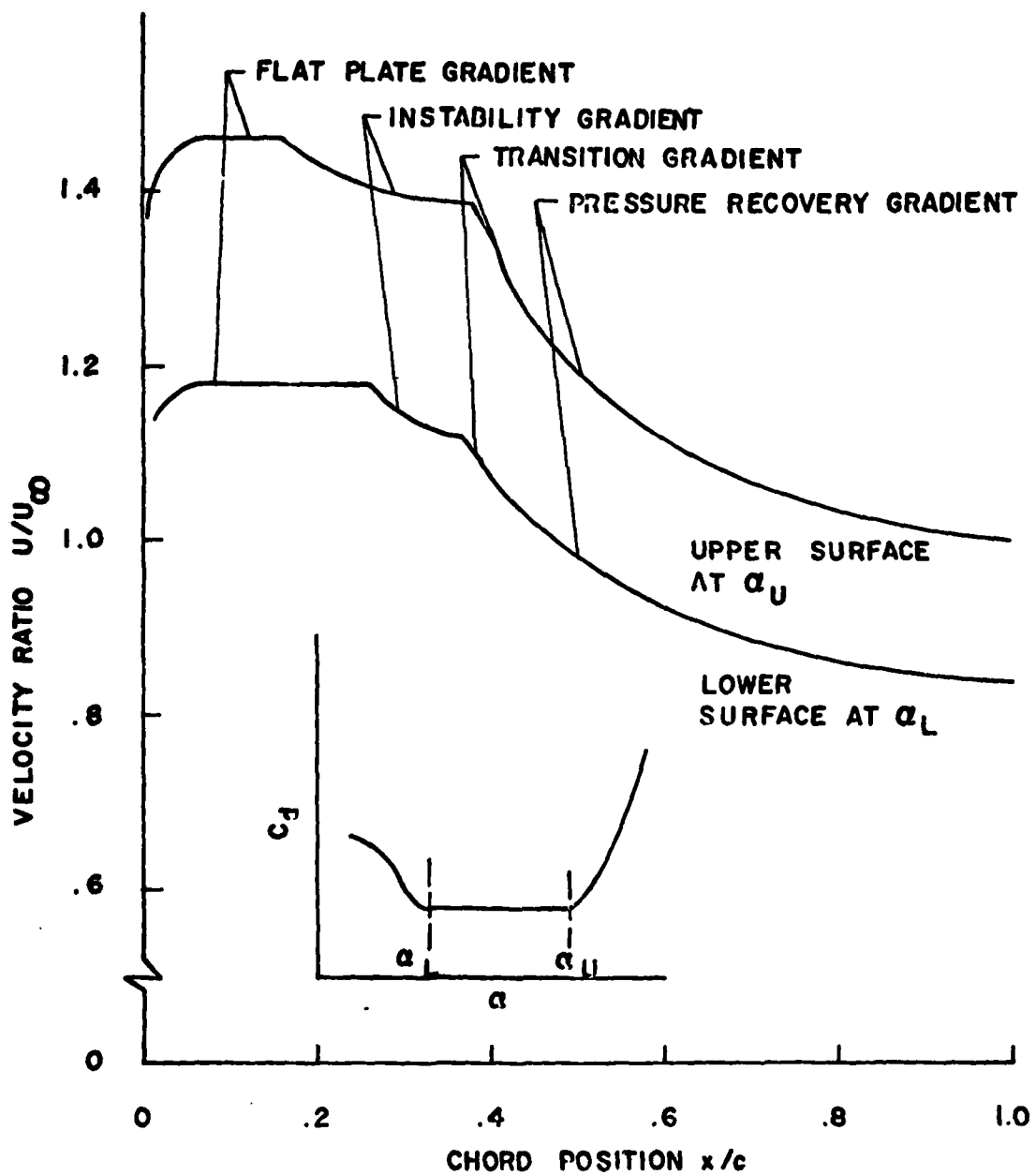
Figure 26 Velocity Gradient Components Used in Airfoil Design
(Ref 13)

$$F(Z) = F(x + iy) = \phi(x,y) + i\psi(x,y) \qquad \text{(C-1)}$$

where ϕ and ψ, the potential and stream functions, are real functions of x and y. The curves ϕ = constant and ψ = constant, form two families of orthogonal curves in the xy plane. The velocity components in the x and y direction are given by

$$u = \frac{\partial \phi}{\partial x} = \frac{\partial \psi}{\partial y} \quad v = \frac{\partial \phi}{\partial y} = -\frac{\partial \psi}{\partial x}$$

The function F(Z) is called a complex stream function. From this function the velocity field is obtained by differentiation in the Complex plane, where

$$\frac{dF}{dZ} = u - iv = \overline{w}\,(Z) \qquad \text{(C-2)}$$

Here $\overline{w} = u - iv$ is the conjugate complex number to $W = u + iv$, which is obtained by reflection of W on the real axis.

For a circular cylinder of radius a, approached in x direction by the undisturbed flow velocity U_∞, the complex stream function is

$$F(Z) = U_\infty\left(Z + \frac{a^2}{Z}\right) \qquad \text{(C-3)}$$

For a plane potential vortex, the stream function is

$$F(Z) = \frac{i\Gamma}{2\pi} \ln Z \qquad \text{(C-4)}$$

where Γ is clockwise circulation.

If we take an analytical function of a complex variable and split it into real and imaginary components:

$$f(Z) = f(x + iy) = \zeta = \xi(x,y) + i\eta(x,y) \qquad \text{(C-5)}$$

The relationship between the complex numbers $z = x+iy$ and $\zeta = \xi + i\eta$ Equation (C-5) can be interpreted geometrically. To each point of

63

complex Z plane is coordinated a point in the complex ζ plane that can be designated as the mirror image of the point in Z plane. When a point in the Z plane moves along a curve, the image point moves along a curve in the ζ plane. The curve is called the image curve to the curve in Z plane. In other words, the Z plane is conformally mapped on to the ζ plane through equation (C-5). The simplest, and probably best known, mapping function is the Joukowsky mapping function,

$$\zeta = f(Z) = Z + \frac{a^2}{Z} \tag{C-6}$$

It maps a circle of radius 'a' about the origin of the 'Z" plane into the twice-passed straight-line (slit) from -2a to +2a in the ζ plane.

The problem of solving the flow about a given body can be tackled by using conformal mapping. Suppose the flow about a body of contour A in the Z plane and its stream function f(Z) are known (usually flow about a circular cylinder is assumed). The flow about a body of contour B in the ζ plane is to be found. For this problem a mapping function

$$\zeta = f(Z) \tag{C-7}$$

is needed which can map contour A of Z plane into contour B of the ζ plane. At the same time the known system of streamlines and potential lines about the body A is being transformed to the unknown system of potential lines and streamlines about body B. The velocity field about body B in the ζ plane is found from the equation.

$$\overline{W}(\zeta) = \frac{dF}{d\zeta} = \frac{dF}{dZ} \cdot \frac{dZ}{d\zeta} = \overline{W}(Z) \frac{dZ}{d\zeta} = \overline{W}(Z) \Big/ \frac{df}{dZ} \tag{C-8}$$

64

$F(Z)$ and $\overline{W}(Z)$ are known from the stream function of the body A. The unknown velocity distribution $\overline{W}(\zeta)$ about body B can be computed from equation (C-8) if the mapping function $\zeta = f(Z)$, that maps body A into body B, is known (Ref 16).

Eppler's Method

The method applied by Eppler (Ref 3) is based on conformal mapping. The three planes involved are shown in Figure 27. In the complex ζ plane we start with infinite parallel flow around the unit circle given by,

$$\zeta = \xi + i\eta = r\, e^{i\phi} \tag{C-9}$$

The circulation Γ is determined such that the rear stagnation point is located at $\zeta = 1$. This flow is defined by the complex potential.

$$F(\zeta) = \phi + i\psi = (e^{-i\alpha}\zeta + e^{i\alpha}\frac{1}{\zeta}) - \frac{\Gamma}{2\pi i} \ln \zeta \tag{C-10}$$

where the circulation,

$$\Gamma = 4\pi \sin \alpha \tag{C-11}$$

This flow is mapped onto the Z plane by means of a function $Z(\zeta)$,

$$Z = x + iy \tag{C-12}$$

If the image is also to be an infinite parallel flow with an angle of attack α around an arbitrary profile, then $Z(\zeta)$ must map the exterior of the ζ circle onto the exterior of the profile in a conformal manner. $\zeta = 1$ must become the trailing edge of the profile and at the same time,

$$z(\infty) \overset{M}{=} \infty \text{ and } (\frac{dZ}{d\zeta})_\infty \overset{M}{=} \text{real} \tag{C-13}$$

The conjugate complex velocity vector $\overline{W}$ in the z plane is

65

$$\bar{w} = Ve^{-i\theta} = \frac{dF}{dZ} = \frac{dF/d\zeta}{dZ/d\zeta} \qquad (C-14)$$

where V is the absolute value of the complex velocity and θ is the argument. The function dF/d is given by

$$\frac{dF}{d\zeta} = e^{-i\alpha} - e^{i\alpha-2} - \frac{\Gamma}{2\pi i} \zeta^{-1} \qquad (C-15)$$

The problem at this stage is to find the mapping function $Z(\zeta)$ such that the velocity on the airfoil, V, is a known function. The function $Z(\zeta)$ is specified on the circle $\zeta = e^{i\phi}$ and not on the airfoil, i.e., not in terms of x but in terms of $V(\phi)$. The relation of x and ϕ is defined as

$$x = \frac{c}{2} (1 + \cos) \qquad (C-16)$$

where c is the chord length of the airfoil. This relation is exact for a flat plate only and becomes inaccurate for airfoils with thickness. According to Eppler (Ref 5), if the function $x(\phi)$ differs too much from equation (C-16) then an iteration can be performed after specifying a new function $V(\phi(x))$, but in practice no such iteration has been found to be necessary.

If the velocity $V(\phi)$ is given, then by taking the logarithm of equation (C-14) we get

$$\ln \bar{w} = \ln V - i\theta = \ln \frac{dF}{d\zeta} - \ln \frac{dZ}{d\zeta} \qquad (C-17)$$

On the circle $\zeta = e^{i\phi}$, $\ln \frac{dZ}{d\zeta}$ is known from the values of $V(\phi)$ and $\frac{dF}{d\zeta}$. Thus the function $\frac{dZ}{d\zeta}$, which is the unknown mapping function, can be determined using complex variables.

In considering the Kutta condiction, and the singularities involved and keeping in view equation (C-15), $dZ/d\zeta$ can be represented as

66

$$\ln \frac{dZ}{d\zeta} = \ln(1 - \frac{1}{\zeta}) + \sum_{m=0}^{\infty} (a_m + i\, b_m)\zeta^{-m} \qquad \text{(C-18)}$$

This form is introduced because the power series does not diverge on any point on the boundary of the circle $\zeta = e^{i\phi}$. Using equation (C-17) we rewrite the above equation as

$$[\ln \frac{dZ}{d\zeta} - \ln(1 - \frac{1}{\zeta})]_{\zeta=e^{i\phi}} = -\ln V(\phi) + i\theta + \ln (\frac{dF}{d\zeta})_{\zeta=e^{i\phi}}$$

$$- \ln(1 - \overline{e}^{i\phi}) = P(\phi) + i\, Q(\phi) \text{ (C-19)}$$

Using the value of $\frac{dF}{d\zeta}$ and equation (C-18) we get the equation for $P(\phi)$, which is the real part of (C-19),

$$P(\phi) = \sum_{m=0}^{\infty} (a_m \cos m\phi + b_m \sin m\phi) = -\ln[\frac{1}{2}|\frac{V(\phi)}{\cos(\phi/2-\alpha)}|] \qquad \text{(C-20)}$$

The coefficients a_m and b_m are the same as coefficients of a real Fourier series and they can be determined as such. But in the actual computation these are not required to be found. Only $Q(\phi)$ is required for the final solution. Now $Q(\phi)$ is equal to

$$\sum_{m=0}^{\infty} (b_m \cos m\phi - a_m \sin m\phi) = \frac{1}{2} \int_0^2 P(\psi) \cos \frac{\psi-\phi}{2} d \qquad \text{(C-21)}$$

The above equation is used to determine $Q(\phi)$.

Now substituting equation (C-20) into equation (C-19) we get

$$\ln(\frac{dZ}{d\zeta})_{e^{i\phi}} = -\ln \frac{V(\phi)}{2|\cos(\phi/2-\alpha)|} + iQ + \ln(1-\overline{e}^{i\phi})$$

$$= \ln \frac{2\cos(\phi/2-\alpha)}{V(\phi)} + iQ + \ln(2i\overline{e}^{i\phi/2}\sin \alpha/2) \qquad \text{(C-22)}$$

or

$$\ln(\frac{dZ}{d\zeta})_{e^{i\phi}} = \mu i \sin \phi/2 \ |\cos (\phi/2-\alpha)| \ \frac{1}{V(\phi)} e^{i(Q-\phi/2)} \qquad \text{(C-23)}$$

But $d\zeta = ie^{i\phi}d\phi$ on the circle so $\frac{dZ}{d\zeta} = ie^{i\phi}(\frac{dZ}{d\zeta})_{e^{i\phi}} =$

$$= \sin \frac{\phi}{2} \ |\cos(\phi/2-\alpha)\frac{1}{V(\phi)}e^{i(Q+\frac{\phi}{2})}$$

$$\text{(C-24)}$$

The above equation can be split into real and imaginary parts to yield,

$$\frac{dx}{d\phi} = -\mu\sin\frac{\phi}{2} \left| \cos(\phi/2-\alpha) \right| \frac{1}{V(\phi)} \cos\left[\frac{\phi}{2} + Q(\phi)\right] \qquad (C-25)$$

$$\frac{dy}{d\phi} = -\mu\sin\frac{\phi}{2} \left| \cos(\phi/2-\alpha) \right| \frac{1}{V(\phi)} \sin\left[\frac{\phi}{2} + Q(\phi)\right] \qquad (C-26)$$

It can be seen that if $Q(\phi)$ is known then the x and y coordinates of the airfoil can be found.

The velocity distribution $V(\phi)$ has to obey certain conditions. At infinity it must satisfy the condition that $Z(\infty) = \infty$ and $\left(\frac{dZ}{d\phi}\right)_\infty = 1$. This requirement indicates that the coefficient of ζ^0 in the expansion of equation (C-18) should be equal to 1. Also, as a result of equation (C-25) and (C-26), a closed airfoil should emerge. This condition implies that the coefficient of ζ^{-1} in $\frac{dZ}{d\zeta}$ (equation C-18) should be zero. Thus from equation 2-18 we get

$$\frac{dZ}{d\zeta} = e^{a_0+ib_0} [1 + (-1 + a_1 + i\, b_1)\, \zeta^{-1} + \ldots] \qquad (C-27)$$

In order to satisfy the conditions given above we have to have the following:

$$a_0 = 0 \qquad b_0 = 0$$

$$a_1 = 1 \qquad b_1 = 1$$

Using the expansion of the Fourier series of equation (C-20) and the above values we get the following integral relationships:

68

$$\pi a_0 = \int_0^{2\pi} P(\phi)\ d\phi = 0 \tag{C-28}$$

$$\pi a_1 = \int_0^{2\pi} P(\phi)\ \cos\phi\ d\phi\ = \pi \tag{C-29}$$

$$\pi b_1 = \int_0^{2\pi} P(\phi)\ \sin\phi\ d\phi\ = 0 \tag{C-30}$$

Now it can be seen that the x and y coordinates of an airfoil can be found using equations (C-20) to (C-26) such that the conditions laid down by equations (C-28) to (C-30) are satisfied. This is the numerical scheme used in the computer program where $V(\phi)$ is specified and coordinates x and y are obtained.

Another important point to be considered is that

$$P(\phi) = -\ln\left[\frac{V^*(\phi,\alpha^*)}{2\left|\cos(\phi/2-\alpha^*)\right|}\right] \tag{C-31}$$

in case we select $\alpha = \alpha^*$ for which the velocity distribution $V^*(\phi,\alpha^*)$ is to occur on the airfoil. This function is independent of α and as a result we can use this function to obtain the velocity distribution at any angle of attack, i.e.,

$$\frac{V(\phi,\alpha)}{\left|\cos(\phi/2-\alpha)\right|} = \frac{V^*(\phi,\alpha^*)}{\left|\cos(\phi/2-\alpha^*)\right|} = f(\phi) \tag{C-32}$$

which can be re-written as

$$V(\phi,\alpha) = V^*(\phi,\alpha^*)\left|\frac{\cos(\phi/2-\alpha)}{\cos(\phi/2-\alpha^*)}\right| \tag{C-33}$$

The velocity distribution is thus specified by α^* and $V^*(\phi,\alpha^*)$.

As the right hand side of equation (C-32) is independent of α so it is not necessary to select one α^* at which the velocity $V^*(\phi,\alpha^*)$

69

is to occur on the airfoil. Different values of α^* can be selected for different segments of the airfoil. For any given segment, velocity $V(\phi,\alpha)$ for any α is identical to the specified $V^*(\phi,\alpha^*)$ only if $\alpha = \alpha^*(\phi)$.

It is necessary to have a continuous velocity distribution over the whole airfoil but that does not require $\alpha^*(\phi)$ to be continuous. Only $V^*(\phi,\alpha^*)$ should compensate for discontinuities of $\alpha^*(\phi)$. If $\alpha^*(\phi)$ is given as piecewise constant, i.e., $\alpha^*(\phi) = \alpha_i^*$ for $\phi_{i-1} \leq \phi \leq \phi_i$ then at each discontinuity in $\alpha^*(\phi)$ the following condition must hold.

$$\lim_{\varepsilon \to 0} \left| \frac{V^*(\phi_i+\varepsilon,\alpha_{i+1}^*)}{\cos(\phi_i/2-\alpha_{i+1}^*)} \right| = \lim_{\varepsilon \to 0} \left| \frac{V^*(\phi_i-\varepsilon,\alpha_i^*)}{\cos(\phi_i/2-\alpha_i^*)} \right| \tag{C-34}$$

At the leading edge there is a problem because of the stagnation point. If segment i includes the front stagnation point then $V^*(\phi,\alpha^*_i) = 0$ has to be given for $\cos(\phi/2-\alpha^*_i) = 0$. This means $P(\phi)$ remains undefined at that point. The problem can be prevented by introducing an arc limit $\phi_{i,\ell e}$ near the leading edge and specifying V^* ahead of this point when the stagnation point is beyond it and vice versa. This can be done if

$$\phi_{i,\ell e} - 2\alpha^*_{i,\ell e} < \pi$$
$$\phi_{i,\ell e} - 2\alpha^*_{i,\ell e+1} > \pi \tag{C-35}$$

which means $\qquad\qquad \alpha^*_{i,\ell e+1} < \alpha^*_{e,\ell e} \tag{C-36}$

70
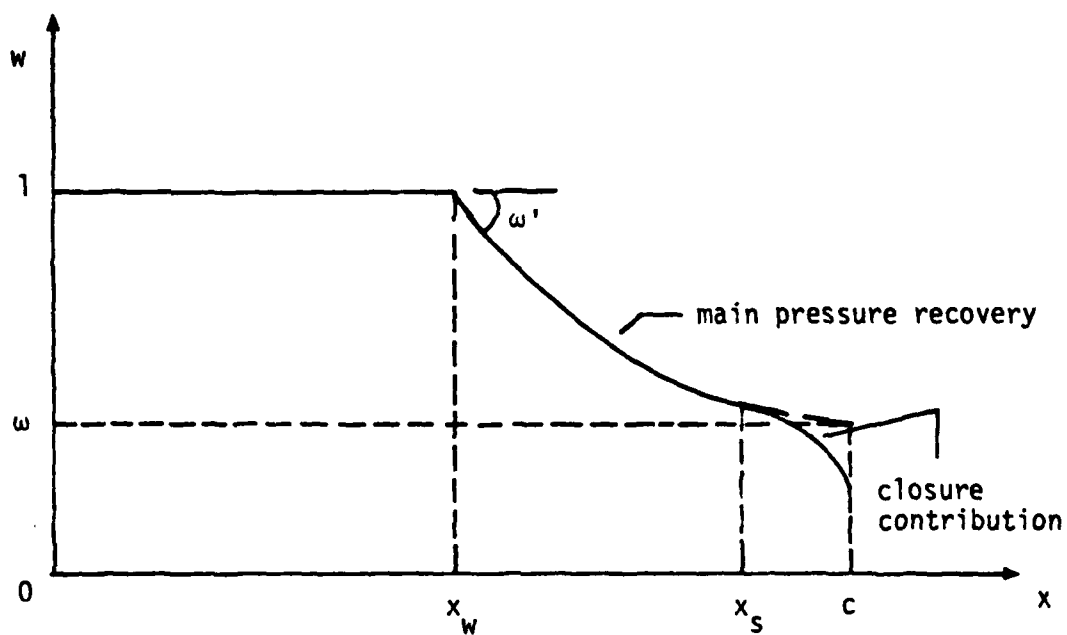
Figure 23. Typical Pressure-Recovery Distribution

71

In the computer program $\phi_{i,\ell e}$ is not specified. It is calculated in the program such that equation (C-28) to (C-30) are satisfied by ensuring that condition 2-36 is met.

Velocity Profile Specification

For the specification of velocity distribution, the circle is divided into Ia arcs. Each arc, i, extends from ϕ_{i-1} to ϕ_i. Thus $\phi_0 = 0$ and $\phi_{Ia} = 2\pi$. The leading edge is $\phi_{i,\ell e}$. For every arc,

$$V(\phi, \alpha^*) = V_i \, W(\phi) \qquad (\phi_{i-1} \leq \phi \leq \phi_i) \tag{C-37}$$

where $W(\phi)$ is a function independent of i. The function $W(\phi)$ allows a main pressure recovery and a closure contribution to be introduced on each surface (Figure   ). It has the following form,

$$W(\phi) = \left[1 + K\left\{\frac{\cos\phi - \cos\phi_W}{1 + \cos\phi_W}\right\}\right]^{-\mu} \left[1 - 0.36\left\{\frac{\cos\phi - \cos\phi_S}{1 - \cos\phi_S}\right\}^2\right]^{K_H} \tag{C-38}$$

for the range $0 \leq \phi \leq \phi_{i,\ell e}$ and

$$W(\phi) = \left[1 + \bar{K}\left\{\frac{\cos\phi - \cos\bar{\phi}_W}{1 + \cos\bar{\phi}_W}\right\}\right]^{-\bar{\mu}} \left[1 - 0.36\left\{\frac{\cos\phi - \cos\bar{\phi}_S}{1 - \cos\bar{\phi}_S}\right\}^2\right]^{\bar{K}_H} \tag{C-39}$$

for the range $\phi_{i,\ell e} \leq \phi \leq 2\pi$.

The property of the term in brackets is such that if $f(\phi) \leq 0$, $\{f(\phi)\} = 0$ and if $f(\phi) > 0$, $\{f(\phi)\} = f(\phi)$. Thus $W(\phi) = 1$ if $\phi > \phi_S$ and $\phi > \phi_W$ in equation (C-38) and if $\phi < \bar{\phi}_W$ and $\phi < \bar{\phi}_S$ in equation (C-39). ϕ_W and ϕ are always $<\pi$ and $\bar{\phi}$ and $\bar{\phi}_W$ are always $>\pi$.

Referring to Figure 28 it can be seen that $\frac{x}{c} = \frac{1}{2}(1 + \cos\phi)$ is used to give an impression of W(x) as given by equation (C-38) and

72

(C-39). The first factor in each equation represents the main pressure recovery and its length is specified by ϕ_W for the upper surface and $\overline{\phi}_W$ for the lower surface. The total amount of pressure recovery and its shape is determined by K and ϕ or $\overline{K}$ and $\overline{\phi}$ depending upon the upper or lower surface. The total amount of main pressure recovery on the upper surface is given by,

$$\omega = 1 + K \left(\frac{1-\cos\phi_W}{1+\cos\phi_W}\right)^{-\mu} \tag{C-40}$$

and the absolute value of the slope of W(x) at $\phi = \phi_W$ is

$$\omega' = \frac{\mu K}{\frac{1}{2}(1+\cos\phi_W)} \tag{C-41}$$

It is possible to specify almost exactly the shape of the pressure recovery by a careful choice of K and μ in equation (C-38).

The pressure recovery can be specified in 3 different modes:

(0) K and μ are specified.

(1) ω' and ω are specified.

(2) μ and ω are specified.

These three modes apply to the lower surface also.

The second factor in equation 2-38 and 2-39 represents the closure contribution. It is normally a small region around the trailing edge. If K_H is > 0 then this term results in a convex velocity decrease as shown in Figure 28. The exponents K_H and $\overline{K}_H$ are not specified rather they are determined by the program.

Thus the total specification of $V(\phi)$ requires only:

(1) The arc limit ϕ_i (except $\phi_{i,\ell e}$).

(2) The values of α_i^* for every arc.

73

(3) Pressure recovery specification $-\phi_W$, μ, K, $\overline{\phi}W'$ $\overline{\mu}$, $\overline{K}$.

(4) The lengths of closure contribution as given by ϕ_S and $\overline{\phi}_S$.

This specification leaves V_i, ϕ_i, ℓ_e, K_H and $\overline{K}_H$ free. There are I_a matching conditions and equations (C-28) to (C-30) must be satisfied. All these conditions can be satisfied in closed form which leads to a transcendental equation for $\phi_{i,\ell e}$. The solution of the equation is obtained by normal numerical methods. The values of K_H,$\overline{K}_H$ and V_i are easily determined from the solution of the transcendental equation.

This concludes the description of Eppler's design method.

Airfoil Analysis Method

The airfoil analysis method employs aerodynamic paneling techniques. In paneling the surface is divided into a large number of very small panels. Then singularities are distributed over the panels. The flow condition requires that the tangential velocity at the control point of each panel be zero. The velocity induced at each panel is estimated by use of available formulae.

The analysis code uses the airfoil co-ordinates obtained from the design method as the edges of the panels (see Figure 29). The singularites used are vortices and they are distributed parabolically along the panel. Thus, this program uses higher order paneling. The flow tangency condition is satisfied

74
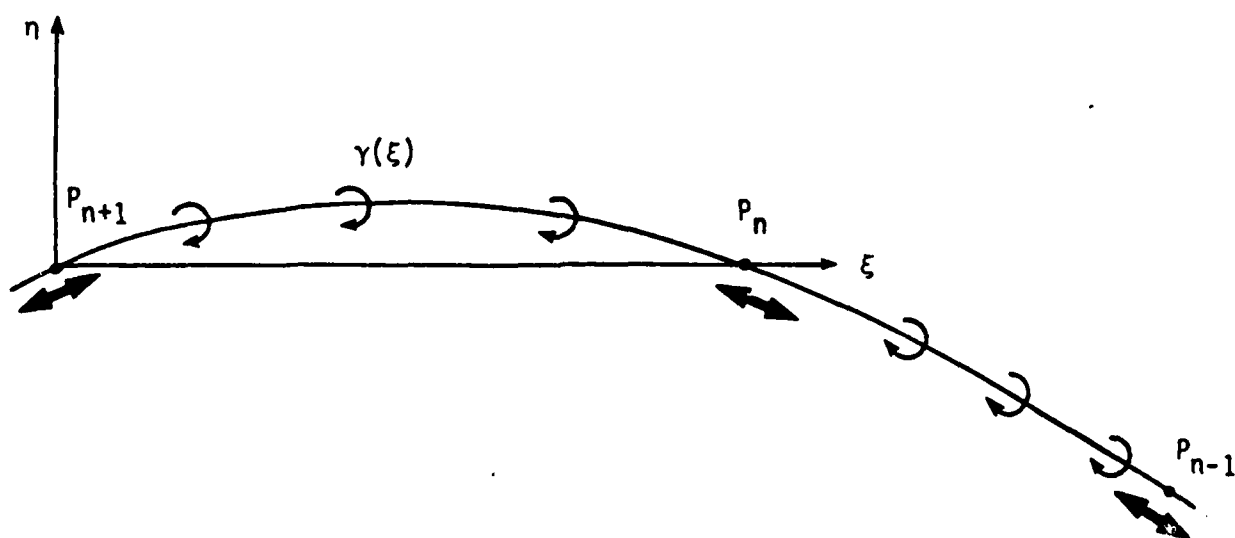
Panel between P_n and P_{n+1}

Shape: Cubic in $\eta(\xi)$

Vorticity: Parabolic

Flow condition: tangential velocity
equals zero at P_n and P_{n+1}

Figure 29 Panel Method (Ref 5)

at each airfoil coordinate (not at the mid point of the panel as is usually done). Zero and 90 degree angles of attack are analyzed because the flow for an arbitrary angle of attack can be derived from these two solutions by superposition. The program includes an option by which additional points can be splined in between the original airfoil coordinates. This option can be utilized to make the solution precise in areas of less panels.

A brief description of the numerical procedure is given in the following pages. This has been taken from Ref 5.

The numerical procedure is based on finding the velocity induced at a point (ξ, η) by the vorticity distribution $\gamma(\xi)$ along a panel which extends from $\xi = 0$ to $\xi = \sigma$ on the ξ-axis as shown in Figure 30. For

$$\gamma(\xi) = \gamma_i \left(1 - \frac{\xi}{\sigma}\right) \tag{C-42}$$

the velocity components are

$$\frac{2\pi}{\gamma_i} W_\xi = \left(1 - \frac{\xi}{\sigma}\right) T + \frac{\eta}{\sigma} \Lambda \tag{C-43}$$

and

$$\frac{2\pi}{\gamma_i} W_\eta = -\left(1 - \frac{\xi}{\sigma}\right) \Lambda + \frac{\eta}{\sigma} T - 1 \tag{C-44}$$

where

$$\Lambda = \ln \frac{\sin \tau_2}{\sin \tau_1}$$

and

$$T = \tau_2 - \tau_1 = \text{arc} \tan \frac{\eta}{\xi - \sigma} - \text{arc} \tan \frac{\eta}{\xi}$$

76
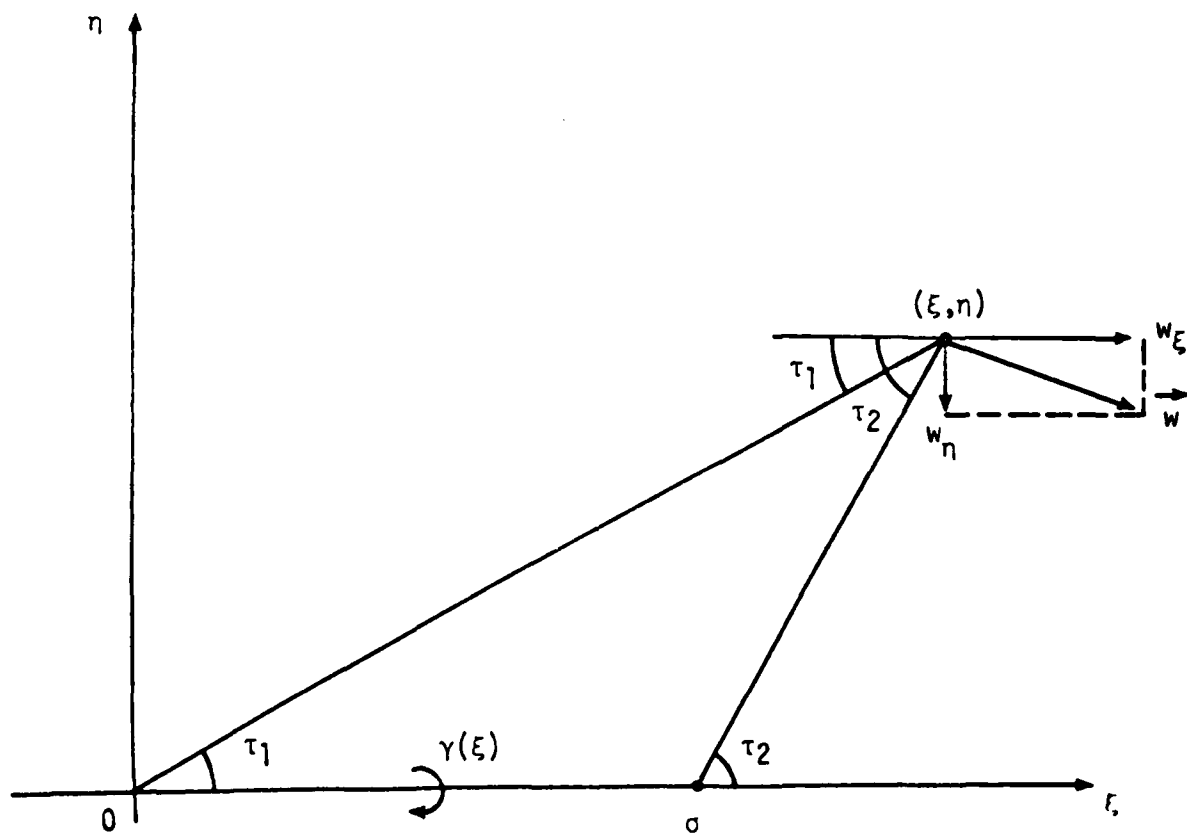
Figure 30   Induced-velocity Vector

Now for

$$\gamma(\xi) = \frac{\xi}{\sigma} \gamma_j \qquad (\text{C-45})$$

the velocity components are

$$\frac{2\pi}{\gamma_j} W_\xi = \frac{\xi}{\sigma} T - \frac{\eta}{\sigma} \Lambda \qquad (\text{C-46})$$

and

$$\frac{2\pi}{\gamma_j} W_\eta = - \frac{\xi}{\sigma}\Lambda - \frac{\eta}{\sigma} T + 1 \qquad (\text{C-47})$$

and for

$$\gamma(\xi) = \frac{\xi}{\sigma} (1 - \frac{\xi}{\sigma}) \gamma_p \qquad (\text{C-48})$$

the velocity components are

$$\frac{2\pi}{\gamma_p} W_\xi = (\frac{\xi}{\sigma} - \frac{\xi^2}{\sigma^2} + \frac{\eta^2}{\sigma^2}) T + \frac{\eta}{\sigma} (2 \frac{\xi}{\sigma} - 1)\Lambda - \frac{\eta}{\sigma} \qquad (\text{C-49})$$

and

$$\frac{2\pi}{\gamma_p} W_\eta = (\frac{\xi^2}{\sigma^2} - \frac{\eta^2}{\sigma^2} - \frac{\xi}{\sigma})\Lambda + \frac{\eta}{\sigma} (2 \frac{\xi}{\sigma} - 1) T - \frac{\xi}{\sigma} + \frac{1}{2} \qquad (\text{C-50})$$

The superposition of vorticities in equations (C-42) and (C-45) results in a linear vorticity distribution with $\gamma(\xi = 0) = \gamma_i$ and $\gamma(\xi = \sigma) = \gamma_j$. The induced velocity for this distribution is given by equations (C-43), (C-44), (C-46) and (C-47). In case of a parabolic vorticity distribution (eqn C-48) the factor γ_p depends on the vorticities on the preceeding and succeeding panels.

If a panel is not straight, it is divided into small subpanels, n_p, in order to compute its induced velocity at the point (ξ, η). n_p is determined by the distance $\frac{\xi}{\sigma}$ and $\frac{\eta}{\sigma}$. If these distances are

78

large enough the camber of the panel is neglected. If the distances are even greater then a global development is introduced in which each panel is replaced by a single vortex.

Special higher order developments are used for the velocity induced at points on the panel itself. At these points, equations (C-43),(C-44),(C-46),(C-47),(C-49) and (C-50) fail. For the vorticity in equation (C-42) the induced tangential velocity at the beginning of a panel (Figure 31) is

$$\frac{2\pi}{\gamma_i} W_t = \frac{5}{6} g_1 + \frac{1}{3} g_2 + \frac{\pi}{2} \tag{C-51}$$

where g_1 and g_2 are the slopes shown in Figure 31. For the vorticity in equation (C-45), the induced tangential velocity is

$$\frac{2\pi}{\gamma_j} W_t = \frac{2}{3} g_1 - \frac{1}{6} g_2 \tag{C-52}$$

and for the vorticity in equation (C-48) it is,

$$\frac{2\pi}{\gamma_p} W_t = \frac{5}{12} g_1 - \frac{1}{6} g_2 \tag{C-53}$$

All these equations allow the computation of the influence of any vorticity distribution on a panel as specified by equation (C-42), (C-45) and (C-48) at any point P. A flow condition at point P results in a linear equation for the unknown γ. Thus a system of n_q linear equations results, where n_q is the number of points defining the airfoil.
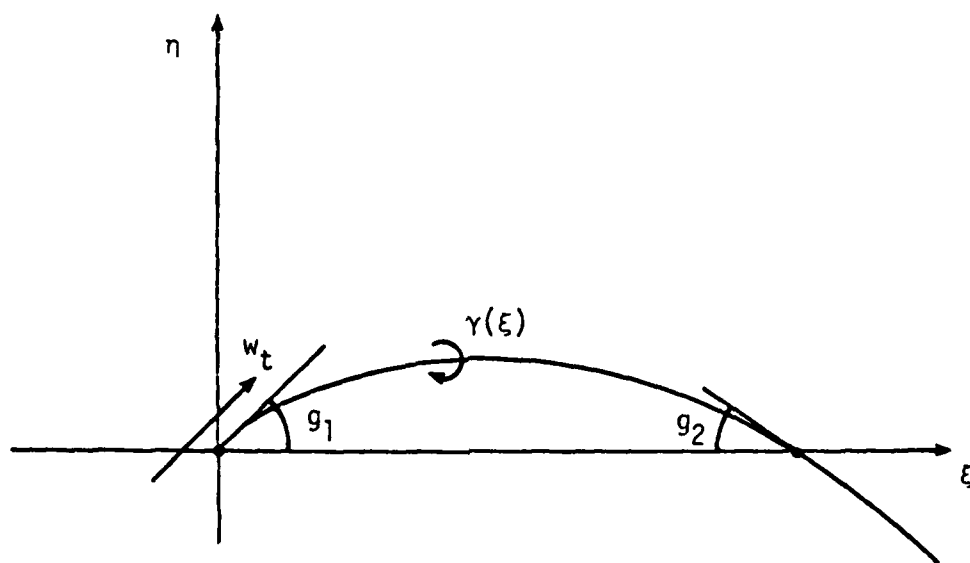
Figure 31 Induced Tangential Velocity on Panel

80

Appendix D

Boundary Layer Analysis Method

The design and analysis of airfoils as described in Appendix C is based on potential flow theory and it does not take into account the effects of viscosity. But in actual flows, viscous effects are always present. Thus the study of the behaviour of boundary layers becomes imperative in all practical designs.

The boundary layer may be defined as a region of flow, very close to the surface of the airfoil (or any other body in flow), within which the velocity varies from zero (in a body fixed co-ordinate system) to the full local stream value at the outer edge of the boundary layer. The analytical solution of the boundary layer equations will be discussed in the following sections with particular stress on the method used by Richard Eppler as described in Ref 4 and 5.

Boundary Layer Equations

A method for the analysis of boundary layers is described in Ref which is called the integral method. According to this method if the tangential velocity component within the boundary layer is $U(x,y)$, the length along the surface and in the flow direction is x, and the length normal to the surface is y, then the potential flow velocity is

$$u(x) = \lim_{y \to h} u(x,y) \qquad (D-1)$$

This displacement thickness is defined as

81

$$\delta_1(x) = \int_o^h (1 - \frac{u}{u_e}) \, dy \qquad \text{(D-2)}$$

where h is larger than δ.

The momentum thickness is defined as

$$\delta_2(x) = \int_o^h (1 - \frac{u}{u_e}) \, \frac{u}{u_e} \, dy \qquad \text{(D-3)}$$

And the energy thickness is defined as

$$\delta_3(x) = \int_o^h [1 - (\frac{u}{u_e})^2] \, \frac{u}{u_e} \, dy \qquad \text{(D-4)}$$

The boundary layer shape factors are defined as

$$H_{12} = \frac{\delta_1}{\delta_2} \qquad \text{(D-5)}$$

$$H_{32} = \frac{\delta_3}{\delta_2} \qquad \text{(D-6)}$$

Assuming that the normal velocity at the surface is V_o and that suction of boundary layer is negative and blowing is positive, the integral momentum equation can be written as

$$\delta_2' + (2 + H_{12}) \, \frac{u_e'}{u_e} \, \delta_2 = C_f + \frac{V_o}{U_e} \qquad \text{(D-7)}$$

The integral energy equation is

$$\delta_3' + 3 \, \frac{u_e'}{u_e} \, \delta_3 = C_D + \frac{V_o}{u_e} \qquad \text{(D-8)}$$

The skin friction coefficient C_f and the dissipation coefficient C_D are defined as follows:

$$C_f = \frac{\tau_o}{\rho u_e^2} \qquad \text{(D-9)}$$

$$C_D = \frac{2}{\rho u_e^3} \int_o^h \tau \frac{\partial u}{\partial y} \, dy \qquad \text{(D-10)}$$

82

END

FILMED

DTIC
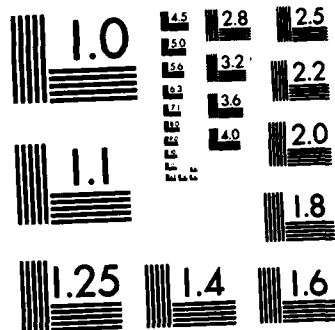
MICROCOPY RESOLUTION TEST CHART

NATIONAL BUREAU OF STANDARDS-1963-A

in all cases τ is the shearing stress and it is defined as

$$\tau = \rho \, \nu \frac{\partial u}{\partial y} \qquad\qquad \text{(D-11)}$$

Now the differential equations (D-7) and (D-8) can be satisfied by every solution $u(x,y)$, of the full partial differential equation for boundary layer flow. That is a project which requires extensive use of digital computers with very large memories. Approximate solutions can, however, be determined by allowing velocity distributions of the form $\frac{u}{u_e} = f(\frac{y}{(x)}, H(x))$, where δ is a thickness factor and H is a shape factor. The thickness factor pertains to the local thickness of the boundary layer and the shape factor relates to the local velocity profile. Normally the shape factor is taken into consideration if it is required to find the velocity profile within the boundary layer. So in normal applications, and specially airfoil design, this factor is neglected and the distributions of δ_1, δ_2 and δ_3 are considered.

Laminar Boundary Layer: Eppler Solution

Using equations (D-10) and D-11) the expressions for C_f and C_D can be re-written as follows:

$$C_f = \frac{\nu}{u_e \delta_2} \frac{\partial f}{\partial \eta} \frac{\delta_2}{\delta} = \frac{\epsilon^*(H_{32})}{R \frac{u}{u_e} \frac{\delta_2}{\ell}} \qquad\qquad \text{(D-12)}$$

and

$$C_D = \frac{2D^*(H_{32})}{R \frac{u}{u_e} \frac{\delta_2}{\ell}} \qquad\qquad \text{(D-13)}$$

83

In this form it is clear that the only concern is to solve for $H_{12}(H_{32})$, $\varepsilon^*(H_{32})$, and $D^*(H_{32})$. The Reynolds number is defined as $R = \frac{u_e \ell}{\nu}$ and the local Reynolds number based on momentum thickness is

$$R_{\delta 2} = \frac{u \delta 2}{\nu} = R \frac{u}{u_e} \frac{\delta_2}{\ell} \tag{D-14}$$

for airfoil boundary layers the reference length ℓ is the airfoil chord length C and the reference velocity u_e is the free stream velocity.

Eppler employed solutions of similar profiles to develop the functional relationships for H_{12}, ε^* and D^* in terms of H_{32}. These are presented graphically in Figure 32. The numerical values are available in Ref 4 and Ref 5. These relations express δ_2' and δ_3' as functions of δ_2 and δ_3 provided the potential flow velocity u(x), suction velocity $V_0(x)$, and the Reynolds number are given. The shape of the boundary layer velocity distribution u(y) can be determined from H_{12} or H_{32}, but as δ_2 and δ_3 are involved, H_{32} is used as the shape factor. The shape factor for a Blausius boundary layer is 1.57258. If $H_{32} \geq 1.57258$, then u(y) has no inflection point. If $H_{32} \leq 1.57258$ then u(y) has an inflection point. The laminar separation limit is set where $\frac{\partial u}{\partial y} = 0$ at y = 0. At this condition $H_{32} = 1.51509$. Also it can be verified that a favorable pressure gradient and $V_0 < 0$ tend to increase H_{32} and vice versa.

The numerical integration of equations (D-7) and (D-8) can be carried out to find the values of δ_2 and δ_3. Knowing the relationships of δ_2 and δ_3 with H_{32}, the value of H_{32} at every 'x' can be found. For the integration procedure, the initial values of δ_2 and δ_3 can

84
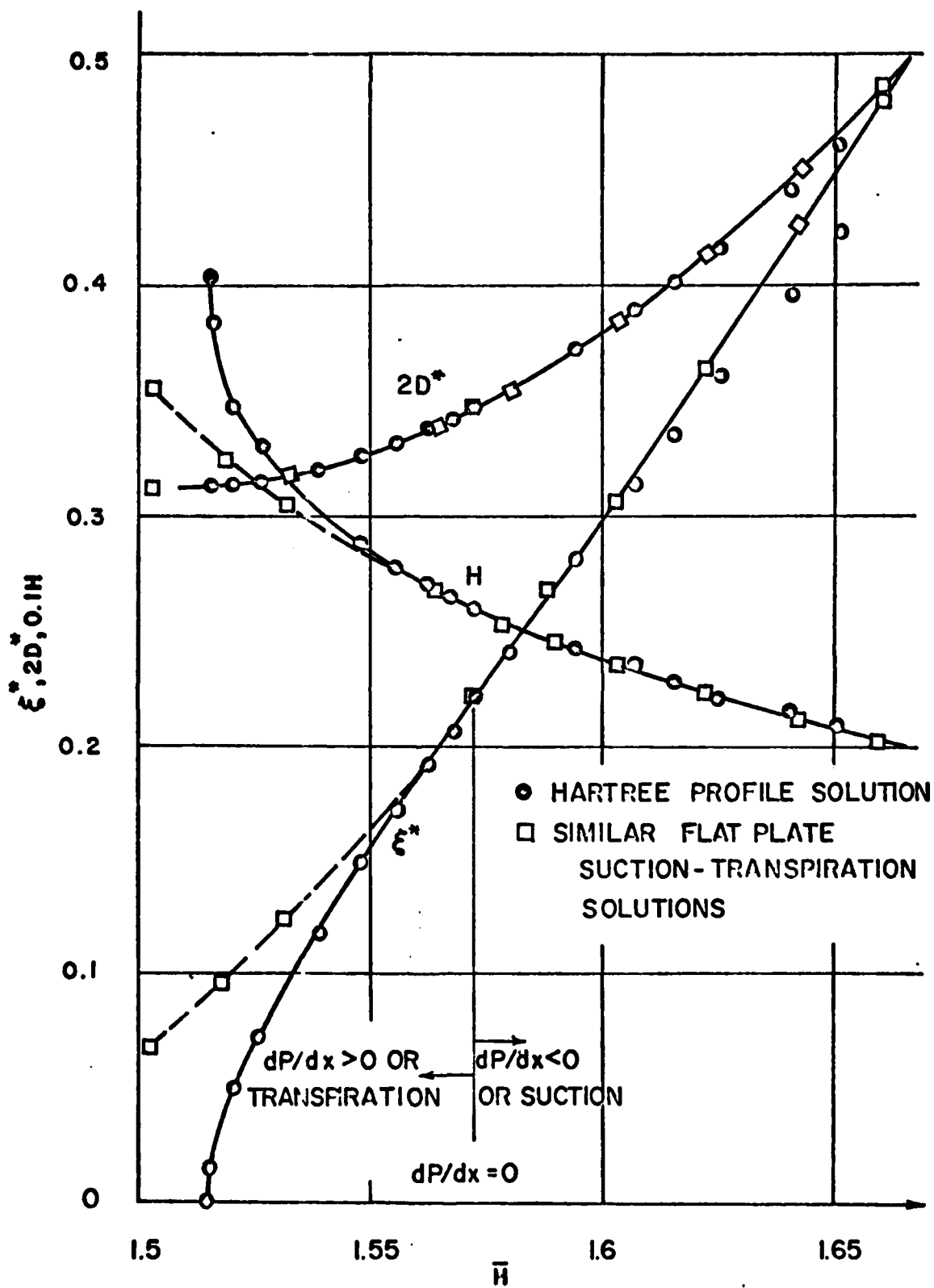
Figure 32 Functional Relationships Between $\bar{H}$ and H, ξ^* and D* (Ref 4)

be derived from closed solutions for the first step of length Δx (see Ref 4,13). Laminar separation is predicted when $H_{32} = 1.51509$. Constant potential flow velocity yields the constant value of $H_{32} = 1.57258$. It has been found by Schlichting (Ref 16) and others that the approximate solutions obtained from this method are quite close to the exact solutions.

Turbulent Boundary Layer: Eppler Solution

The analysis of turbulent boundary layers is carried out in the same manner as laminar boundary layers but in this case the derivation of expressions for H_{12}, C_f and C_D is quite involved. Here selected velocity distributions are not used, as was done in case of laminar flow. Rather some empirical relations are employed to solve this problem. The derivation of these expressions was carried out by Wieghardt, Ludwieg-Tillman, and Rotta. The complete derivations are available in Ref 4 but only the final results are presented here.

$$H_{12} = \frac{11}{48} \frac{H_{32} + 15}{H_{32} - 59} \tag{D-15}$$

$$C_f = 0.045716 \ [(H_{12}-1) \frac{u_e \delta_2}{\nu}]^{-0.232} e^{-1.260 H_{12}} \tag{D-16}$$

$$C_D = 0.01 \ [(H_{12}-1) \frac{u_e \delta_2}{\nu}]^{-1/6} \tag{D-17}$$

The above equations indicate that there is not a single value of H_{32}, for turbulent boundary layers, at which separation occurs. According to this method it can only be said that

$$H_{32} > 1.58 \rightarrow \text{no separation}$$

$$H_{32} < 1.46 \rightarrow \text{sure separation}$$

In the computer program, a turbulent boundary layer is assumed to have separated at a value of $H_{32} = 1.46$ because the H_{32} values obtained by the above procedure are low under adverse pressure gradients.

Transition and Laminar Separation Bubbles

It is important to predict the location of transition from laminar to turbulent flow because the equations are different for the two regimes. Laminar flow is governed by equations (D-13), (D-14) and the solutions of similar profiles wehreas turbulent flow is government by equations (D-15), (D-16) and (D-17). The transition criterion used by Eppler is as follows:

$$\ln R_2 \geq 18.4 H_{32} - 21.74 - 0.36r \tag{D-18}$$

where 'r' is the roughness factor. The idea is that transition occurs if $\ln R_{\delta 2}$ is as indicated in equation (D-18), which was derived empirically.

The roughness factor of zero represents a smooth surface and turbulence free initial flow conditions; it corresponds to natural transition. Disturbances caused by insects, a rough surface, or by a turbulent free stream are represented by $r = 4$. Roughness factor of zero was used in this study.

Many times laminar separation occurs before the criterion laid down in equation (D-18) is satisfied. In such cases the procedure is to switch to turbulent laws and continue calculation. But, often in real flows, laminar separation is followed by turbulent

87

re-attachment (Ref 4,5). The small area of laminar separation before the turbulent attachment is called a "laminar separation bubble." The adverse effects of laminar separation bubbles have already been discussed in Appendix A.

The results of Eppler's boundary layer method exhibit a certain bubble analogy. If the local Reynolds number $R_{\delta 2}$ is small enough, the method indicates either a very slowly increasing shape factor H_{32} or a decreasing H_{32} which rapidly reaches the turbulent separation value of $H_{32} = 1.46$. For a slowly increasing H_{32} a bubble extending at least up to $H_{32} = 1.58$ should be expected. This is possible after laminar separation or in very steep adverse pressure gradients following transition. As the presence of a bubble analog indicates the possibility of separation in real flows, so it is important to avoid the bubble analog in computations.

Section Characteristics

This section will be devoted to the procedures followed by Eppler (Ref 5) in order to determine the section characteristics of airfoils.

The drag estimation under normal circumstances is carried out by using the Squire-Young formula, i.e.,

$$c_d = 2\delta_{2, te} \; (\frac{u_{te}}{u_\infty}) \; \frac{5 + H_{12,te}}{2} \qquad (D-19)$$

where 'te' refers to conditions at the trailing edge. The use of this formula in cases where the flow at the trailing-edge is near separation, results in very high c_d values. Actually (D-19) was not

derived to cater for such conditions. Empirical modifications were
carried out to cover such situations and the result is:

$$c_d = 2\delta_{2,\text{ te}} \left(\frac{u_{\text{te}}}{u_\infty}\right) \frac{5 + H^*_{12,\text{te}}}{2} \qquad \text{(D-20)}$$

where

$$H^*_{12,\text{te}} = H_{12,\text{te}} \quad \text{for } H_{12,\text{te}} \leq 2.5$$
$$= 2.5 \quad \text{for } H_{12,\text{te}} \geq 2.5 \qquad \text{(D-21)}$$

The above relation is applied to the trailing-edge for upper and
lower surfaces separately.

In case of separation, the momentum thickness δ_2 is corrected
as follows:

$$\delta_{2,\text{te}} = \delta_{2,\text{sep}} \left(\frac{u_{\text{sep}}}{u_{\text{te}}}\right) \frac{5 + H_{12,\text{sep}}}{2} \qquad \text{(D-22)}$$

where u_{sep} is the local velocity at which separation occurs. As
$H_{32} = 1.46$ for turbulent separation so $H_{12,\text{sep}} = 2.803$ and as such
c_d from equation (D-19) will be

$$c_d = c_{d,\text{sep}} \left(\frac{u_{\text{sep}}}{u_{\text{te}}}\right)^{0.15}$$

The above expression shows that a penalty in the form of drag in-
crease results from separation.

Lift and pitching moment coefficients are basically determined
by potential flow methods but some viscous effect corrections are
applied to them.

For no separation the lift curve slope is kept at 2π. This means
that the potential flow thickness effects are offset by the boundary
layer displacement effects. So if α_o is the zero lift angle as shown
in Figure 33, then the lift coefficient with no separation will be

89
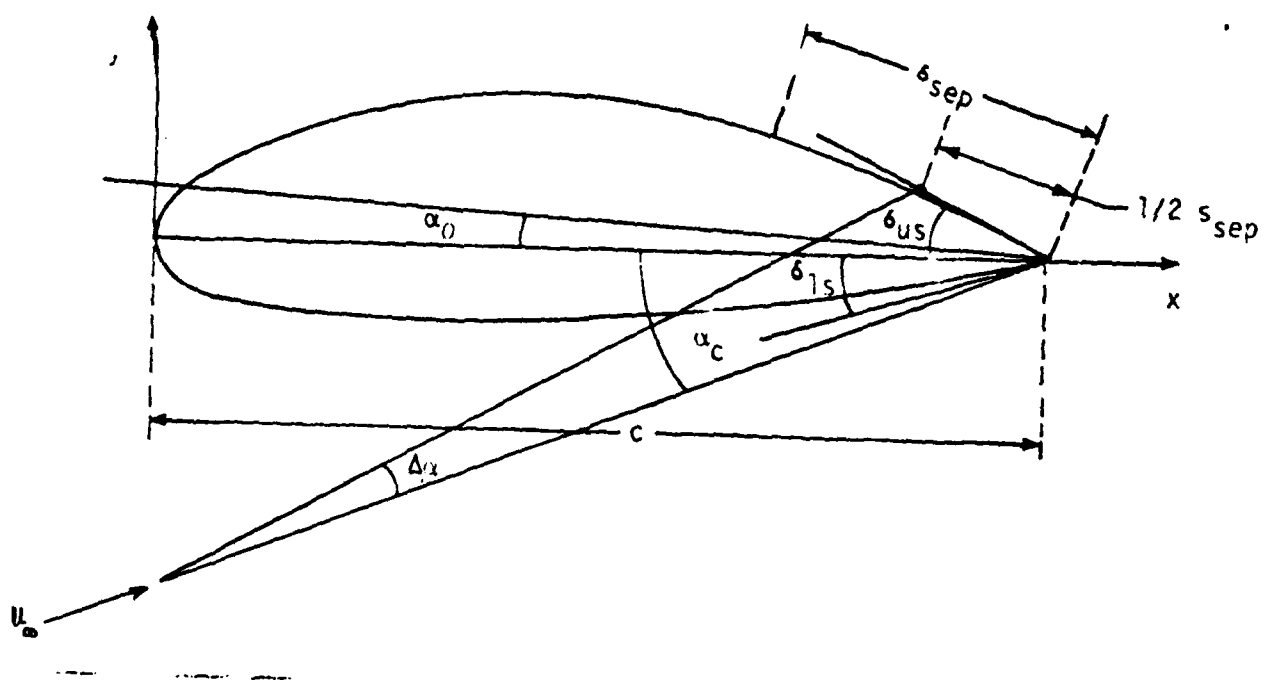
Figure 33 Lift-coefficient Correction due to Separation

90

$$C_{\ell ns} = 2\pi(\alpha_c + \alpha_o) \qquad \text{(D-23)}$$

where α_c is the angle of attack with respect to the chord line.

In case a separation is predicted on the upper surface and its length is S_{sep} then an angle of attack correction is applied.

$$\Delta\alpha \simeq -\frac{1/2 \; S_{sep}}{C}(\delta_{us} + \alpha_c) \qquad \text{(D-24)}$$

where δ_{us} is the slope of the upper surface near the trailing-edge (see Figure 33).

The lift coefficient correction will be

$$\Delta c_\ell = 2\pi\Delta\alpha = -\pi \; \frac{S_{sep}}{C}(\delta_{us} + \alpha_c) \qquad \text{(D-25)}$$

Similar corrections are applied if separation is indicated on the lower surface. A positive Δc_ℓ on the upper surface or a negative Δc_ℓ for the lower surface are not allowed, because they are unrealistic.

Summary

The basic boundary layer concepts were briefly covered followed by derivation of boundary layer solution equations. In the solutions, special emphasis was laid on Eppler's solution methods as they are of primary interest in this project. The chapter was concluded with the estimation procedures used to determine section characteristics like c_ℓ, c_d and c_m.

Appendix E

Detailed Results: Airfoil 2500

The detailed results for airfoil 2500 are presented in this appendix. On the first two pages, the x and y coordiantes of the airfoil are given under columns marked x and y. The C_p values at each coordinate are listed in the subsequent columns. Every column indicates C_p values for a different angle of attack. All angles of attack are with respect to the chord line. The last line on page 94 indicates the value of zero lift angle of attack and C_{m_o}.

The last four pages of the appendix contain a summary of the results obtained by viscous flow analysis. For every Reynolds number (1.5 to 6.5 million) and angle of attack (-5° to $+11^o$), the amount of turbulent flow, amount of separation, and the value of C_d is given for the upper and lower surfaces, separately. The values of turbulent flow and separation are given as fractions of the chord length, i.e. s.sep = .03 implies that there is separated flow on 3% of chord length.

The values of C_l, C_d and C_{m_o} for each set of Reynolds number and angle of attack are also listed in these data.

AIRFOIL 2504   15.01%

PRESSURE DISTRIBUTIONS FOR THE ABOVE ANGLES OF ATTACK RELATIVE TO THE CHORD LINE

N	X	Y	-5.00	-4.00	-3.00	-2.00	-1.00	0.00	1.00	2.00	3.00	5.00	7.00	11.00

ALPHA = 5.27 DEGREES   CM0 = -.1282   ETA = 1.133

SUMMARY   AIRFOIL 2500   ANGLE OF ATTACK RELATIVE TO THE CHORD LINE   ALPHAO = 3.87 DEGREES
% INDICATES BUBBLE ANALOG LONGER THAN .030

	R = 150000 RU = 3			R = 250000 RU = 3			R = 350000 RU = 3		
ALPHA = -5.00 DEGREES	S TURB	S SEP	CD	S TURB	S SEP	CD	S TURB	S SEP	CD
UPPER	.2136	.1174	.00258	.2165	.0548	.0021	.2185	.0354	.0018
LOWER	.9984	.0472	.0060	.9984	.0438	.0055	.9984	.0414	.0052
TOTAL	CL = -.056	CD = .0085		CL = .065	CD = .0076		CL = .022	CD = .0070	
	CM = -.1125			CM = -.1234			CM = -.1271		

	R = 150000 RU = 3			R = 250000 RU = 3			R = 350000 RU = 3		
ALPHA = -4.00 DEGREES	S TURB	S SEP	CD	S TURB	S SEP	CD	S TURB	S SEP	CD
UPPER	.2148	.1233	.00261	.2176	.0606	.0022	.2195	.0400	.0019
LOWER	.9977	.0453	.0054	.9977	.0419	.0050	.9977	.0395	.0047
TOTAL	CL = .039	CD = .0080		CL = .102	CD = .0071		CL = .122	CD = .0066	
	CM = -.1136			CM = -.1249			CM = -.1291		

	R = 150000 RU = 3			R = 250000 RU = 3			R = 350000 RU = 3		
ALPHA = -3.00 DEGREES	S TURB	S SEP	CD	S TURB	S SEP	CD	S TURB	S SEP	CD
UPPER	.2159	.1279	.00281	.2187	.0710	.0023	.2206	.0451	.0020
LOWER	.9962	.0436	.0049	.9962	.0402	.0045	.9962	.0372	.0042
TOTAL	CL = .133	CD = .0076		CL = .194	CD = .0068		CL = .221	CD = .0063	
	CM = -.1151			CM = -.1255			CM = -.1309		

	R = 150000 RU = 3			R = 250000 RU = 3			R = 350000 RU = 3		
ALPHA = -2.00 DEGREES	S TURB	S SEP	CD	S TURB	S SEP	CD	S TURB	S SEP	CD
UPPER	.2172	.1322	.00291	.2199	.0811	.0024	.2218	.0502	.0021
LOWER	.9931	.0422	.0044	.9931	.0387	.0041	.9931	.0350	.0039
TOTAL	CL = .227	CD = .0073		CL = .285	CD = .0065		CL = .319	CD = .0060	
	CM = -.1167			CM = -.1261			CM = -.1326		

	R = 150000 RU = 3			R = 250000 RU = 3			R = 350000 RU = 3		
ALPHA = -1.00 DEGREES	S TURB	S SEP	CD	S TURB	S SEP	CD	S TURB	S SEP	CD
UPPER	.2184	.1365	.00318	.2212	.0904	.0025	.2239	.0556	.0022
LOWER	.9931	.0833	.00128	.9939	.0869	.00693	.9931	.0568	.0009
TOTAL	CL = .341	CD = .0042		CL = .396	CD = .0034		CL = .428	CD = .0031	
	CM = -.1237			CM = -.1320			CM = -.1371		

	R = 150000 RU = 3			R = 250000 RU = 3			R = 350000 RU = 3		
ALPHA = 0.00 DEGREES	S TURB	S SEP	CD	S TURB	S SEP	CD	S TURB	S SEP	CD
UPPER	.2128	.1446	.00328	.2225	.0976	.0026	.2244	.0614	.0023
LOWER	.9924	.0828	.00118	.9932	.0803	.00098	.9937	.0798	.00078
TOTAL	CL = .434	CD = .0043		CL = .488	CD = .0035		CL = .533	CD = .0031	
	CM = -.1293			CM = -.1331			CM = -.1409		

% INDICATES BUBBLE ANALOG LONGER THAN .030   ANGLE OF ATTACK RELATIVE TO THE CHORD LINE   ALPHA = 5.57 DEGREES

| | R = 150000 NU = 3 | R = 250000 NU = 3 | R = 350000 NU = 3 |

ALPHA = 1.00 DEGREES

	S TURB	S SEP	CD	S TURB	S SEP	CD	S TURB	S SEP	CD
UPPER	.2213	.1446	.0034%	.2240	.1648	.0028	.2258	.0709	.0024
LOWER	.0918	.0823	.0103	.0926	.0798	.0098%	.0931	.0774	.0078%
TOTAL	CL = .526 CD = .0044			CL = .578 CD = .0036			CL = .622 CD = .0031		
	CM = -.1200			CM = -.1341			CM = -.1414		

ALPHA = 2.00 DEGREES

	S TURB	S SEP	CD	S TURB	S SEP	CD	S TURB	S SEP	CD
UPPER	.2229	.1495	.0036%	.2256	.1118	.0029	.2274	.0802	.0026
LOWER	.0913	.0819	.0103	.0921	.0793	.0098%	.0926	.0768	.0082%
TOTAL	CL = .618 CD = .0045			CL = .668 CD = .0037			CL = .711 CD = .0032		
	CM = -.1205			CM = -.1352			CM = -.1420		

ALPHA = 3.00 DEGREES

	S TURB	S SEP	CD	S TURB	S SEP	CD	S TURB	S SEP	CD
UPPER	.2247	.1524	.0038%	.2273	.1188	.0031	.3665	.0744	.0043
LOWER	.0909	.0815	.0098%	.0916	.0788	.0078%	.0922	.0763	.0065%
TOTAL	CL = .716 CD = .0047			CL = .767 CD = .0038			CL = .821 CD = .0049		
	CM = -.1301			CM = -.1362			CM = -.1462		

ALPHA = 5.00 DEGREES

	S TURB	S SEP	CD	S TURB	S SEP	CD	S TURB	S SEP	CD
UPPER	.3073	.1052	.0051	.5833	.0987	.0079	.7344	.0959	.0093
LOWER	.0901	.0409	.0098%	.0908	.0780	.0066%	.0914	.0752	.0052%
TOTAL	CL = .977 CD = .0059			CL = .987 CD = .0086			CL = .991 CD = .0098		
	CM = -.1446			CM = -.1450			CM = -.1464		

ALPHA = 7.00 DEGREES

	S TURB	S SEP	CD	S TURB	S SEP	CD	S TURB	S SEP	CD
UPPER	.9498	.1166	.0158	.9529	.1092	.0146	.8584	.1043	.0138
LOWER	.0894	.0803	.0078%	.0901	.0772	.0066%	.0907	.0742	.0058%
TOTAL	CL = 1.158 CD = .0168			CL = 1.170 CD = .0151			CL = 1.178 CD = .0143		
	CM = -.1471			CM = -.1487			CM = -.1497		

ALPHA = 11.00 DEGREES

	S TURB	S SEP	CD	S TURB	S SEP	CD	S TURB	S SEP	CD
UPPER	1.0455	.1347	.0251	1.0455	.1287	.0230	1.0455	.1245	.0217
LOWER	.0883	.0794	.0066%	.0891	.0758	.0064%	.0896	.0722	.0048%
TOTAL	CL = 1.537 CD = .0256			CL = 1.548 CD = .0234			CL = 1.556 CD = .0221		
	CM = -.1556			CM = -.1568			CM = -.1576		

SUMMARY AIRFOIL 2800   ANGLE OF ATTACK RELATIVE TO THE CHORD LINE   ALPHA = 5.87 DEGREES
S INDICATES BUBBLE ANALOG LONGER THAN .020

R = 450000 RU = 3   R = 550000 RU = 3   R = 650000 RU = 3

ALPHA = -5.00 DEGREES
        S TURB S SEP   CD   S TURB S SEP   CD   S TURB S SEP   CD
UPPER   .2290   .0292   .0017   .2212   .0252   .0016   .2232   .0223   .0015
LOWER   .9984   .0396   .0050   .9964   .0375   .0048   .9984   .0355   .0047
TOTAL   CL = .027 CD = .0067   CL = .030 CD = .0064   CL = .031 CD = .0062
        CM = -.1282   CM = -.1288   CM = -.1291

ALPHA = -4.00 DEGREES
        S TURB S SEP   CD   S TURB S SEP   CD   S TURB S SEP   CD
UPPER   .2219   .0317   .0018   .2222   .0275   .0017   .2232   .0244   .0016
LOWER   .9977   .0369   .0045   .9977   .0346   .0044   .9977   .0326   .0042
TOTAL   CL = .129 CD = .0063   CL = .132 CD = .0060   CL = .134 CD = .0058
        CM = -.1306   CM = -.1313   CM = -.1317

ALPHA = -3.00 DEGREES
        S TURB S SEP   CD   S TURB S SEP   CD   S TURB S SEP   CD
UPPER   .2221   .0343   .0018   .2233   .0298   .0017   .2243   .0266   .0016
LOWER   .9962   .0344   .0041   .9962   .0328   .0039   .9962   .0301   .0038
TOTAL   CL = .231 CD = .0059   CL = .235 CD = .0057   CL = .237 CD = .0055
        CM = -.1330   CM = -.1338   CM = -.1343

ALPHA = -2.00 DEGREES
        S TURB S SEP   CD   S TURB S SEP   CD   S TURB S SEP   CD
UPPER   .2232   .0377   .0019   .2244   .0322   .0018   .2254   .0289   .0017
LOWER   .9931   .0321   .0037   .9931   .0298   .0036   .9931   .0278   .0035
TOTAL   CL = .332 CD = .0053   CL = .337 CD = .0054   CL = .340 CD = .0052
        CM = -.1353   CM = -.1365   CM = -.1371

ALPHA = -1.00 DEGREES
        S TURB S SEP   CD   S TURB S SEP   CD   S TURB S SEP   CD
UPPER   .2245   .0424   .0020   .2256   .0348   .0019   .2266   .0312   .0018
LOWER   .2977   .0323   .0013   .4277   .0303   .0017   .5222   .0281   .0019
TOTAL   CL = .433 CD = .0033   CL = .441 CD = .0036   CL = .444 CD = .0037
        CM = -.1376   CM = -.1394   CM = -.1401

ALPHA = 0.00 DEGREES
        S TURB S SEP   CD   S TURB S SEP   CD   S TURB S SEP   CD
UPPER   .2258   .0473   .0021   .2269   .0385   .0020   .2279   .0337   .0019
LOWER   .0942   .0759   .0072   .1947   .0271   .0009   .3215   .0263   .0012
TOTAL   CL = .530 CD = .0028   CL = .548 CD = .0029   CL = .547 CD = .0031
        CM = -.1441   CM = -.1416   CM = -.1429

SUMMARY AIRFOIL 2500   ANGLE OF ATTACK RELATIVE TO THE CHORD LINE   ALPHAO = 5.27 DEGREES

t INDICATES BUBBLE ANALOG LOWER THAN .030

R = .450000   MU = 3   R = .550000   MU = 3   R = .650000   MU = 3

ALPHA = 1.00 DEGREES
	S TURB	S SEP	CD		S TURB	S SEP	CD		S TURB	S SEP	CD
UPPER	.2272	.8535	.0022		.2961	.0479	.0028		.4148	.0584	.0039
LOWER	.0936	.0751	.0061t		.0938	.0729	.0063t		.0642	.0708	.0053t
TOTAL		CL = .646	CD = .0028		CL = .651	CD = .0034			CL = .637	CD = .0044
		CM = -.1468			CM = -.1468				CM = -.1439	

ALPHA = 2.00 DEGREES
	S TURB	S SEP	CD		S TURB	S SEP	CD		S TURB	S SEP	CD
UPPER	.3437	.0605	.0036		.4674	.0696	.0048		.5520	.0707	.0054
LOWER	.0930	.0744	.0063t		.0934	.0721	.0061t		.0937	.0699	.0059t
TOTAL		CL = .738	CD = .0042		CL = .724	CD = .0053			CL = .722	CD = .0059
		CM = -.1464			CM = -.1442				CM = -.1437	

ALPHA = 3.00 DEGREES
	S TURB	S SEP	CD		S TURB	S SEP	CD		S TURB	S SEP	CD
UPPER	.5115	.0800	.0057		.6683	.0795	.0065		.6790	.0777	.0070
LOWER	.0926	.0738	.0065t		.0929	.0714	.0065t		.0932	.0691	.0065t
TOTAL		CL = .812	CD = .0062		CL = .812	CD = .0070			CL = .814	CD = .0074
		CM = -.1446			CM = -.1445				CM = -.1448	

ALPHA = 5.00 DEGREES
	S TURB	S SEP	CD		S TURB	S SEP	CD		S TURB	S SEP	CD
UPPER	.8184	.0928	.0099		.8663	.0900	.0101		.8998	.0872	.0103
LOWER	.0918	.0725	.0065t		.0921	.0699	.0064t		.0924	.0673	.0063t
TOTAL		CL = .995	CD = .0104		CL = .999	CD = .0106			CL = 1.003	CD = .0107
		CM = -.1470			CM = -.1475				CM = -.1480	

ALPHA = 7.00 DEGREES
	S TURB	S SEP	CD		S TURB	S SEP	CD		S TURB	S SEP	CD
UPPER	.9626	.1004	.0133		.9659	.0973	.0120		.9686	.0946	.0126
LOWER	.0911	.0712	.0064t		.0914	.0683	.0064t		.0917	.0656	.0064t
TOTAL		CL = 1.184	CD = .0137		CL = 1.189	CD = .0133			CL = 1.194	CD = .0130
		CM = -.1505			CM = -.1511				CM = -.1517	

ALPHA = 11.00 DEGREES
	S TURB	S SEP	CD		S TURB	S SEP	CD		S TURB	S SEP	CD
UPPER	1.0455	.1213	.0208		1.0455	.1181	.0201		1.0455	.1153	.0196
LOWER	.0900	.0686	.0063t		.0903	.0644	.0063t		.0906	.0553	.0063t
TOTAL		CL = 1.562	CD = .0211		CL = 1.568	CD = .0204			CL = 1.573	CD = .0199
		CM = -.1581			CM = -.1587				CM = -.1588	

Appendix F

Detailed Results: Airfoil 2510

The detailed results for airfoil 2510 are presented in this appendix. On the first two pages, the x and y coordinates of the airfoil are given under columns marked x and y. The C_p value at each coordinate are listed in the subsequent columns. Every column indicates C_p values for a different angle of attack. All angles of attack are with respect to the chord line. The last line on page 10) indicates the value of zero lift angle of attack and C_{m_o}.

The last four pages of the appendix contain a summary of the results obtained by viscous flow analysis. For every Reynolds number (1.5 to 6.5 million) and angle of attack (-5° to $\_11^o$), the amount of turbulent flow, amount of separation, and the value of C_d is given for the upper and lower surfaces, separately. The values of turbulent flow and separation are given as fractions of the chord length, i.e. s.sep - .03 implies that there is separated flow on 3% of chord length.

The values of C_1, C_d and C_{m_o} for each set of Reynolds number and angle of attack are also listed in these data.

AIRFOIL 2S10   15.04%

PRESSURE DISTRIBUTIONS FOR THE ABOVE ANGLES OF ATTACK RELATIVE TO THE CHORD LINE

N	X	V	-5.00	-4.00	-3.00	-2.00	-1.00	0.00	1.00	2.00	3.00	5.00	7.00	11.00
44	.38305	-.05398	-.482	-.426	-.370	-.315	-.250	-.205	-.151	-.097	-.044	.060	.160	.358
45	.43178	-.05215	-.467	-.417	-.367	-.317	-.267	-.217	-.168	-.118	-.071	.025	.118	.298
46	.49116	-.04859	-.387	-.345	-.302	-.259	-.216	-.173	-.130	-.088	-.045	.039	.122	.283
47	.53167	-.04362	-.260	-.225	-.190	-.154	-.119	-.083	-.047	-.012	.024	.095	.168	.304
48	.59326	-.03636	-.151	-.122	-.093	-.064	-.034	-.005	.025	.055	.086	.146	.206	.325
49	.63525	-.02932	-.058	-.034	-.010	.014	.038	.063	.088	.113	.139	.190	.242	.345
50	.68687	-.02241	.021	.040	.060	.080	.101	.121	.143	.164	.185	.229	.273	.363
51	.73729	-.01604	.088	.104	.120	.137	.154	.171	.189	.207	.225	.263	.301	.379
52	.78564	-.01052	.144	.157	.171	.184	.199	.213	.228	.244	.259	.291	.324	.393
53	.83101	-.00626	.191	.202	.213	.225	.236	.249	.261	.274	.287	.315	.343	.403
54	.87252	-.00277	.231	.239	.248	.258	.267	.278	.288	.299	.310	.334	.358	.411
55	.90931	-.00064	.263	.270	.277	.285	.293	.301	.310	.319	.328	.348	.369	.416
56	.94061	.00050	.289	.294	.300	.306	.312	.319	.326	.334	.342	.358	.377	.416
57	.96581	.00091	.322	.326	.330	.334	.339	.344	.350	.356	.362	.376	.391	.425
58	.98448	.00078	.363	.365	.368	.371	.374	.378	.382	.387	.392	.402	.415	.443
59	.99646	.00029	.398	.399	.400	.402	.404	.406	.409	.412	.416	.424	.434	.458
60	1.00000	-.00000	.413	.413	.413	.414	.415	.418	.418	.420	.422	.428	.435	.464

ALPHAO = 4.32 DEGREES   CM0 = -.1226   ETA = 1.120

SUMMARY AIRFOIL 2810
ANGLE OF ATTACK RELATIVE TO THE CHORD LINE   ALPHAO = 4.38 DEGREES
* INDICATES BUBBLE ANALOG LONGER THAN .030

R = 150000 RU = 3   R = 250000 RU = 3   R = 350000 RU = 3

ALPHA = -5.00 DEGREES
              S TURB   S SEP   CD   S TURB   S SEP   CD   S TURB   S SEP   CD
UPPER   .2878   .2282   .0023*   .2116   .0114   .0018   .2142   .0025   .0016
LOWER   1.0039   .0126   .0063   1.0039   .0046   .0057   1.0039   .0005   .0054
TOTAL   CL = -.097 CD = .0084   CL = -.081 CD = .0075   CL = -.076 CD = .0070
         CM = -.1144   CM = -.1180   CM = -.1198

ALPHA = -4.00 DEGREES
              S TURB   S SEP   CD   S TURB   S SEP   CD   S TURB   S SEP   CD
UPPER   .2805   .0468   .0023*   .2132   .0147   .0019   .2158   .0056   .0017
LOWER   1.0013   .0016   .0055   1.0013   .0000   .0058   1.0013   .0000   .0049
TOTAL   CL = .002 CD = .0078   CL = .025 CD = .0068   CL = .032 CD = .0065
         CM = -.1148   CM = -.1200   CM = -.1218

ALPHA = -3.00 DEGREES
              S TURB   S SEP   CD   S TURB   S SEP   CD   S TURB   S SEP   CD
UPPER   .2112   .0554   .0024*   .2149   .0190   .0020   .2174   .0086   .0017
LOWER   .5378   .0000   .0028   .5504   .0000   .0025   .5584   .0000   .0024
TOTAL   CL = .102 CD = .0052   CL = .131 CD = .0045   CL = .139 CD = .0041
         CM = -.1157   CM = -.1221   CM = -.1241

ALPHA = -2.00 DEGREES
              S TURB   S SEP   CD   S TURB   S SEP   CD   S TURB   S SEP   CD
UPPER   .2131   .0674   .0025   .2167   .0235   .0021   .2192   .0117   .0018
LOWER   .5251   .0000   .0026   .5399   .0000   .0024   .5491   .0000   .0022
TOTAL   CL = .199 CD = .0051   CL = .236 CD = .0044   CL = .246 CD = .0041
         CM = -.1161   CM = -.1241   CM = -.1264

ALPHA = -1.00 DEGREES
              S TURB   S SEP   CD   S TURB   S SEP   CD   S TURB   S SEP   CD
UPPER   .2158   .0795   .0027   .2186   .0281   .0022   .2216   .0149   .0019
LOWER   .5176   .0000   .0024   .5284   .0000   .0022   .5392   .0000   .0021
TOTAL   CL = .294 CD = .0051   CL = .340 CD = .0044   CL = .352 CD = .0040
         CM = -.1162   CM = -.1259   CM = -.1287

ALPHA = 0.00 DEGREES
              S TURB   S SEP   CD   S TURB   S SEP   CD   S TURB   S SEP   CD
UPPER   .2171   .0893   .0028   .2206   .0328   .0023   .2230   .0190   .0020
LOWER   .5122   .0000   .0023   .5193   .0000   .0021   .5283   .0000   .0020
TOTAL   CL = .390 CD = .0051   CL = .444 CD = .0044   CL = .457 CD = .0040
         CM = -.1167   CM = -.1277   CM = -.1308

102

2810
0 INDICATES BUBBLE ANALOG LONGER THAN .030

ANGLE OF ATTACK RELATIVE TO THE CHORD LINE   ALPHA0 = 4.38 DEGREES

	R = 150000 RU = 3			R = 250000 RU = 3			R = 350000 RU = 3		
ALPHA = 1.00 DEGREES	S TURB	S SEP	CD	S TURB	S SEP	CD	S TURB	S SEP	CD
UPPER	.2194	.0979	.0030*	.2228	.0407	.0024	.2852	.0234	.0021
LOWER	.5067	0.0000	.0022	.5144	0.0000	.0020	.5195	0.0000	.0018
TOTAL			.0051			.0044			.0040
	CL = .487 CD = -.1172			CL = .544 CD = -.1287			CL = .562 CD = -.1327		
ALPHA = 2.00 DEGREES	S TURB	S SEP	CD	S TURB	S SEP	CD	S TURB	S SEP	CD
UPPER	.2216	.1063	.0031*	.2252	.0489	.0026	.4149	.0336	.0039
LOWER	.5407	0.0000	.0020	.5092	0.0000	.0019	.5147	0.0000	.0018
TOTAL			.0052			.0044			.0057
	CL = .583 CD = -.1177			CL = .644 CD = -.1295			CL = .660 CD = -.1331		
ALPHA = 3.00 DEGREES	S TURB	S SEP	CD	S TURB	S SEP	CD	S TURB	S SEP	CD
UPPER	.2245	.1143	.0032*	.4326	.0449	.0046	.6092	.0473	.0059
LOWER	.4949	0.0000	.0019	.5035	0.0000	.0018	.5096	0.0000	.0017
TOTAL			.0052			.0064			.0076
	CL = .678 CD = -.1182			CL = .755 CD = -.1331			CL = .753 CD = -.1325		
ALPHA = 5.00 DEGREES	S TURB	S SEP	CD	S TURB	S SEP	CD	S TURB	S SEP	CD
UPPER	.9521	.0790	.0121	.9521	.0692	.0110	.9546	.0625	.0104
LOWER	.4772	0.0000	.0017	.4897	0.0000	.0016	.4976	0.0000	.0015
TOTAL			.0138			.0126			.0119
	CL = .929 CD = -.1299			CL = .941 CD = -.1323			CL = .949 CD = -.1339		
ALPHA = 7.00 DEGREES	S TURB	S SEP	CD	S TURB	S SEP	CD	S TURB	S SEP	CD
UPPER	.9720	.0896	.0142	.9720	.0806	.0130	.9734	.0740	.0123
LOWER	.4469	0.0000	.0015	.4690	0.0000	.0014	.4808	0.0000	.0013
TOTAL			.0157			.0143			.0136
	CL = 1.126 CD = -.1318			CL = 1.138 CD = -.1341			CL = 1.146 CD = -.1358		
ALPHA = 11.00 DEGREES	S TURB	S SEP	CD	S TURB	S SEP	CD	S TURB	S SEP	CD
UPPER	1.0291	.1215	.0224	1.0291	.1133	.0203	1.0291	.1072	.0191
LOWER	.2733	0.0000	.0009	.3464	0.0000	.0009	.3862	0.0000	.0009
TOTAL			.0231			.0218			.0200
	CL = 1.496 CD = -.1318			CL = 1.509 CD = -.1340			CL = 1.510 CD = -.1358		

103

SUMMARY AIRFOIL 2510
* INDICATES BUBBLE ANALOG LOWER THAN .030   ANGLE OF ATTACK RELATIVE TO THE CHORD LINE   ALPHAO = 4.30 DEGREES

R = 450000 NU = 3   R = 550000 NU = 3   R = 550000 NU = 3   R = 650000 NU = 3

ALPHA = -5.00 DEGREES
        1 S TURB   S SEP   CD   8 S TURB   S SEP   CD   3 S TURB   S SEP   CD
UPPER   .2162   0.0000   .0015   .8178   0.0000   .0050   .2191   0.0000   .0014
LOWER   1.0039   0.0000   .0051   1.0039   0.0000   .0050   1.0039   0.0000   .0049
TOTAL   CL = -.074 CD = .0068   CL = -.074 CD = .0064   CL = -.074 CD = .0062
        CM = -.1196   CM = -.1196   CM = -.1196

ALPHA = -4.00 DEGREES
        1 S TURB   S SEP   CD   2 S TURB   S SEP   CD   3 S TURB   S SEP   CD
UPPER   .2177   .0003   .0015   .2193   0.0000   .0015   .2206   .0000   .0014
LOWER   1.0013   0.0000   .0047   1.0013   0.0000   .0046   1.0013   0.0000   .0045
TOTAL   CL = .035 CD = .0063   CL = .036 CD = .0060   CL = .036 CD = .0059
        CM = -.1226   CM = -.1227   CM = -.1227

ALPHA = -3.00 DEGREES
        1 S TURB   S SEP   CD   2 S TURB   S SEP   CD   3 S TURB   S SEP   CD
UPPER   .2193   .0031   .0016   .2209   0.0000   .0015   .2222   0.0000   .0014
LOWER   .5640   0.0000   .0023   .5684   0.0000   .0022   .5858   0.0000   .0023
TOTAL   CL = .143 CD = .0039   CL = .146 CD = .0038   CL = .146 CD = .0037
        CM = -.1251   CM = -.1257   CM = -.1257

ALPHA = -2.00 DEGREES
        1 S TURB   S SEP   CD   2 S TURB   S SEP   CD   3 S TURB   S SEP   CD
UPPER   .2210   .0059   .0017   .2226   .0022   .0016   .2238   0.0000   .0015
LOWER   .5555   0.0000   .0022   .5604   0.0000   .0021   .5643   0.0000   .0021
TOTAL   CL = .251 CD = .0039   CL = .254 CD = .0037   CL = .256 CD = .0036
        CM = -.1276   CM = -.1284   CM = -.1288

ALPHA = -1.00 DEGREES
        1 S TURB   S SEP   CD   2 S TURB   S SEP   CD   3 S TURB   S SEP   CD
UPPER   .2229   .0089   .0018   .2244   .0048   .0017   .2576   .0047   .0018
LOWER   .5467   0.0000   .0020   .5523   0.0000   .0020   .5567   0.0000   .0019
TOTAL   CL = .358 CD = .0038   CL = .361 CD = .0036   CL = .361 CD = .0038
        CM = -.1300   CM = -.1309   CM = -.1310

ALPHA = 0.00 DEGREES
        1 S TURB   S SEP   CD   2 S TURB   S SEP   CD   3 S TURB   S SEP   CD
UPPER   .2248   .0119   .0019   .3283   .0158   .0026   .4343   .0222   .0033
LOWER   .5374   0.0000   .0038   .5440   0.0000   .0019   .5482   0.0000   .0018
TOTAL   CL = .464 CD = .0038   CL = .461 CD = .0044   CL = .454 CD = .0051
        CM = -.1324   CM = -.1316   CM = -.1301

104

Appendix G

Detailed Results: Airfoil 2700

The detailed results for airfoil 2700 are presented in this appendix. On the first two pages, the x and y coordinates of the airfoil are given under columns marked x and y. The C_p values at each coordinate are listed in the subsequent columns. Every column indicates C_p values for a different angle of attack. All angles of attack are with respect to chord line. The last line on page 108 indicates the value of zero lift angle of attack and C_{m_0}.

The last four pages of the appendix contain a summary of the results obtained by viscous flow analysis. For every Reynolds number (1.5 to 6.5 million) and angle of attack (-5° to +11°), the amount of turbulent flow, amount of separation, and the value of C_d is given for the upper and lower surfaces, separately. The values of turbulent flow and separation are given as fractions of the chord length, i.e. s.sep = .03 implies that there is separated flow over 3% of chord length.

The values of C_1, C_d and C_{m_0} for each set of Reynolds number and angle of attack are also listed in these data.

106

AIRFOIL E700

PRESSURE DISTRIBUTIONS FOR THE ABOVE ANGLES OF ATTACK RELATIVE TO THE CHORD LINE

CHORD = -.1112   ETA = 1.118

ALPHAS = -4.04 DEGREES

SUMMARY AIRFOIL 2700   ANGLE OF ATTACK RELATIVE TO THE CHORD LINE   ALPHANG = 4.04 DEGREES
* INDICATES BUBBLE ANALOG LONGER THAN .030

R = 150000 NU = 3   R = 250000 NU = 3   R = 350000 NU = 3

ALPHA = -8.00 DEGREES
	S TURB	S SEP	CD		S TURB	S SEP	CD		S TURB	S SEP	CD
UPPER	.2470	.0495	.0022		.2521	0.0000	.0018		.2556	0.0000	.0017
LOWER	1.0035	.0060	.0063		1.0035	0.0000	.0058		1.0035	0.0000	.0054
TOTAL	CL = -.110 CD = .0085			CL = -.106 CD = .0076			CL = -.106 CD = .0072		
	CM = -.1067			CM = -.1076			CM = -.1078		

ALPHA = -4.00 DEGREES
	S TURB	S SEP	CD		S TURB	S SEP	CD		S TURB	S SEP	CD
UPPER	.2493	.0131	.0023		.2543	0.0000	.0019		.2577	0.0000	.0018
LOWER	1.0015	0.0000	.0056		1.0015	0.0000	.0052		1.0015	0.0000	.0050
TOTAL	CL = -.064 CD = .0079			CL = -.064 CD = .0072			CL = -.064 CD = .0068		
	CM = -.1085			CM = -.1105			CM = -.1105		

ALPHA = -2.00 DEGREES
	S TURB	S SEP	CD		S TURB	S SEP	CD		S TURB	S SEP	CD
UPPER	.2516	.0175	.0025		.2565	.0027	.0021		.2597	0.0000	.0018
LOWER	.5552	0.0000	.0028		.5486	0.0000	.0026		.5569	0.0000	.0024
TOTAL	CL = .102 CD = .0053			CL = .113 CD = .0046			CL = .114 CD = .0043		
	CM = -.1105			CM = -.1130			CM = -.1135		

ALPHA = -2.00 DEGREES
	S TURB	S SEP	CD		S TURB	S SEP	CD		S TURB	S SEP	CD
UPPER	.2540	.0226	.0026		.2587	.0058	.0022		.2619	0.0000	.0019
LOWER	.5215	0.0000	.0026		.5373	0.0000	.0024		.5469	0.0000	.0023
TOTAL	CL = .207 CD = .0052			CL = .220 CD = .0045			CL = .224 CD = .0042		
	CM = -.1124			CM = -.1154			CM = -.1165		

ALPHA = -1.00 DEGREES
	S TURB	S SEP	CD		S TURB	S SEP	CD		S TURB	S SEP	CD
UPPER	.2565	.0279	.0027		.2611	.0090	.0023		.2642	.0023	.0021
LOWER	.5136	0.0000	.0025		.5248	0.0000	.0022		.5363	0.0000	.0021
TOTAL	CL = .312 CD = .0052			CL = .327 CD = .0045			CL = .333 CD = .0042		
	CM = -.1141			CM = -.1177			CM = -.1190		

ALPHA = 0.00 DEGREES
	S TURB	S SEP	CD		S TURB	S SEP	CD		S TURB	S SEP	CD
UPPER	.2591	.0343	.0029		.2635	.0123	.0024		.2666	.0051	.0022
LOWER	.5077	0.0000	.0023		.5154	0.0000	.0021		.5245	0.0000	.0020
TOTAL	CL = .415 CD = .0052			CL = .434 CD = .0045			CL = .440 CD = .0042		
	CM = -.1156			CM = -.1200			CM = -.1215		

109

SUMMARY AIRFOIL 2700
S INDICATES BUBBLE ANALOG LOWER THAN .030   ANGLE OF ATTACK RELATIVE TO THE CHORD LINE   ALPHA = 4.04 DEGREES

R = 150000   NU = 3   R = 250000   NU = 3   R = 350000   NU = 3

ALPHA = 1.00 DEGREES
	S TURB	S SEP	CD		S TURB	S SEP	CD		S TURB	S SEP	CD
UPPER	.2618	.0444	.0031		.2662	.0160	.0025		.2682	.0082	.0023
LOWER	.5017	0.0000	.0022		.5101	0.0000	.0020		.5156	0.0000	.0018
TOTAL	CL = .514 CD = .0053				CL = .540 CD = .0045				CL = .547 CD = .0042		
	CM = -.1163				CM = -.1221				CM = -.1238		

ALPHA = 2.00 DEGREES
	S TURB	S SEP	CD		S TURB	S SEP	CD		S TURB	S SEP	CD
UPPER	.2647	.0549	.0032		.2690	.0210	.0027		.3631	.0167	.0032
LOWER	.4951	0.0000	.0021		.5044	0.0000	.0019		.5104	0.0000	.0018
TOTAL	CL = .611 CD = .0053				CL = .644 CD = .0046				CL = .648 CD = .0054		
	CM = -.1166				CM = -.1239				CM = -.1248		

ALPHA = 3.00 DEGREES
	S TURB	S SEP	CD		S TURB	S SEP	CD		S TURB	S SEP	CD
UPPER	.2670	.0717	.0034		.3724	.0260	.0038		.5581	.0339	.0052
LOWER	.4877	0.0000	.0020		.4982	0.0000	.0018		.5049	0.0000	.0017
TOTAL	CL = .701 CD = .0055				CL = .748 CD = .0056				CL = .740 CD = .0069		
	CM = -.1155				CM = -.1255				CM = -.1237		

ALPHA = 5.00 DEGREES
	S TURB	S SEP	CD		S TURB	S SEP	CD		S TURB	S SEP	CD
UPPER	.6090	.0565	.0075		.8951	.0672	.0100		.9338	.0598	.0099
LOWER	.4689	0.0000	.0017		.4828	0.0000	.0016		.4917	0.0000	.0015
TOTAL	CL = .919 CD = .0092				CL = .918 CD = .0116				CL = .927 CD = .0114		
	CM = -.1213				CM = -.1212				CM = -.1229		

ALPHA = 7.00 DEGREES
	S TURB	S SEP	CD		S TURB	S SEP	CD		S TURB	S SEP	CD
UPPER	.9761	.0669	.0139		.9701	.0855	.0127		.9716	.0778	.0120
LOWER	.4332	0.0000	.0015		.4581	0.0000	.0014		.4726	0.0000	.0013
TOTAL	CL = 1.094 CD = .0154				CL = 1.108 CD = .0140				CL = 1.119 CD = .0133		
	CM = -.1189				CM = -.1215				CM = -.1235		

ALPHA = 11.00 DEGREES
	S TURB	S SEP	CD		S TURB	S SEP	CD		S TURB	S SEP	CD
UPPER	1.025	.1377	.0217		1.0285	.1272	.0199		1.0285	.1201	.0187
LOWER	.2160	0.0000	.0008		.3159	0.0000	.0009		.3630	0.0000	.0009
TOTAL	CL = 1.453 CD = .0225				CL = 1.468 CD = .0207				CL = 1.475 CD = .0196		
	CM = -.1173				CM = -.1197				CM = -.1214		

SUMMARY: AIRFOIL   2700   ANGLE OF ATTACK RELATIVE TO THE CHORD LINE   ALPHAO = 4.04 DEGREES
% INDICATES BUBBLE ANALOG LONGER THAN .030

R = 450000 RU = 3	R = 550000 RU = 3	R = 650000 RU = 3

ALPHA = -5.00 DEGREES

	TURB	S SEP	CD		TURB	S SEP	CD		TURB	S SEP	CD
UPPER	.2552	0.0000	.0016		.2603	0.0000	.0016		.2520	0.0000	.0015
LOWER	1.0035	0.0000	.0053		1.0035	0.0000	.0052		1.0035	0.0000	.0051
TOTAL	CL = -.106 CD = .0069			CL = -.106 CD = .0067			CL = -.106 CD = .0066
	CM = -.1076			CM = -.1076			CM = -.1076

ALPHA = -4.00 DEGREES

UPPER	.2602	0.0000	.0017		.2622	0.0000	.0016		.2639	0.0000	.0016
LOWER	1.0015	0.0000	.0049		1.0015	0.0000	.0047		1.0015	0.0000	.0046
TOTAL	CL = .004 CD = .0066			CL = .004 CD = .0064			CL = .004 CD = .0062
	CM = -.1165			CM = -.1165			CM = -.1165

ALPHA = -3.00 DEGREES

UPPER	.2622	0.0000	.0018		.2642	0.0000	.0017		.2658	0.0000	.0016
LOWER	.5629	0.0000	.0024		.5674	0.0000	.0023		.6303	0.0000	.0025
TOTAL	CL = .114 CD = .0041			CL = .114 CD = .0040			CL = .114 CD = .0048
	CM = -.1135			CM = -.1135			CM = -.1135

ALPHA = -2.00 DEGREES

UPPER	.2643	0.0000	.0018		.2662	0.0000	.0018		.2678	0.0000	.0017
LOWER	.5537	0.0000	.0022		.5588	0.0000	.0021		.5629	0.0000	.0021
TOTAL	CL = .224 CD = .0040			CL = .224 CD = .0039			CL = .224 CD = .0038
	CM = -.1165			CM = -.1165			CM = -.1165

ALPHA = -1.00 DEGREES

UPPER	.2665	0.0000	.0019		.2684	0.0000	.0018		.2699	0.0000	.0018
LOWER	.5442	0.0000	.0021		.5501	0.0000	.0020		.5547	0.0000	.0020
TOTAL	CL = .334 CD = .0040			CL = .334 CD = .0038			CL = .334 CD = .0037
	CM = -.1195			CM = -.1195			CM = -.1195

ALPHA = 0.00 DEGREES

UPPER	.2689	.0012	.0020		.2752	0.0000	.0019		.2943	.0076	.0028
LOWER	.5341	0.0000	.0019		.5411	0.0000	.0018		.5466	0.0000	.0019
TOTAL	CL = .443 CD = .0039			CL = .444 CD = .0038			CL = .438 CD = .0048
	CM = -.1223			CM = -.1228			CM = -.1200

III

INFOIL 2700   ANGLE OF ATTACK RELATIVE TO THE CHORD LINE   ALPHA = 4.04 DEGREES
* INDICATES BUBBLE ANALOG LONGER THAN .030

R = .450000 MU = 3   R = .550000 MU = 3   R = .650000 MU = 3

ALPHA = 1.00 DEGREES
        S TURB S SEP   CD   S TURB S SEP   CD   S TURB S SEP   CD
UPPER   .3315   .0052 .0026   .4548   .0158 .0035   .5403   .0192 .0040
LOWER   .5263   0.0000 .0018   .5310   0.0000 .0018   .5377   0.0000 .0017
TOTAL   CL = .547 CD = .0044   CL = .546 CD = .0053   CL = .537 CD = .0058
             CM = -.1238   CM = -.1221   CM = -.1214

ALPHA = 2.00 DEGREES
        S TURB S SEP   CD   S TURB S SEP   CD   S TURB S SEP   CD
UPPER   .5076   .0248 .0043   .6049   .0270 .0049   .6720   .0272 .0053
LOWER   .5148   0.0000 .0017   .5181   0.0000 .0017   .5264   0.0000 .0016
TOTAL   CL = .640 CD = .0060   CL = .638 CD = .0066   CL = .638 CD = .0069
             CM = -.1230   CM = -.1225   CM = -.1225

ALPHA = 3.00 DEGREES
        S TURB S SEP   CD   S TURB S SEP   CD   S TURB S SEP   CD
UPPER   .6677   .0355 .0059   .7476   .0349 .0064   .7952   .0333 .0066
LOWER   .5097   0.0000 .0016   .5134   0.0000 .0016   .5164   0.0000 .0015
TOTAL   CL = .738 CD = .0075   CL = .739 CD = .0080   CL = .740 CD = .0081
             CM = -.1233   CM = -.1235   CM = -.1238

ALPHA = 5.00 DEGREES
        S TURB S SEP   CD   S TURB S SEP   CD   S TURB S SEP   CD
UPPER   .9550   .0545 .0098   .9578   .0569 .0095   .9602   .0478 .0092
LOWER   .4979   0.0000 .0014   .5027   0.0000 .0014   .5064   0.0000 .0014
TOTAL   CL = .933 CD = .0112   CL = .937 CD = .0109   CL = .940 CD = .0106
             CM = -.1241   CM = -.1250   CM = -.1257

ALPHA = 7.00 DEGREES
        S TURB S SEP   CD   S TURB S SEP   CD   S TURB S SEP   CD
UPPER   .9737   .0765 .0115   .9753   .0652 .0111   .9772   .0607 .0109
LOWER   .4817   0.0000 .0013   .4883   0.0000 .0012   .4935   0.0000 .0012
TOTAL   CL = 1.127 CD = .0128   CL = 1.133 CD = .0124   CL = 1.139 CD = .0121
             CM = -.1251   CM = -.1264   CM = -.1276

ALPHA = 11.00 DEGREES
        S TURB S SEP   CD   S TURB S SEP   CD   S TURB S SEP   CD
UPPER   1.0255 .1145 .0179   1.0255 .1095 .0173   1.0255 .1052 .0168
LOWER   .3983   0.0000 .0009   .4156   0.0000 .0009   .4317   0.0000 .0009
TOTAL   CL = 1.467 CD = .0188   CL = 1.484 CD = .0182   CL = 1.500 CD = .0177
             CM = -.1228   CM = -.1240   CM = -.1251

Appendix H

Brief Description of Boundary Layer Analysis
Method Designed by Shang et al

A computer code, using the eddy viscosity model for analysis of boundary layers, was employed for verification of results achieved by using Eppler's boundary layer analysis method. A brief description of the method used in solving the boundary problem is given here.

The method is based on the solution of three basic equations i.e. continuity, momentum, and energy equations. They are:

Continuity:

$$\frac{\partial}{\partial x}(r^j \rho u) + \frac{\partial}{\partial y}[r^j \rho(V + \frac{\rho'V'}{\rho})] = 0 \qquad (H-1)$$

Momentum:

$$\rho[u\frac{\partial u}{\partial x} + (V + \frac{\rho'V'}{\rho})\frac{\partial u}{\partial y}] = -\frac{dP}{dx} + \frac{1}{r^j}\frac{\partial}{\partial y}[r^j(\mu\frac{\partial u}{\partial y} + \rho\,u'V')] \qquad (H-2)$$

Energy:

$$\rho[u\frac{\partial u}{\partial x}(C_pT) + (V + \frac{\partial'V'}{\partial})\frac{\partial}{\partial y}(C_pT)] = u\frac{dp}{dx} + \frac{1}{r^j}\frac{\partial}{\partial y}[r^j\frac{K\ell}{C_p}\frac{\partial}{\partial y}(C_pT)]$$

$$+\mu(\frac{\partial u}{\partial y})^2 + \frac{1}{r^j}\frac{\partial}{\partial y}[r^j(-C_p\rho V'T')] - \rho u'V'\frac{\partial u}{\partial y} \qquad (H-3)$$

These equations were modified by using the following factors

$$V = V + \frac{\rho'V'}{\rho}$$
$$\varepsilon = -\rho\frac{u'V'}{\partial u/\partial y} \qquad (H-4)$$
$$K_T = -C_p\rho\frac{V'T'}{\partial T/\partial y}$$

113

Also included were the following two laws:

Perfect gas law:

$$p = C_p \left(\frac{\gamma-1}{\gamma}\right) \rho\, T \tag{H-5}$$

Sutherland viscosity law:

$$\frac{\mu}{\mu_e} = \left(\frac{T}{T_e}\right)^{1.5} \frac{T_e+S}{T+S} \quad \text{(air only)} \tag{H-6}$$

The system thus has two algebraic expressions and three non-linear partial differential equations. But it still had a singularity at $x = 0$ (leading edge). This was avoided by using a transformation of variables. The transformation of Probstein-Elliott and Levy-Lees is used. It can be written as:

$$\xi(x) = \int_0^x \rho_e\, u_e/\mu_e\, r_o^{2j}\, dx \tag{H-7}$$

$$\eta(x,y) = \frac{\rho_e u_e r_o^j}{2\xi} \int_0^y t^j \frac{\rho}{\rho_e}\, dy \tag{H-8}$$

$$\left(\frac{\partial}{\partial x}\right)_y = \rho_e u_e \mu_e\, r_o^{2j} \left(\frac{\partial}{\partial \xi}\right)_\eta + \left(\frac{\partial \eta}{\partial x}\right)\left(\frac{\partial}{\partial \eta}\right)_\xi \tag{H-9}$$

$$\left(\frac{\partial}{\partial y}\right)_x = \frac{\rho_e u_e r_o^{2j} t^j}{\partial \xi} \left(\frac{\rho}{\rho_e}\right)\left(\frac{\partial}{\partial \eta}\right)_\xi \tag{H-10}$$

$$F = \frac{u}{u_e} \tag{H-11}$$

$$\theta = \frac{T}{T_e} \tag{H-12}$$

$$V = \frac{2\xi}{\rho_e u_e \mu_e r_o^{2j}} \left(F \frac{\partial \eta}{\partial x} + \frac{\rho V r_o^j t^j}{\partial \xi}\right) \tag{H-13}$$

$$\ell = \frac{\rho \mu}{\rho_e \mu_e} \tag{H-14}$$

$$\alpha = \frac{u_e^2}{C_p T_e} \tag{H-15}$$

114

$$\beta = \frac{\partial \xi}{u_e} \frac{du_e}{d\xi} \tag{H-16}$$

Continuity:

$$\frac{\partial F}{\partial \eta} + \partial \xi \; \frac{\partial F}{\partial \xi} + F = 0 \tag{H-17}$$

Momentum:

$$\partial \xi \; F \frac{\partial F}{\partial \xi} + V \frac{\partial F}{\partial \eta} - \frac{\partial}{\partial \eta} (t^{2j} \; \ell \; \bar{c} \; \frac{\partial}{\partial \eta}) + \beta \; (F^2 - \_) = 0 \tag{H-18}$$

Energy:

$$\partial \xi F \frac{\partial \theta}{\partial \xi} + V \frac{\partial \theta}{\partial \eta} - \frac{\partial}{\partial \eta} (t^{2j} \frac{\ell}{pr} \varepsilon \frac{\partial \theta}{\partial \eta}) - \alpha \; \ell t^{2j} \varepsilon (\frac{\partial F}{\partial \eta})^2 = 0 \tag{H-19}$$

where $\varepsilon = 1 + \frac{\varepsilon}{\mu} \Gamma$ and $\varepsilon = 1 + \frac{\varepsilon}{\mu} \frac{Pr}{Pr_t} \Gamma$

These equations are cast into a finite difference scheme and are
used to study the behaviour of the boundary layer. The transformation
from the real (x,y) plane to the (ξ, η) plane cast the boundary layer
into a rectangular grid of nodes. The value of F, $\underline{\theta}$ and V was com-
puted at each node in the grid. This procedure was carried out
along the surface of the test object (e.g. airfoil). Based on the
results obtained at each node the following quantities were computed:

   Boundary layer momentum thickness

   Boundary layer displacement thickness

   Local skin friction co-efficient

   Local Mach number

   Local Reynolds number

   Reynolds number based on momentum thickness

   Reynolds number based on displacement thickness

   Ratio of local and free stream density of air

115

Ratio of local and free stream temperature

Stanton number (for heat transfer)

These parameters are enough to enable a thorough analysis of the boundary layer at any point on the surface. The computer code also has the capability of providing the velocity and temperature profile within the boundary layer at any number of points.

The input to the program includes the specification of free stream Mach number, Reynolds number and temperature in addition to the ratio of specific heats, the laminar and turbulent prandtl number, the number and location of points (on the surface) on which data is needed, and the specification the C_p value at each point on the surface.

Readers interested in further details of this program are referred to Ref 18 and Ref 2.

Vita

Iftikhar Ahmad was born on 1 June 1953 in Gujranwala, Pakistan. He did his matriculation and F.Sc. with distinction from P.A.F. College Sargodha in 1969 and 1971 respectively. He joined P.A.F. College of Aeronautical Engineering in 1972. He graduated in first division from CAE in 1976 with a Bachelor of Aerospace Engineering degree. He was commissioned in the P.A.F., as a flying officer upon graduation. As an engineering officer, he was assigned to various duties in the P.A.F. and did several professional courses. He was detailed for a Master's course in Aeronautical Engineering at the Air Force Institute of Technology in June 1981. He is a member of the Institute of Engineers, Pakistan.

Permanent address: E/485 Street No-2
Medina Colony, Walton
Lahore, Pakistan

REPORT DOCUMENTATION PAGE	READ INSTRUCTIONS BEFORE COMPLETING FORM

1. REPORT NUMBER	2. GOVT ACCESSION NO.	3. RECIPIENT'S CATALOG NUMBER
AFIT/GAE/AA/82D-1	AD-A124 757	

4. TITLE (and Subtitle)	5. TYPE OF REPORT & PERIOD COVERED
Design and Analysis of a Subcritical Airfoil for High Altitude Long Endurance Flight.	MS Thesis
	6. PERFORMING ORG. REPORT NUMBER

7. AUTHOR(s)	8. CONTRACT OR GRANT NUMBER(s)
Iftikhar Ahmad Flt Lt PAF	

9. PERFORMING ORGANIZATION NAME AND ADDRESS	10. PROGRAM ELEMENT, PROJECT, TASK AREA & WORK UNIT NUMBERS

11. CONTROLLING OFFICE NAME AND ADDRESS	12. REPORT DATE
	December 1982
	13. NUMBER OF PAGES

14. MONITORING AGENCY NAME & ADDRESS(if different from Controlling Office)	15. SECURITY CLASS. (of this report)
	UNCLASSIFIED
	15a. DECLASSIFICATION/DOWNGRADING SCHEDULE

16. DISTRIBUTION STATEMENT (of this Report)

Approved for Public Release; Distribution Unlimited

17. DISTRIBUTION STATEMENT (of the abstract entered in Block 20, if different from Report)

18. SUPPLEMENTARY NOTES

19. KEY WORDS (Continue on reverse side if necessary and identify by block number)

Airfoil Design   Inverse Design of Airfoils
Eppler Computer Code   High Lift to Drag Ratio

20. ABSTRACT (Continue on reverse side if necessary and identify by block number)

An airfoil was designed using the 'inverse design' method. The airfoil was tailored to meet the requirements of high altitude, long endurance missions. The cruise Mach number was 0.65 so compressibility effects were included. In the procedure used, a basic airfoil was generated to meet the thickness and moment requirements. It was then refined to ensure desired behaviour of the boundary layer at the operating angles of attack. Computer codes designed by Richard Eppler were used for this study. Results thus obtained were compared with results obtained by analysis of the airfoil using a viscous flow computer code based on eddy viscosity model.

DD $_{1 \text{ JAN } 73}^{\text{FORM}}$ 1473   EDITION   1 NOV 65 IS OBSOLETE   UNCLASSIFIED

END

FILMED

3-83

DTIC